AIX-MARSEILLE UNIVERSITÉ

Ecole Doctorale Physique et sciences de la matière

CEA/DES/IRESNE/DER/SPRC/LEPh

Thèse présentée pour obtenir le grade universitaire de Docteur

Discipline: Physique et Sciences de la matiere
Spécialité: Energie, Rayonnement et plasma

Giorgio VALOCCHI

Modélisation neutronique de coeurs complexes en cinétique multidimensionnelle : application au coeur ASTRID faible vidange et à la préparation d'expériences de validation

Neutronic modeling of complex cores in multidimentional kinetics: Application to the low void worth core ASTRID and to the preparation of a validation experiment

Soutenance le 14/05/2020 devant le jury composé de:

Ivan KODELI	IJS & CCFE/UKAEA	Rapporteur
Elsa MERLE	CNRS, LPSC	Rapporteur
Annick BILLEBAUD	CNRS, LPSC	Examinateur
Jean TOMMASI	CEA Cadarache	Directeur de thèse
Piero RAVETTO	Politecnico di Torino	Directeur de thèse

Résumé

Le comportement cinétique d'un réacteur nucléaire est régi par des phénomènes opérant sur différentes échelles de temps. De ce fait, les calculs cinétiques directs sont parmi les calculs les plus exigeants en termes de ressources en physique des réacteurs et se révèlent généralement inabordables, même avec les supercalculateurs les plus avancés.

L'approche courante consiste à décrire le comportement cinétique d'un réacteur en utilisant la cinétique ponctuelle, c'est-à-dire un modèle à paramètres intégraux dans lequel le réacteur est modélisé pour ainsi dire comme un point et décrit par un ensemble de paramètres cinétiques globaux. Cette approche implique que ces quantités sont constantes sur l'ensemble du cœur et n'est pas en mesure de représenter les effets spatiaux qui pourraient résulter de l'hétérogénéité. Les alternatives nécessitent généralement de calculer le flux sur l'ensemble du réacteur avec un pas de temps qui dépend de l'échelle de temps de ces phénomènes. Le temps moyen de génération des neutrons étant typiquement de l'ordre de la microseconde, cela pourrait obliger à répéter le calcul du flux un nombre de fois inacceptable.

L'objectif de cette thèse est de mettre en œuvre et d'appliquer des modèles d'ordre réduit capables de simuler correctement des transitoires de réacteur caractérisés par un comportement complexe tout en étant raisonnables en termes de ressources requises (temps, mémoire).

Les résultats présentés montrent comment des systèmes hétérogènes peuvent évoluer en présentant des effets spatiaux non négligeables qui ne peuvent pas être modélisés avec des approches standard, telles que la cinétique ponctuelle, mais peuvent être représentés en utilisant des techniques plus avancées qui gardent cependant un besoin en ressources du même ordre de grandeur.

Abstract

The kinetic behavior of a nuclear reactor is governed by phenomena taking place on different time scales. Due to this, direct kinetic calculations are among the most resource-demanding calculations in reactor physics and usually result in being not affordable even with the most advanced supercomputers.

The common approach is to describe the kinetic behavior of a reactor by using point kinetics that is a lumped parameter model where the reactor is modeled as it were point-like and described by a set of global kinetic parameters. This approach implies that those quantities are constant over the whole core and is not able to capture spatial effects that could arise from heterogeneity. The alternatives usually require to compute the flux on the whole reactor with a time step that depends on the time scale of these phenomena. Being the typical mean neutron generation time of the order of the μs, this could force to repeat flux calculation a non-affordable amount of times.

The aim of this thesis is to implement and apply reduced-order models able to properly simulate reactor transients characterized by complex behavior while being affordable in terms of resource-demand (time, memory).

The results presented show how heterogeneous systems can evolve presenting spatial effects that can not be modeled with standard approaches, as point kinetics, but can be represented using more advanced techniques that have resource demand in the same order of magnitude.

Résumé étendu

Introduction

La description physique d'un réacteur nucléaire est une tâche complexe impliquant plusieurs disciplines ; celle qui se concentre sur le comportement des neutrons est appelée physique des réacteurs ou neutronique. Cette discipline est largement étudiée et comprend des concepts issus des mathématiques, de la physique, de l'ingénierie et de l'informatique. Une description approfondie de tous les concepts nécessaires pour calculer le flux de neutrons dans un réacteur dépasse l'objet de ce chapitre, qui vise plutôt à fixer la notation et la terminologie et à servir comme révision rapide des concepts de base. Le lecteur intéressé par de plus amples informations trouvera plusieurs références dans le texte.

Dans la section 1.1, il est fait un bref aperçu des principaux concepts qui se retrouvent habituellement dans la physique des réacteurs. Dans un premier temps, les principales quantités utilisées pour décrire le comportement des neutrons dans un réacteur, le flux de neutrons et les sections nucléaires, sont présentées. Ensuite, le principal modèle mathématique utilisé pour décrire le flux de neutrons dans un réacteur, l'équation linéaire de Boltzmann, est présenté ; ce faisant, les différents termes apparaissant dans l'équation de Boltzmann, le terme total, la fission, la diffusion et le terme de flux sont décrits individuellement et quelques commentaires sur l'hypothèse principale liée à chacun d'entre eux sont ajoutés au cours de leur description. Ensuite, quelques formulations simplifiées qui peuvent être utilisées pour décrire une configuration en régime stationnaire d'un réacteur sont présentées ; ces formulations sont des problèmes à valeur propre et sont appelées modes ω, α et k. Les formulations en régime stationnaire de l'équation de Boltzmann sont introduites en raison de leur intérêt pour les applications les plus fréquentes et pour fournir une première référence des tâches à effectuer lors d'une analyse typique de la physique des réacteurs. Pour chacune de ces formulations, nous décrivons brièvement l'hypothèse par laquelle elles sont obtenues et les principaux inconvénients associés à chacune d'entre elles.

Le chapitre se termine par la section 1.3 qui est consacrée au code APOLLO3 qui a été principalement utilisé au cours de ce travail.

Perturbation Theory in Reactor Physics

Le chapitre 2 présente quelques-unes des techniques appartenant à la classe des méthodes de la théorie des perturbations en physique des réacteurs. Comme le précédent, ce chapitre ne prétend pas être exhaustif et il vise à introduire certains des concepts théoriques fondamentaux liés à ces techniques tout en fixant la notation et la terminologie. La dernière partie du chapitre est consacrée à une discussion un peu plus détaillée des développements nécessaires à la mise

en œuvre de ces méthodes et de l'optimisation qui a été faite au cours de cette thèse.

La section 2.1 présente le concept de flux adjoint de manière similaire à ce qui a eté fait pour le flux direct dans le chapitre précédent. Elle aborde ensuite la signification physique de cette quantité, en montrant qu'elle peut être considérée comme l'importance du neutron dans un réacteur critique, c'est-à-dire le niveau relatif de la réaction en chaine stable qu'il permet d'entretenir.

La section 2.2 décrit la théorie dite des perturbations standard grâce à laquelle il est possible de calculer l'effet sur la réactivité d'une petite perturbation du système. L'expression finale reliant le changement de réactivité à la perturbation des opérateurs est obtenue au moyen de techniques variationnelles.

La section 2.3 décrit la théorie dite de la perturbation généralisée qui permet d'étendre la possibilité de calculer l'effet d'une petite perturbation à tout rapport bilinéaire homogène d'ordre zéro. Le formalisme est similaire à celui de la théorie de la perturbation standard mais introduit des nouvelles importances définies par des quantités qui doivent être calculées spécifiquement pour chaque rapport bilinéaire.

La section 2.4 montre comment les techniques mentionnées précédemment peuvent être utilisées pour calculer la sensibilité et l'incertitude liées aux données nucléaires des principales grandeurs d'intérêt dans la physique des réacteurs.

Enfin, la section 2.5 est consacrée à la description de la mise en œuvre de ces méthodes dans la plate-forme neutronique APOLLO3. La description reste générale, mais elle aborde les principales particularités des mises en œuvre effectuées au cours de ce travail. Dans la sous-section relative à la théorie des perturbations standard, on introduit le concept de champ qui est largement utilisé dans APOLLO3 ; il s'agit d'une structure de données qui permet des niveaux multiples et qui est utilisée pour stocker les principales quantités qui sont décrites sur des mailles. Grâce à ces champs, un algorithme est implémenté qui permet de calculer en deux étapes les produits scalaires impliquant un opérateur :

- Dans un premier temps, le produit scalaire entre les flux adjoint et direct est calculé sans integrer sur le variables nécessaires au calcul d'un opérateur spécifique.
- Ensuite, ce champ est utilisé pour calculer la valeur du produit scalaire en introduisant les données relatives à l'opérateur.

Comme trois types d'opérateurs différents apparaissent dans l'équation de Boltzmann, trois champs différents sont définis dans un premier temps. Cette procédure permet d'éviter de traiter plusieurs fois les mêmes données géométriques, car ces opérations sont gourmandes en mémoire et lentes du point de vue du calcul. Un effort important est consacré à l'optimisation du traitement des données géométriques, y compris pendant le calcul des champs, car cela a un impact énorme sur le temps de calcul total. La dernière partie

est consacrée à la mise en œuvre de la théorie des perturbations généralisée. Comme la procédure est similaire à celle de la théorie des perturbations standard, cette sous-section contient quelques commentaires sur le filtrage, une procédure visant à améliorer la stabilité numérique du calcul des importances.

Reduced Order Models in Reactor Kinetics

Ce chapitre présente une discussion des principaux modèles d'ordre réduit disponibles pour étudier la cinétique des réacteurs. Après un examen des principales approches, le chapitre se concentre sur la description des mises en œuvre effectuées au cours de ce travail.

La section 3.1 contient un aperçu des différentes méthodes. Après une brève introduction, la première présentée est la cinétique ponctuelle. La méthode décrit le réacteur comme s'il était ponctuel au moyen d'un ensemble d'équations différentielles ordinaires ; en particulier, si on utilise d pour indiquer le nombre de familles de précurseurs, la cinétique ponctuelle est décrite par un ensemble de $d+1$ équations différentielles ordinaires. Après avoir présenté la description mathématique de la méthode, l'accent est mis sur l'équation de Nordheim. Il est montré dans quelles conditions l'équation de Nordheim peut être obtenue à partir de l'équation cinétique ponctuelle et certaines des interprétations physiques possibles sont discutées juste après. En particulier, un formalisme matriciel est introduit et il est montré comment les valeurs propres de la matrice d'évolution, qui sont les solutions de l'équation de Nordhaim, peuvent être considérées comme les temps de réponse caractéristiques du système. Le comportement de ces valeurs propres est brièvement discuté et l'approximation du saut prompt est abordée à titre d'exemple.

La deuxième classe de méthodes abordées est celle de la cinétique multipoint. Ces méthodes partagent de nombreuses caractéristiques avec la cinétique ponctuelle mais permettent d'ajouter des degrés de liberté dans la description du système. L'idée derrière ces méthodes est que le système peut être divisé en plusieurs régions et que chacune d'entre elles peut être décrite par un point couplé aux autres ; cela se fait en calculant les fonctions d'importance qui sont propres à chaque région et la façon de le faire définit la version spécifique de la cinétique multipoint. Parmi les différentes versions disponibles, la première qui a été discutée est celle proposée par Avery. Dans cette version, nous définissons les importances directes et adjointes qui sont profondément liées au flux direct et adjoint et à la fin, en utilisant n pour le nombre de régions et d pour le nombre de familles de précurseurs, nous obtenons un système de $n(n+d)$ équations différentielles ordinaires. La deuxième version de la cinétique multipoint discutée est celle proposée par Kobayashi qui utilise comme fonction d'importance quelque chose de plus similaire à une fonction de Green et qui conduit à un nombre plus petit d'équations différentielles : $n(1+d)$. Les similitudes et les différences de ces méthodes sont brièvement discutées et la formulation compacte, analogue à celle introduite pour la cinétique ponctuelle, est également introduite pour ces méthodes.

Après ces méthodes, la classe des méthodes dites quasi-statiques est présentée. Une brève présentation des méthodes adiabatiques, quasi-statiques améliorées et quasi-statiques de type correcteur-prédicteur est faite. Enfin, la section se termine par un aperçu des méthodes directes disponibles pour résoudre numériquement l'équation de Boltzmann.

La section 3.2 traite des données qui sont nécessaires pour les calculs cinétiques mais qui ne sont pas utilisées lors des calculs statiques. La raison pour laquelle ces données sont détaillées est que, n'étant pas utilisées pour les calculs statiques, elles ont été mises en œuvre à partir de zéro pendant ce travail. Un bref examen des modèles précurseurs utilisés par les deux principales bibliothèques de données nucléaires et de leurs différences est effectué et les idées fondamentales qui les sous-tendent sont présentées. Le travail se concentre ensuite sur les modèles de précurseurs utilisés par le JEFF, la bibliothèque de données nucléaires européenne, puisqu'il s'agit de celle utilisée par le CEA. En raison des contraintes imposées par le code que nous utilisons (APOLLO3) et des particularités du modèle de précurseurs adopté dans le JEFF, une stratégie de préparation permettant d'utiliser ces données directement dans le calcul du coeur a été mise en place. La première sous-section explique comment cela a été possible pour le spectre de fission retardée, tandis que la deuxième sous-section décrit comment cela a été mis en œuvre pour la fraction de neutrons retardés.

La section 3.3 décrit comment la cinétique ponctuelle a été mise en œuvre dans APOLLO3. Dans ce cas également, la discussion reste générale et seules les idées principales sont abordées. En particulier, l'implémentation est telle que les paramètres cinétiques sont calculés par APOLLO3 et fournis dans un environnement python où ils sont effectivement utilisés pour résoudre le système d'équations différentielles ordinaires au moyen de bibliothèques open source.

La section 3.4 décrit la mise en œuvre de la cinétique multipoint dans APOLLO3. La première sous-section est consacrée à l'implémentation d'Avery. En raison de la nécessité de calculer les importances directes et adjointes et de les utiliser pour calculer plusieurs coefficients, il faut trouver un compromis entre le temps de calcul et l'occupation de la mémoire. Les alternatives sont de calculer toutes les importances une fois et de les stocker toutes ou de stocker seulement une importance directe et une importance adjointe par fois mais de recalculer certaines d'entre elles plusieurs fois. Pour nos applications, la mémoire est considérée comme un goulot d'étranglement plus que le temps de calcul et c'est pourquoi la deuxième solution a été préférée. L'implémentation de Kobayashi, qui n'a qu'une seule sorte d'importance, est, du point de vue algorithmique, simple et n'est pas particulièrement détaillée.

Kinetic Parameters

Ce chapitre présente les résultats obtenus en appliquant la théorie des perturbations pour calculer la sensibilité et l'incertitude de la fraction effective de

	TRIPOLI4	APOLLO3	Δ
K_{eff}	1.036026±4pcm	1.03367	235 pcm
Λ	0.6350±0.0014 μs	0.6140 μs	0.021 μs (3%)
β	371±1.6 pcm	370.2 pcm	0.8 pcm (0,2%)
Time	90366 s	1100 s	

ASTRID BD 16/10 - Paramètres cinétiques

neutrons retardés (bêta effectif) aux données nucléaires de deux configurations. La première est le réacteur rapide à caloporteur sodium ASTRID et la seconde est le cœur EPICURE qui est un réacteur à eau thermique.

ASTRID

La section 4.1 est consacrée au coeur ASTRID. ASTRID est l'acronyme de Advanced Sodium Technological Reactor for Industrial Demonstration et était censé être le premier prototype d'un SFR de 4ème génération en France. La

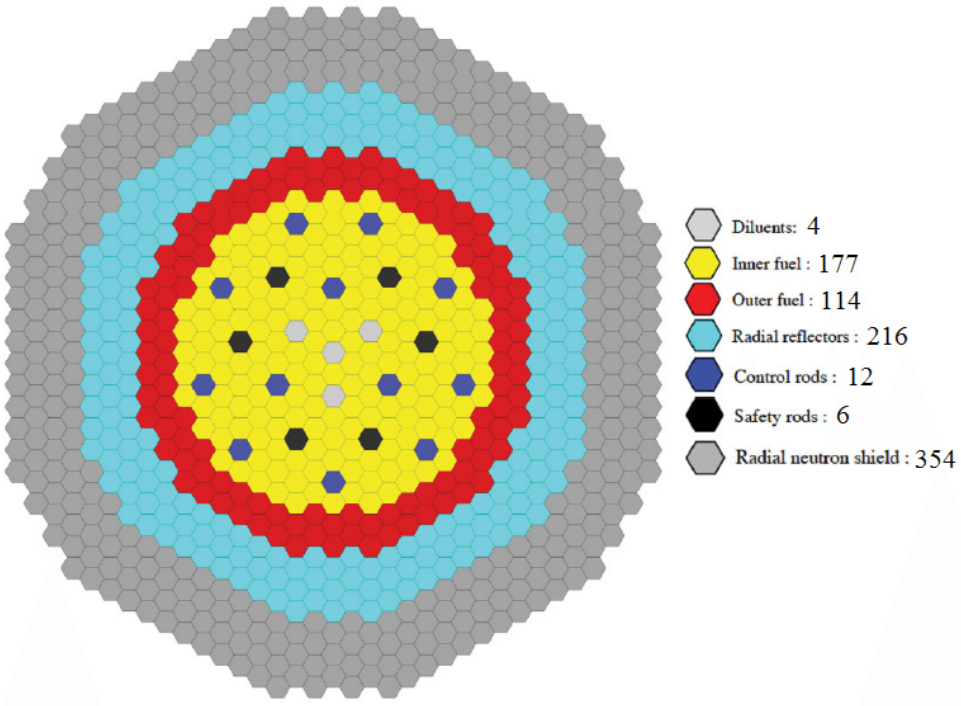

ASTRID CFV V1

première partie est consacrée à la validation d'une partie de la mise en œuvre décrite dans le chapitre précédent. En particulier, le temps moyen de génération des neutrons et la fraction retardée effective sont comparés à ceux calculés à l'aide d'un code de Monte Carlo (TRIPOLI4). Les résultats sont en bon accord et le léger écart dans le temps moyen de génération des neutrons peut s'expliquer grâce à la simplification de la description du coeur et à un biais connu du calcul multigroupe détaillé plus loin dans le chapitre.

Isotope	Capture	Fission	Elastic	Inelastic	NXN	ν_{tot}	ν_d	χ	TOTAL
^{16}O	0.06	-	0.09	0.00	-	-	-	-	0.11
^{23}Na	0.00	-	0.04	0.03	-	-	-	-	0.05
^{50}Cr	0.01	-	0.00	0.00	-	-	-	-	0.01
^{52}Cr	0.00	-	0.00	0.01	-	-	-	-	0.01
^{54}Fe	0.01	-	0.01	0.01	-	-	-	-	0.02
^{56}Fe	0.02	-	0.06	0.09	-	-	-	-	0.12
^{57}Fe	0.00	-	0.00	0.00	-	-	-	-	0.01
^{58}Ni	0.03	-	0.00	0.00	-	-	-	-	0.03
^{235}U	0.00	0.00	-0.00	0.00	0.00	-0.00	0.04	0.00	0.04
^{238}U	0.12	0.48	-0.06	-0.09	0.04	-0.02	**1.50**	0.01	**1.58**
^{238}Pu	0.00	0.01	0.00	0.00	0.00	0.06	0.11	0.09	0.15
^{239}Pu	0.02	0.07	-0.01	-0.02	-0.01	0.06	**1.32**	0.34	**1.36**
^{240}Pu	-0.04	0.32	-0.00	0.02	0.01	0.01	0.23	0.05	0.40
^{241}Pu	0.02	0.04	0.00	0.01	0.00	0.02	0.70	0.22	0.74
^{242}Pu	0.01	0.00	0.00	0.01	0.00	0.01	0.20	0.02	0.21
^{241}Am	0.00	0.00	-0.00	0.00	0.00	0.01	0.01	0.00	0.01
TOTAL	0.13	0.59	0.11	0.03	0.04	0.08	**2.14**	0.42	**2.27**

Propagation de l'incertitude (en %) du bêta effectif pour le coeur ASTRID CFV V1. Les valeurs négatives représentent des valeurs imaginaires, c'est-à-dire des contributions négatives à la variance globale.

Les résultats relatifs au coeur ASTRID sont présentés à l'aide d'un diagramme circulaire (qui n'est pas reproduit dans ce résumé) et de deux tableaux. Le diagramme circulaire montre la contribution relative à la fraction retardée effective des principaux isotopes. La contribution dominante provient du ^{238}U, en raison de son bêta important, suivi du ^{239}Pu qui est le principal isotope de fission puis des autres isotopes du Pu. Les résultats relatifs à la sensibilité de la fraction nucléaire retardée effective sont présentés dans le premier tableau qui n'est pas reproduit dans ce résumé ; ils montrent qu'elle est principalement sensible aux contributions directes (Fission , ν_d , ν_{tot} , χ) et que les effets indirects sont au plus d'un ordre de grandeur plus faibles. Le deuxième tableau, que l'on peut également voir dans ce résumé, contient les résultats relatifs à la propagation au beta effectif de l'incertitude due aux données nucléaires. Il montre comment les contributions directes sont la principale source d'incertitude et en particulier le nombre de neutrons retardés par fission qui, parmi les contributeurs directs, est celui qui présente la plus grande incertitude dans les bibliothèques de données nucléaires.

EPICURE

Le second système analysé est un coeur du programme expérimental EPICURE UM17x17 qui fut étudié dans l'installation EOLE du CEA Cadarache. Ce système possède un spectre thermique et a été utilisé pour valider les mises en œuvre effectuées au cours de cette thèse. Les résultats ont permis de montrer comment l'approximation multigroupe, lorsqu'elle est utilisée avec peu de groupes d'énergie, est la source d'erreur dominante pour ce qui concerne le

	TRIPOLI4	IDT	MINARET 26G	MINARET 281G
K_{eff}	1.048557±2.2pcm	1.04678	1.04712	1.04655
Λ	18.62487±0.003 μs	-	17.73 μs	18.36
β	648.6 ± 0.8 pcm	-	647.1 pcm	648.7 pcm

EPICURE - Paramètres cinétiques

Isotope	Capture	Elastic	Inelastic	NXN	Fission	ν_{tot}	ν_d	χ	TOTAL
^{1}H	0.04	0.14	0.00	0.00	-	-	-	-	0.15
^{16}O	0.05	0.08	0.00	0.00	-	-	-	-	0.10
^{90}Zr	0.00	0.01	0.02	0.00	-	-	-	-	0.02
^{91}Zr	0.00	0.00	0.01	0.00	-	-	-	-	0.01
^{92}Zr	0.00	0.01	0.01	0.00	-	-	-	-	0.01
^{94}Zr	0.00	0.01	0.01	0.00	-	-	-	-	0.01
^{235}U	0.04	0.00	0.00	0.00	0.04	-0.07	**2.23**	0.11	**2.23**
^{238}U	0.01	0.00	0.15	0.04	0.02	0.04	0.57	0.04	0.60
^{239}Pu	0.10	0.00	0.00	0.00	0.13	-0.04	0.50	0.16	0.55
^{240}Pu	0.07	0.00	0.00	0.00	0.02	0.00	0.00	0.00	0.08
^{241}Pu	0.02	0.00	0.00	0.00	0.01	0.03	0.17	0.10	0.20
^{242}Pu	0.06	0.00	0.00	0.00	0.00	0.00	0.00	0.00	0.06
^{241}Am	0.03	0.00	0.00	0.00	0.00	0.00	0.00	0.00	0.03
TOTAL	0.16	0.16	0.16	0.04	0.14	-0.06	**2.36**	0.22	**2.39**

Propagation de l'incertitude (en %) du bêta effectif pour l'expérience EPICURE UM17x17. Les valeurs négatives représentent des valeurs imaginaires, c'est-à-dire des contributions négatives à la variance globale.

temps moyen de génération des neutrons.

En ce qui concerne la fraction effective de neutrons retardés, la principale contribution provient de le ^{235}U, suivi de le ^{238}U, puis des isotopes du Pu. Les résultats sur les sensibilités et les incertitudes sont similaires à ceux du cas précédent, compte tenu de la contribution différente des divers isotopes à la fission : le bêta effective est principalement sensible aux contributions directes ; parmi les diverses contributions directes, le nombre de neutrons retardés par fission est la principale source d'incertitude.

Transient Analysis

Dans ce chapitre, trois types des transitoires sont examinés à l'aide des techniques présentées dans le chapitre 3.

ASTRID

Le premier transitoire est une éjection instantanée d'une barre de commande située dans le coeur ASTRID. Le coeur est simulé en utilisant la cinétique ponctuelle puis la cinétique multipoint avec trois régions symétriques. Les résultats montrent un bon accord pour ce qui concerne l'évolution de la popula-

tion totale de neutrons entre la cinétique ponctuelle et la cinétique multipoint, tant dans le formalisme d'Avery que dans celui de Kobayashi.

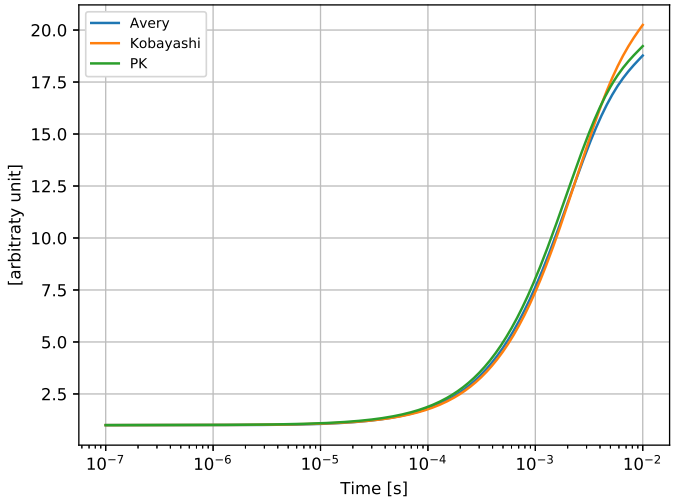

Transitoire ASTRID - évolution de la population totale de neutrons

Les résultats montrent également que la redistribution de la population de neutrons entre les trois régions a lieu avant le saut prompt, ce qui est confirmé par l'analyse des valeurs propres de la matrice d'évolution : deux d'entre elles correspondent à des transitoires plus rapides que celui du saut prompt, correspondant à des changements de populations relatives entre les régions.

Coupled Fast-Thermal reactor

Le second système analysé est un réacteur couplé rapide-thermique , modélisé avec une géométrie 1D. Cette configuration comporte 6 régions homogènes différentes, une zone rapide, un absorbeur, un zone de transition, un convertisseur, une région thermique et un réflecteur à eau. Seules la zone rapide, la zone de transition, le convertisseur et la région thermique sont fissiles. Ce système a été choisi en raison des propriétés cinétiques très différentes de chaque région afin de mettre en évidence les différences entre la cinétique ponctuelle et les cinétiques multipoints.

Les résultats montrent en effet des écarts importants dans la population totale de neutrons entre la cinétique ponctuelle et la cinétique multipoint tout en montrant des différences mineures entre les diverses approches de cinétique multipoint utilisées. Dans ce cas également, la redistribution de la population de neutrons procède le saut prompt mais, dans ce cas, en plus de permettre une évolution des populations relatives par région, elle est associée à un changement dans la population totale de neutrons que la cinétique ponctuelle ne peut pas reproduire.

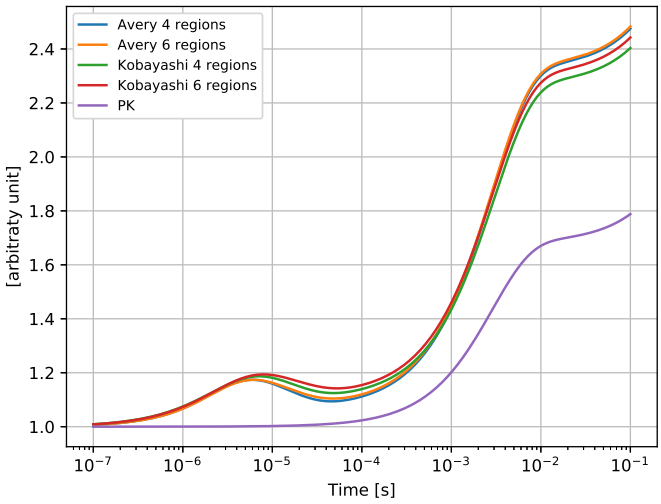

Transitoire 1D - évolution de la population totale de neutrons

MUSE

Le dernier cas analysé est un transitoire de l'expérience MUSE-4 menée dans l'installation nucléaire MASURCA du CEA Cadarache. L'objectif de l'expérience était de simuler un réacteur ADS en utilisant une source externe de neutrons couplée à un cœur sous-critique rapide.

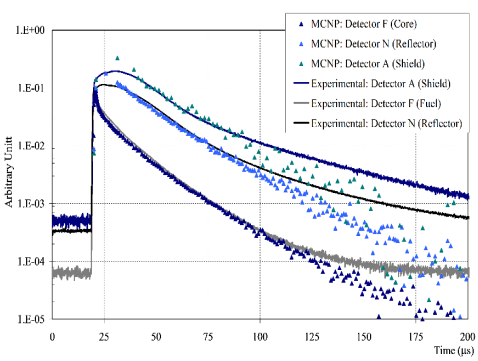

données originales de l'expérience

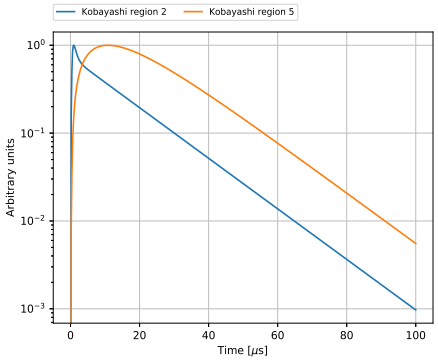

données obtenues par ce travail

Transitoire MUSE - Comparaison entre les données expérimentales et les données calculées par ce travail (légende : région 2 = coeur, région 5 = réflecteur).

Les résultats obtenus montrent que si la cinétique ponctuelle est incapable de capter les effets rapides, la cinétique multipoint est capable de reproduire à la fois le pic dans la région centrale et le retard du détecteur dans le réflecteur, ce qui donne des résultats qualitatifs similaires à ceux qui ont été mesurés. Les divergences restantes s'expliquent par le fait que l'historique complet du système n'est pas modélisé, ce qui peut conduire à une mauvaise description

de la population de précurseurs existante : en effet , expérimentalement on réalise de longues séquences de pulses avec une fréquence de l'ordre du kHz , pendant des durées totales de l'ordre de l'heure : les précurseurs peuvent se mettre à l'équilibre ; alors que les calculs modélisent un pulse isolé dans un système vide de neutrons et précurseurs .

Conclusion

Ces travaux ont permis de mieux délimiter les capacités des principaux modèles d'ordre réduit disponibles en matière de cinétique des réacteurs.

Les analyses sur le bêta effectif (ou la fraction effective de neutrons retardés) montrent que ce paramètre est principalement sensible aux contributions directes.

En ce qui concerne les différences entre la cinétique ponctuelle et la cinétique multipoint pour le cas où les propriétés cinétiques sont homogènes, les deux techniques de modélisation fournissent des résultats similaires pour la population neutronique totale mais pour les autres cas analysés, des différences importantes apparaissent entre les deux. En outre, l'analyse des valeurs propres de la matrice d'évolution montre que les effets sur la redistribution des populations de neutrons ont lieu avant le saut prompt.

En perspective de ce travail, il y a l'application de la théorie des perturbations généralisée à d'autres paramètres cinétiques, en particulier au temps moyen de génération des neutrons.

En ce qui concerne la cinétique multipoint, il est intéressant de développer rigoureusement le formalisme afin d'inclure une source de neutrons dans l'équation et de comparer les résultats avec des calculs plus précis, comme la cinétique directe ou les simulations de Monte Carlo, et de reconstruire l'historique d'irradiation du cas MUSE pour une comparaison réelle des données simulées avec les données expérimentales.

Remerciements

Although I was willing to take more time to write these lines, the recent events changed my perspective and the nature of this moment. From being a goal I imagined to celebrate with all of you, it turned out to be the end of a chapter that we will share in a much less tangible way. This moment, that represents the end of my formal education, it is actually a milestone in the path of my development as a person, a development to which each of you had a significant role. Even though you will not be here to prove it in person, I owe this achievement to you and I really struggle to find appropriate words to express my gratitude.

Having always preferred to cultivate my relationships one to one, I do not find any appropriate way to categorize you into groups to fulfill the acknowledgments task within one page; a solution that however, since the contribution that each of you had to my development has been unique, I would have found largely unsatisfactory. So I will not try and instead I will address the few words which follow to those that directly contributed to this PhD.

First of all, I want to thank all the members of the jury, since you have shown an extremely constructive attitude and, despite the world pandemic, the related discomfort, the uncertainty, and the setbacks, you kept encouraging me, helping with the organization and improving the work from a scientific point of view. I really appreciated it.

I want to particularly thank Jean and Piero, you are, although in a different way, two extremely inspiring models, both from the professional and the human point of view. The scrupulousness, the passion, the easiness, the humility, the competence, and the dedication I see in you are something I deeply admire.

Most of the merit of this achievement, however, goes to my family, not only for their everyday support, that however has been almost unconditional and more than generous, but also for the more important role that you had in my development. Papà, you taught me the importance of effort and perseverance. Mamma, you taught me the importance of equilibrium and motivation. Francesca, you taught me the importance of empathy and communication. Not only by spoken words but with an everyday example. I had the biggest of the luck of living with three different but great persons, from which I had and I have the privilege of learning each day, those and other lessons.

I also want to thank all my colleagues, old or new, at the same level or at high-ranking, that I had the honor of meeting during this PhD, and that now I have the honor of joining for an hopefully much longer and fruitful period to come, as permanent staff. The easiness and competence you have shown in the challenges we met build a work and human environment I did not think was possible. Among these colleagues, I want to explicitly thank Pascal, you acted as a ghost supervisor and as a friend, motivating and helping me to overcame several blocking point in a way no one else could have done.

Even though some of them can be seen as colleagues, I want to thank a group

of actual and ex PhD and students I met, not only for your human contribution, but for the extremely powerful team you proved to be. No work is done alone, and beyond the expected contributions of supervisors, that however has been far above the due, this army of friend helped me in solving problems, organizing, perfecting talks, proofreading and formatting. Their contribution has been fundamental in the conclusion of this work, and if any merit will come from it, I definitely have to share it with them.

Finally I want to thank Valeria, probably the last person I met and with whom I built a close human relationship, but who came in my life as naturally as if you have always been here. Aside from the huge contribution to my personal growth and to the one which came as part of the PhD team, during the last period, you never made me feel the discomfort of the lockdown, you kept motivating and supporting me, you inspired me with your diligence, you helped me to loosen the stress and you took care of all the organization that was possible to delegate to another person. For these and other reasons, I love you.

Contents

List of Figures

List of Tables

Liste des abréviations

BD	Basic Design
CEA	Commissariat à l'énergie atomique et aux énergies alternatives
CFV	Coeur à Faible reactivite de Vidange
ENDF	Evaluated Nuclear Data File
GPT	Generalized perturbation theory
IQM	Improved Quasi Static
JEFF	Joint Evaluated Fission and Fusion Nuclear Data Library
l.h.s.	left hand side
MPK	Multipoint Kinetics
PCQM	Predictor Corrector Quasi Static
PK	Point Kinetics
PWR	Pressurized Water Reactor
r.h.s.	right hand side
SFR	Sodium Fast Reactor
SPT	Standard perturbation theory

Chapter 1

Introduction

Contents

This chapter aims at introducing the reader to the topic of this thesis, fixing the notation, clarifying the reasons that motivated this work and presenting the basic mathematical and computational tools that have been used. The contents in this chapter, far from being exhaustive, condense the main concepts about computational reactor physics needed to read this thesis; this is done in a few pages but it can not substitute a prior knowledge of the topic. Good references to use as supplement for this section are [1, 2] for the foundations and [3, 4] with a focus on the algorithmic part. Section 1.1 describes the Boltzmann equation that is the reference mathematical model in reactor physics. Section 1.2 describes a way to proceed in order to solve a typical problem in reactor physics and provides a justification of this thesis. Section 1.3 describes the computer code used during this work.

1.1 The Boltzmann Equation

One of the aims of reactor physics is the study of the neutron flux (ϕ) in a nuclear reactor. The neutron flux is a scalar quantity and represents the total length traveled by all the neutrons per unit volume and unit time in a given direction. It is expressed as the product of the neutron density in the phase space (n) and the speed (v)

$$\phi(\hat{\Omega}, E, \vec{r}, t) = n(\hat{\Omega}, E, \vec{r}, t)v(E) \quad , \tag{1.1}$$

where variables describing the phase space are the energy (E), the direction versor ($\hat{\Omega}$) and the position in space ($\vec{r}$) and the flux and the neutron density can be function of time (t).

Neutrons in a reactor can interact with the nuclei they encounter and the probability of this to happen is measured by cross-sections. Cross-sections, that have units of a surface, depends from the nucleus, the type of reaction, the energy of the incoming particle and, although being different from the geometrical cross-section, can be regarded has the surface seen by the neutrons. It is common practice to distinguish between microscopic cross-section (σ $[m^2]$), that is a property of each nucleus, and macroscopic cross-section (Σ $[m^{-1}]$), that can be regarded as the total cross-section by unit volume seen by neutrons and that can be obtained by the microscopic one by multiplying it for the nuclei density. Keeping this analogy, the number of neutrons undergoing a given reaction, in a given time interval, can be obtained as the product of the flux and the macroscopic cross section (Σ).

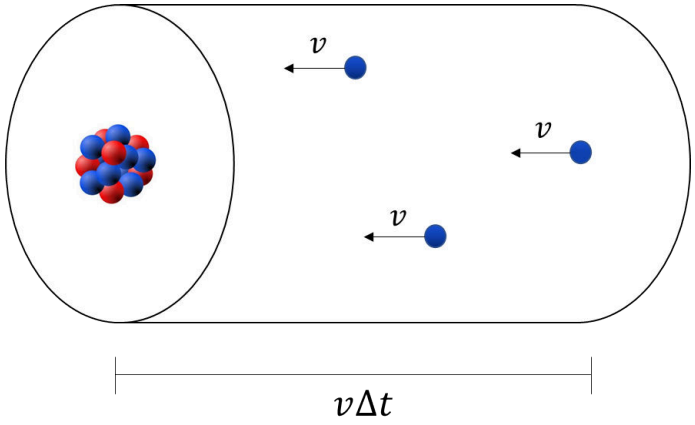

Figure 1.1 – Visual representation of a cross-section

Neutrons can interact in different ways with atoms. It is common practice to group those reactions in three groups:

- Capture, that is when the neutron is captured by the atom.
- Scattering, that is when the neutron is removed from its position in the phase space and remitted in a new one.
- Fission that is when an atom absorb a neutron, breaks apart, and emits several neutrons.

All these reactions make the neutron disappear from its original point in the phase-space, the sum of their cross-sections is therefore called total cross-section. The total rates of neutrons disappearing from a point in the phase space can simply be obtained by multiplying the flux by the total cross section (Σ_t). For further convenience this can be expressed in compact operator notation as follows:

$$\mathcal{T}\phi = \Sigma_t(E, \vec{r}, t)\phi(\hat{\Omega}, E, \vec{r}, t) \quad , \tag{1.2}$$

where the dependence of the various terms on the variables of the phase space is explicitly noted in the right hand side (r.h.s.). In Eq. 1.2 it has been assumed that the cross section does not dependent on the incoming direction $\hat{\Omega}$. Since in a typical reactor all materials are either amorphous or polycrystalline with very small crystals that have different orientations this is usually a good approximation; however, for very specific cases (e.g. where there is a crystal lattice that exhibits preferential directions) this assumption can be relaxed.

The new neutrons generated by fission can be obtained by means of the fission cross-section, the production operator can be defined as follows:

$$\mathcal{F}\phi = \int_{\infty} dE' \, \frac{\chi(E \leftarrow E', \vec{r}, t)}{4\pi} \oint_{4\pi} d\hat{\Omega}' \, \nu\Sigma_f(E', \vec{r}, t)\phi(\hat{\Omega}', E', \vec{r}, t) \quad , \tag{1.3}$$

where χ is the fission spectrum, Σ_f is the macroscopic fission cross section and $\nu(E, \vec{r}, t)$ is the average number of neutrons per fission. Here not only the cross-section seen by the incoming neutrons but also the neutrons produced are considered to be emitted isotropically. To be precise not only the cross-section but also ν and χ depend on the fissile isotope, therefore, rigorously, the new neutrons produced should be computed specifically for each fissile isotope, adding the individual reaction rates and outgoing neutrons.

Most of the neutrons produced by fission are emitted almost instantaneously, these neutrons are called prompt; a small fraction of them, instead, is emitted by decay of some fission products and therefore those neutrons are called delayed neutrons. These delayed neutron are usually grouped in precursors families according to similar decay times (more details are provided in section 3.2).

When dealing with the fission operator the convention adopted in this manuscript is that $\mathcal{F}$ without subscript refers to the total fission operator, meaning the operator taking into account both prompt and delayed neutrons, with subscript p to the prompt one, with subscript di to the $i-th$ delayed family and with subscript d to the total delayed operator; this translates in Eq. 1.3 by replacing the total neutron yields per fission (ν) and spectrum (χ) with the prompt ones (ν_p and χ_p), with the delayed ones (ν_d and χ_d) or with the ones of $i-th$ family ones (ν_i and χ_i).

Finally, the scattering operator ($\mathcal{S}$), representing the neutrons appearing in point in phase space $(\hat{\Omega}, E, \vec{r})$ can be expressed as follows:

$$\mathcal{S}\phi = \int_{\infty} dE' \oint_{4\pi} d\hat{\Omega}' \, \Sigma_s(\hat{\Omega} \cdot \hat{\Omega}', E \leftarrow E', \vec{r}, t) \, \phi(\hat{\Omega}', E', \vec{r}, t) \quad , \tag{1.4}$$

where Σ_s is the macroscopic scattering cross-section for neutrons with energy E' to be scattered to energy E and to be deflected by an angle whose cosine is $\mu = \hat{\Omega} \cdot \hat{\Omega}'$. This term, concerning its dependence on the angular part, is usually developed in Legendre polynomials (P^l) as follows:

$$\Sigma_s(\mu, E \leftarrow E', \vec{r}, t) = \sum_{l=0}^{\infty} \frac{2l+1}{4\pi} \Sigma_s^l(E \leftarrow E', \vec{r}, t) P^l(\mu) \quad , \tag{1.5}$$

where Σ_s^l is the scattering cross-section of order l. This formulation has convenient numerical properties when combined with the harmonics of the flux. Flux harmonics (or moments) of order l, m are the projections of the flux on the spherical harmonics ($Y^{l,m}$):

$$\Phi^{l,m}(E, \vec{r}, t) = \oint_{4\pi} d\hat{\Omega} Y^{l,m}(\hat{\Omega}) \phi(\hat{\Omega}, E, \vec{r}, t) \tag{1.6}$$

extensive discussion of those can be found in the following references [3, 4].

On top of those interactions, neutrons naturally stream from one point to another due to their motion. The term describing this phenomena can be obtained considering an infinitesimal volume around the point $\vec{r}$. The difference

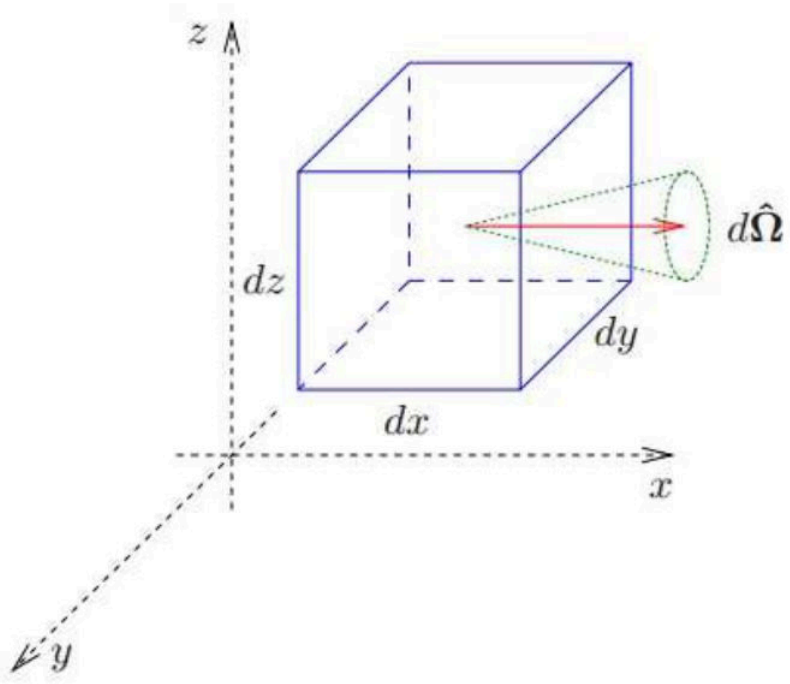

Figure 1.2 – Infinitesimal volume around a traveling neutron

between the neutrons entering in the volume from one face and the ones leaving the volume from the opposite one can be computed as the difference of the neutron flux on two faces multiplied for their surface. Dividing for the volume of the cube and taking the limit to zero we obtain:

$$\lim_{h \to 0} \frac{\phi(\hat{\Omega}, E, \vec{r} + h\hat{\Omega}, t) - \phi(\hat{\Omega}, E, \vec{r}, t)}{h} = \hat{\Omega} \cdot \nabla \phi \tag{1.7}$$

where the r.h.s. is usually referred as the streaming term.

The scattering and the total term are usually grouped together with the streaming term in the net neutron loss operator:

$$\mathcal{A}\phi = \left[\hat{\Omega} \cdot \nabla + \mathcal{T} - \mathcal{S}\right] \phi \quad . \tag{1.8}$$

All these operators can be combined together in a balance equation to describe the neutron flux in a nuclear reactor; the result is the Boltzmann equation:

$$\begin{cases} \frac{1}{v}\frac{\partial \phi}{\partial t} + \mathcal{A}\phi = \mathcal{F}_p\phi + \sum_i \frac{\chi_i}{4\pi}\lambda_i C_i \\ \frac{\chi_i}{4\pi}\frac{dC_i}{dt} = \mathcal{F}_{di}\phi - \lambda_i \frac{\chi_i}{4\pi} C_i \end{cases} , \tag{1.9}$$

where χ_i is the emission spectrum and λ_i the decay constant of the $i-th$ delayed neutron family, $\phi(\hat{\Omega}, E, \vec{r}, t)$ is the time dependent neutron flux and $C_i(\vec{r}, t)$ is the concentration of precursors of the i-th family.

To write this equation several assumptions have been made:

- Continuous medium assumption: neutrons and nuclei are modeled not by point particles but by the notions of neutron and isotope density.
- Neglecting neutron-neutron interaction: in a standard reactor, neutron density is of the order of 10^8 neutron/cm^3 while atom density is of the order of 10^{22} atoms/cm^3, allowing to neglect neutron neutron interaction that would have lead to a non-linear equation.
- Neglecting neutron decay: neutron life time due to β decay is of the order of 15 min while typical neutron life time in a pressurized water reactor (PWR) is of few tens of μs.
- Neutron are not relativistic particles: maximal fission neutron energy is around 20 MeV while neutron mass is around 0.9 GeV.

1.1.1 ω-modes

When interested in the asymptotic behaviour of the reactor, a separable solution of the form:

$$\begin{cases} \phi(\hat{\Omega}, E, \vec{r}, t) = \psi(\hat{\Omega}, E, \vec{r}) e^{\omega t} \\ C_i(\vec{r}, t) = C_i(\vec{r}) e^{\omega t} \end{cases} \tag{1.10}$$

can be substituted in Eq. 1.9. The resulting equation, once the exponential in time has been factored out, is the following:

$$\left[\frac{\omega}{v} + \mathcal{A}\right]\psi = \left[\mathcal{F}_p + \sum_i \frac{\lambda_i}{\lambda_i + \omega}\mathcal{F}_{di}\right]\psi \quad , \tag{1.11}$$

where the term ω/v behaves as a total cross-section. The solutions of Eq. 1.11 are known as ω-modes and represent the possible shapes of the flux in asymptotic cases. Although no rigorous mathematical result exists about the nature of the solutions of this equation [1], some insight about it can be obtained by extrapolating results from similar versions of this equation (i.e. k-modes equation) [5]. In particular there are infinitely many values of ω that are solutions of this equation, they can be complex and the real part can go from minus to plus infinity; however, the solution with the larger real part (ω_0) is expected to be simple, real and the associated eigenvector (ψ_0) is expected to be non negative everywhere. ω_0 is also called the dominant eigenvalue because, when

time tends to infinity, due to the exponential solution, it represents the last remaining mode; therefore ω_0 represents the asymptotic rate of growth and ψ_0 the asymptotic shape. A stable system has $\omega_0 = 0$ and, in this case, it is called critical. When $\omega_0 > 0$ the system is said supercritical otherwise ($\omega_0 < 0$) it is said subcritical.

This equation, however, is rarely employed since it is non linear in ω and imposes to distinguish between prompt and delayed neutrons in the fission operator also during the flux calculation.

1.1.2 α-modes

When reactor is close to equilibrium, Eq. 1.11 can be further simplified by neglecting the time dependence of the precursors concentration and considering them instantaneously at equilibrium with the flux. This is equivalent in considering ω negligible with respect to λ_i. The resulting equation is the following:

$$\left[\frac{\alpha}{v} + \mathcal{A}\right]\psi = \mathcal{F}\psi \quad , \tag{1.12}$$

where at the place of the prompt and delayed fission operator appears the total one. Also in this equation there are infinite solutions, with α that can be complex and with the real part going from minus to plus infinity. As before the dominant one is expected to be real, simple and the associated eigenvector is expected to be non negative everywhere. Clearly, when α assumes values that are very different from zero, the system evolves rapidly and the assumption that precursors are instantaneously at equilibrium with the flux is not a good approximation anymore. Looking at Eq. 1.11 we can notice how, if ω gets very large, the term concerning the delayed neutrons can be neglected and Eq. 1.11 reduce to the α equation where the fission production operator is substituted with the prompt one:

$$\left[\frac{\alpha}{v} + \mathcal{A}\right]\psi = \mathcal{F}_p\psi \quad . \tag{1.13}$$

This equation is a good approximation when the system is prompt critical, that is when only prompt neutrons are sufficient to sustain the chain reaction and the system experiences very fast evolution.

1.1.3 k-modes

The problem with the equations presented so far is that the terms α/v and ω/v can be complex and the dominant eigenvalue can be negative; this, in some situation (e.g. coolant void), can make the whole left hand side (l.h.s). negative, with an impact on the stability of the solving algorithms used to integrate the Boltzmann equation [3]. For this reason, usually, other formulation are preferred. Neglecting completely the time derivative leads to a formulation that does not always guarantee the existence of a solution. To have one, the standard procedure is to introduce an eigenvalue k resulting in the following

equation:

$$\mathcal{A}\psi = \frac{\mathcal{F}}{k}\psi \quad . \tag{1.14}$$

This formulation, known as k-modes (or critical problem), is a linear problem that can have different eigenvalues with $max(\nu) > k_0 > k_1.. > 0$. The dominant one ($k_0$) is proved to exist and to be positive and the associated eigenvector (ψ_0) is non negative everywhere [5]. k_0 is also known as k-effective or multiplication factor since it represents the ratio of the number of neutron in a generation over the number of the previous one. To have a parallelism with the previous formulations a system is stable when k-effective is equal to one, and in this situation (ω and α equal to 0) the three formulations coincide.

Since Eq. 1.14 is a liner eigenvalue problem and the main interest is in its dominant eigenvalue, its discretization can be easily solved by means of a power iteration method [3].

1.2 Deterministic transport

Computing the neutron flux is a demanding task and at present two major approaches are available, a probabilistic one, called the Monte Carlo method, that consists in simulating the evolution of a statistically representative subset of neutrons, and a deterministic one, consisting in integrating directly the Boltzmann equation. While the Monte Carlo method permits to simulate a reactor with very few simplifying hypotheses, it has a very high computational cost and therefore is often used as reference to validate less accurate models. The deterministic approach instead relies on several simplifications, being detailed later in this section, that make it extremely attractive from the computational point of view and therefore has been the main approach used in this work.

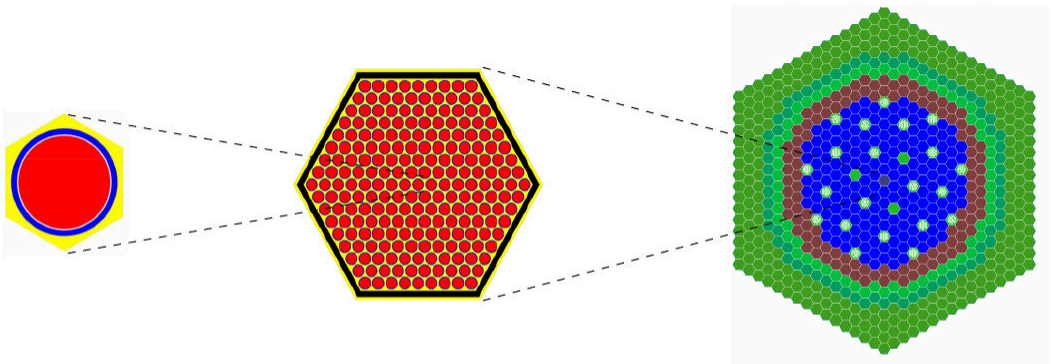

Figure 1.3 – Typical SFR geometries and dimensions

To have an idea of the order of magnitude of the number of unknowns involved

in a typical steady-state problem, the reader can look at Fig. 1.3 showing a standard sodium fast reactor (SFR). To estimate the number of sub-volume needed to properly discretize this kind of reactor, is sufficient to consider that a cell, in its simplest description, is made up by the fuel, a gap between the fuel and the cladding, the cladding, and the coolant; using a sub volume for each of the materials mentioned above will lead to 4 volumes for a single cell. A typical fast reactor has around 250 fuel pins per sub-assembly and 300 fuel assemblies in the core; considering a reference active height of 2 meters and using 100 planes to catch the axial effects would lead to a total number of $4\times250\times300\times100=3\times\ 10^7$ spatial volumes.

Regarding the energy variable, an example of the energy dependence of the total cross-section of 2 of the main isotopes can be seen in Fig. 1.4. As can be

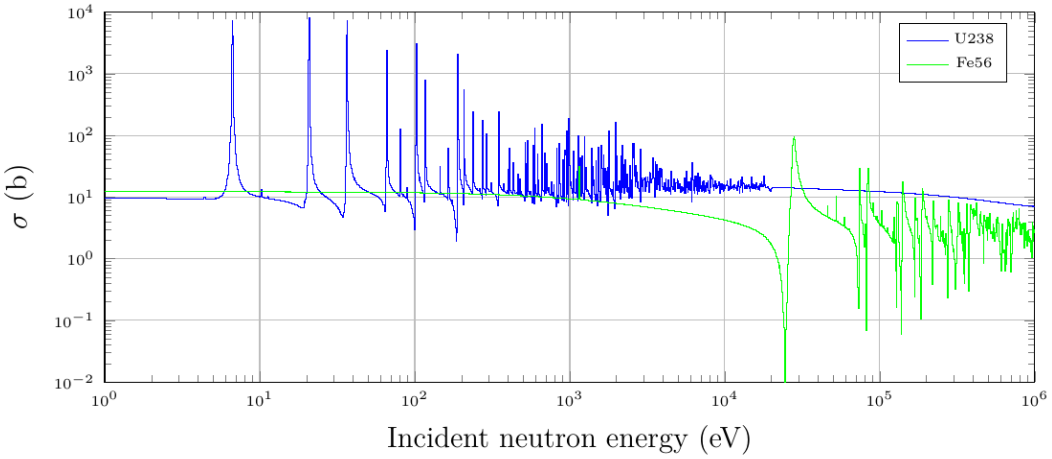

Figure 1.4 – ^{238}U and ^{56}Fe total cross-section

seen the cross-sections have complicated energy dependence with resonances that lead to important changes in total amplitude in very short energy range; this implies that for a proper discretization of the energy variable about 10^5 energy points would be necessary. Assuming to use 100 directions for the remaining angular variable this would lead to 3×10^{14} unknowns. Pretending to model this problem on a computer and using 8 bytes (the dimension of a double) for each of the unknowns will lead to the use of around 2.4 PetaByte of computer memory.

To overcome this problem several simplifications are employed in a classical calculation. For what concerns the energy variable the standard way to handle it in deterministic calculations is through the multi group approximation [3]. Since the most energetic neutrons produced by fission have an energy of about 20 MeV, and, except for very slow neutrons, neutrons only lose energy by scattering, the energy range of interest can be restricted from 0 to 20 MeV; this interval is subdivided in N_g sub-intervals or energy groups and the Boltzmann equation is then integrated over each of them. The usual ordering is such that the first groups are the most energetic ones, meaning: $E_0 > E_1 > E_2... >$

$E_{N_g} > E_{N_{g+1}} = 0$ where E_g is considered the upper bound of each group. Defining the multigroup flux as:

$$\phi^g(\hat{\Omega}, \vec{r}, t) = \int_{E_{g+1}}^{E_g} dE\ \phi(\hat{\Omega}, E, \vec{r}, t) \quad , \quad 0 < g < N_g \tag{1.15}$$

the multigroup cross-section can be obtained by imposing conservation of the reaction rates in this way:

$$\Sigma^g(\hat{\Omega}, \vec{r}, t) = \frac{\int_{E_{g+1}}^{E_g} dE\ \Sigma(E, \vec{r}, t)\phi(\hat{\Omega}, E, \vec{r}, t)}{\phi^g(\hat{\Omega}, \vec{r}, t)} \quad , \quad 0 < g < N_g \quad . \tag{1.16}$$

An important issue with this approach is that, even if the original cross-section is isotropic, the multi group cross-section acquires an angular dependence due to the weighting procedure. Another drawback is that to produce these cross-sections a weight flux, that is the output of the calculation, has to be provided as input. In current applications a representative weight flux, having only the main characteristics of the actual flux, is used to produce initial cross sections with many energy groups (typically 281 for PWR and 1968 for SFR), then a self-shielding procedure is used to account for nuclear resonances, those cross-sections are used to compute a local flux, that is used in turn to condense those cross-sections with a coarse energy group structure (from 33 to 2 groups) that is used for the final core calculation.

All these steps are formalized in the so called calculation schemes that implement several phases of dimension reduction that lead to problems that can be easily handled by modern computers. Together with the energy variable described before, the various steps perform various simplifications on the other variables. The proper definition of a calculation scheme and the identification of its uncertainty is a complicated task and is specific for each type of reactor, some good references are [3, 4, 6]. A detailed description of a calculation scheme is beyond the purpose of this work, therefore discussion will be limited to the description of the main steps that characterize a typical calculation scheme usually employed at CEA:

- Nuclear data pre-processing: Nuclear data are integrated starting from continuous functions of energy to multigroup cross section (typically 281 for PWR or 1968 for SFR), using a reference spectrum. This process can be done with public software (as NJOY [7]) or with internal one. During this process each isotope is considered individually and no other information is needed.
- Self-shielding calculation: this step allows to take into account the effects of resonances on average group cross-sections by performing calculations on very simple geometries. This step is usually done together with the following one, directly by the so called lattice solver of APOLLO3.
- Lattice calculation: this step, by means of a steady-state calculation (k-mode usually 2D), permits to further reduce the energy unknowns and the spatial ones by condensing the cross-section on a coarser energy mesh

(typically from 281 to 2 for PWR or from 1981 to 33 for SFR) and homogenizing the materials.

- Core calculation: this step allows to compute the actual flux in the reactor and the desired quantities on geometries where the materials are homogeneous and with a coarse group structure.

Even with all these procedures, steady-state core calculations have computation times that range from tens of minutes to several hours. The fact that the mean neutron generation lifetime in a fast reactor is smaller than 1 μs explain the challenges behind time dependent calculation. The present work aims to investigate some of the various techniques available to model neutronic transients providing new insight on their application and highlighting their limits.

1.3 APOLLO3

APOLLO3® is a deterministic code under development at CEA to perform neutronic calculation in the context nuclear reactor physics [8]. It is developed in FORTRAN, C++ and Python and it has been designed to unify and replace the existing codes used by CEA, EDF and AREVA. The aim is integrate the functionalities of APOLLO2 and CRONOS2 that are currently used for PWR and of ERANOS that is currently used for SFR; it also includes a generic perturbation module [9] that allows a high level data and fluxes manipulation, that has been the starting point of this work and to which we contributed with more than 4000 code lines. The APOLLO3 code includes several solvers that are divided in lattice and core ones. The main lattice solvers are IDT, based on the short characteristic method [10], and TDT, based on the long characteristic method [11]. On the core side, the main solvers are MINOS, based on SPN or diffusion approximation, MINARET, based on the S_N approximation, and PASTIS, based on the P_N approximation. More details about the solvers or the numerical approximations they implement can be found in [8] and in the references provided therein. The solver mainly used in this work is MINARET, due to its deep integration in the perturbation module [9]. This solver uses discontinuous Galerkin finite elements for the spatial discretization and the discrete ordinate method for the angular dependence [12]. MINARET will also allow to go beyond the diffusion approximation, a simplification that is usually adopted when dealing with core-side calculations.

Chapter 2

Perturbation Theory in Reactor Physics

Contents

The purpose of this chapter is to introduce the reader to perturbation theory in reactor physics and how it can be used to analyse problems that typically occur in this field. As for the previous one, the purpose of this chapter is to serve as a reference for the notation and definitions and can be integrated with the references provided in the various section. Section 2.1 presents the adjoint problem and its physical meaning, then section 2.2 describes the so called standard perturbation theory (SPT) and section 2.3 gives an overview of the so called generalized perturbation theory (GPT). Section 2.4 describes how these methods can be used to quantify the uncertainty related to nuclear data. Finally Section 2.5 briefly describes how these methods have been implemented in the APOLLO3 code during this work.

2.1 The Adjoint Boltzmann Equation

If the time variable is neglected the scalar product between two functions f and g can be defined in the following way:

$$\langle f, g \rangle = \oint_{4\pi} d\hat{\Omega} \int_{\infty} dE \int_{V} d\vec{r}\; f(\hat{\Omega}, E, \vec{r})\; g(\hat{\Omega}, E, \vec{r}) \quad . \tag{2.1}$$

With this definition of the scalar product, the adjoint (denoted with the superscript *) of an operator $\mathcal{B}$ obeys the following relation:

$$\langle f, \mathcal{B}g \rangle = \langle \mathcal{B}^* f, g \rangle \qquad \forall f, g \tag{2.2}$$

The adjoint formulation of the Boltzmann equation has a physical meaning (that it will be shown to be a kind of neutron importance [13]) and that is frequently used in reactor physics. Adjoint operators derived from the ones described in section 1.1 can be defined by multiplying the forward ones for the adjoint flux, integrating over the phase space variables and "deriving" with respect of the forward flux. The operator including the total cross-section (Eq. 1.2) is self-adjoint, meaning that, being a simple multiplication, it is equal to the direct one:

$$\mathcal{T}^* \phi^* = \Sigma_t(E, \vec{r}) \phi^*(\hat{\Omega}, E, \vec{r}) \quad . \tag{2.3}$$

To obtain the adjoint production operator it is sufficient to revert the energies appearing in Eq. 1.3. This lead to the inversion of the $\nu\Sigma_f$ with the χ term:

$$\mathcal{F}^* \phi^* = \nu\Sigma_f(E, \vec{r}, t) \int_\infty dE' \frac{\chi(E' \leftarrow E, \vec{r}, t)}{4\pi} \oint_{4\pi} d\hat{\Omega}' \; \phi^*(\hat{\Omega}', E', \vec{r}) \quad . \tag{2.4}$$

Also the scattering operator can be obtained by reverting the energies in Eq. 1.4:

$$\mathcal{S}^* \phi^* = \int_\infty dE' \oint_{4\pi} d\hat{\Omega}' \; \Sigma_s(\hat{\Omega} \cdot \hat{\Omega}', E' \leftarrow E, \vec{r}) \; \phi^*(\hat{\Omega}', E', \vec{r}) \quad , \tag{2.5}$$

where rigorously also directions have to be reverted; since $\hat{\Omega} \cdot \hat{\Omega}'$ is commutative, their order in Eq. 2.5 is not important.

To define the adjoint of the streaming operator is necessary to specify the boundary conditions of the problem. In reactor physics, usually, the typical analysis focuses on a system that does not interact with the environment; a convenient way to model this condition is consider the reactor surrounded by void. Mathematically, void boundary condition implies that no neutrons enter in the system from the boundary. Using $\hat{n}$ to denote the direction perpendicular to the boundary (Γ) and oriented toward the exterior, the latter condition can be expressed:

$$\phi(\hat{\Omega}, E, \vec{r}, t) = 0 \quad , \qquad \forall \vec{r} \in \Gamma \quad and \quad \hat{n} \cdot \hat{\Omega} < 0 \quad . \tag{2.6}$$

Since the adjoint flux can be interpreted physically as the neutron importance (as will be clarified in the next section), and neutrons can't react with the system anymore once they cross the boundary, the void condition for the adjoint flux is the following:

$$\phi^*(\hat{\Omega}, E, \vec{r}, t) = 0 \quad , \qquad \forall \vec{r} \in \Gamma \quad and \quad \hat{n} \cdot \hat{\Omega} > 0 \quad . \tag{2.7}$$

Due to those boundary conditions the term $\phi^* \phi$ vanish over the whole boundary. Exploiting the following identity:

$$\nabla \cdot \hat{\Omega} \phi^* \phi = \phi^* \hat{\Omega} \cdot \nabla \phi + \phi \; \hat{\Omega} \cdot \nabla \phi^* \quad , \tag{2.8}$$

and considering that once integrated over the whole domain the l.h.s. vanishes (thanks to the divergence theorem), we can conclude that the adjoint streaming operator is simply the opposite of the forward one.

Accordingly to the definitions provided so far the net loss operator defined in Eq. 1.8 become:

$$\mathcal{A}^*\phi^* = \left[-\hat{\Omega}\cdot\nabla + \mathcal{T}^* - \mathcal{S}^*\right]\phi^* \quad . \tag{2.9}$$

As for the forward case the k-mode equation can be written as follows:

$$\mathcal{A}^*\phi^* = \frac{\mathcal{F}^*}{k}\phi^* \quad , \tag{2.10}$$

for which the same discussion as for the forward case can be done. Moreover it can be shown how forward and adjoint fluxes obey orthogonality relations. In order to do so, Eq. 2.10 can be multiplied by ϕ_i (that is $i-th$ harmonics of the forward problem) and subtracted to the forward equation multiplied by ϕ_j^* (that is $j-th$ harmonics of the adjoint problem):

$$\begin{aligned}\left\langle\left(\mathcal{A}^* - \frac{\mathcal{F}^*}{k_j}\right)\phi_j^*, \phi_i\right\rangle - \left\langle\phi_j^*, \left(\mathcal{A} - \frac{\mathcal{F}}{k_i}\right)\phi_i\right\rangle = \\ \left(\frac{1}{k_i} - \frac{1}{k_j}\right)\left\langle\phi_j^*\mathcal{F}\phi_i\right\rangle = 0 \quad .\end{aligned} \tag{2.11}$$

Since the dominant eigenvectors are non negative everywhere [5], Eq. 2.11 implies that $k_i = k_j$ for $i = j$ and $\left\langle\phi_j^*\mathcal{F}\phi_i\right\rangle = 0$ for $i \neq j$.

2.1.1 Physical meaning

To show the physical meaning of the adjoint flux, let's take a critical system and, for simplicity, let's write the time dependent Boltzmann equation with the total production operator, then add a source term:

$$\frac{1}{v}\frac{\partial\phi}{\partial t} + \mathcal{A}\phi = \mathcal{F}\phi + S \quad . \tag{2.12}$$

Consider an initial situation where $\phi(\hat{\Omega}, E, \vec{r}, 0) = 0$ everywhere and the source is of the form $S = \delta(\hat{\Omega} - \hat{\Omega}_0, E - E_0, \vec{r} - \vec{r}_0, t)$ where δ is the Dirac generalised function. This situation is equivalent to a critical system where no neutron exists and a single one, with energy E_0 and direction $\hat{\Omega}_0$ is introduced at position $\vec{r}_0$ at time equal 0. Take the scalar product of the previous equation with the adjoint dominant k-mode and integrate over time, from $t = 0$ to a generic time t; the resulting equation is the following:

$$\left\langle\phi_0^*, \frac{1}{v}\int_0^t \frac{\partial\phi}{\partial t}dt'\right\rangle = \int_0^t \left\langle\phi_0^*, \left(\mathcal{F} - \mathcal{A}\right)\phi\right\rangle dt' + \int_0^t \left\langle\phi_0^*, S\right\rangle dt' \quad . \tag{2.13}$$

The first term, since $\phi(\hat{\Omega}, E, \vec{r}, 0) = 0$, is equal to $\left\langle\phi_0^*(\hat{\Omega}, E, \vec{r}), \frac{1}{v}\phi(\hat{\Omega}, E, \vec{r}, t)\right\rangle$. The second one, due to the fact that the system is critical (therefore

$(\mathcal{F}^* - \mathcal{A}^*)\,\phi^* = 0$), vanishes and the last one, being S a Dirac delta, is simply equal to $\phi_0^*(\hat{\Omega}_0, E_0, \vec{r}_0)$. As time goes to infinity all the higher modes vanish and the only one left is the dominant one, therefore, for $t \to \infty$, $\phi(\hat{\Omega}, E, \vec{r}, t) \to \lambda\psi_0(\hat{\Omega}, E, \vec{r})$ where ψ_0 is the dominant eigenvector and λ is a real number representing the amplitude of the final flux. Substitute $\phi = \lambda\psi_0$ in Eq. 2.13 and solve for lambda:

$$\lambda = \frac{\phi_0^*(\hat{\Omega}_0, E_0, \vec{r}_0)}{\left\langle \phi_0^*, \frac{1}{v}\psi_0 \right\rangle} \quad , \tag{2.14}$$

the results is that the adjoint flux at the phase space point where the neutron is injected into the system is proportional to the final amplitude. This shows why the adjoint flux is usually referred as neutron importance.

2.2 Standard Perturbation Theory

One of the most popular applications of the adjoint flux is its use to compute the effects on reactivity ρ of a small perturbation of the system [13]. Assuming the k-modes formulation, the reactivity of a system can be defined as follows:

$$\rho = \frac{k-1}{k} \tag{2.15}$$

Starting from the k-mode equation (Eq. 1.14) imagine to have a small perturbation; keeping only first order terms, the k-modes equation can be expanded in the following way:

$$d\left[\left(\mathcal{A} - \frac{\mathcal{F}}{k}\right)\phi\right] = \left(d\mathcal{A} - \frac{d\mathcal{F}}{k}\right)\phi + \left(\mathcal{A} - \frac{\mathcal{F}}{k}\right)d\phi + \frac{dk}{k^2}\mathcal{F}\phi = 0 \quad . \tag{2.16}$$

Since dk/k^2 is equal to the differential of the reactivity $d\rho$, this term can be collected and, by multiplying Eq. (2.16) by a weight function $f(\hat{\Omega}, E, \vec{r})$ such as the scalar product $\langle f, \mathcal{F}\phi \rangle$ is non-zero, the explicit expression for a reactivity variation can be obtained as follows:

$$d\rho = -\frac{\left\langle f, \left(d\mathcal{A} - \frac{d\mathcal{F}}{k}\right)\phi \right\rangle + \left\langle f, \left(\mathcal{A} - \frac{\mathcal{F}}{k}\right)d\phi \right\rangle}{\langle f, \mathcal{F}\phi \rangle} \tag{2.17}$$

By using the adjoint flux as the weight function, the second term in Eq. 2.17 vanishes and the equation reduces to the compact form usually employed to compute sensitivities.

$$d\rho = -\frac{\left\langle \phi^*, \left(d\mathcal{A} - \frac{d\mathcal{F}}{k}\right)\phi \right\rangle}{\langle \phi^*, \mathcal{F}\phi \rangle} \tag{2.18}$$

Notice that for no matter which perturbation, as long it is small, it is sufficient to compute the reference forward and adjoint flux to obtain its impact on the reactivity.

2.3 Generalized Perturbation Theory

The previous formulation allows to compute the sensitivity of the reactivity to the parameters used to compute the flux. That formalism can be extended [14] and applied to any bilinear ratio R homogeneous of order zero that means that the following relation holds:

$$R(\Sigma, a\phi^*, b\phi) = R(\Sigma, \phi^*, \phi) \qquad \forall a, b \qquad , \tag{2.19}$$

where ϕ and ϕ^* are the forward and adjoint flux and Σ represents the set of parameters used to compute those fluxes. To focus on critical systems two fixed Lagrange multipliers, ψ^* and ψ can be introduced to impose the constraints of Eq. 1.14 and 2.10. Then a functional $\mathcal{L}$ can be defined the in following way:

$$\mathcal{L} = R - \left\langle \psi^*, \left(\mathcal{A} - \frac{\mathcal{F}}{k}\right)\phi \right\rangle - \left\langle \left(\mathcal{A}^* - \frac{\mathcal{F}^*}{k}\right)\phi^*, \psi \right\rangle \quad , \tag{2.20}$$

and its variation is equal to:

$$\begin{aligned} d\mathcal{L} = &\left\langle \frac{\partial R}{\partial \Sigma}, d\Sigma \right\rangle + \left\langle \frac{\partial R}{\partial \phi}, d\phi \right\rangle + \left\langle \frac{\partial R}{\partial \phi^*}, d\phi^* \right\rangle \\ &- \left\langle \psi^*, \left(\mathcal{A} - \frac{\mathcal{F}}{k}\right) d\phi \right\rangle - \left\langle \left(\mathcal{A}^* - \frac{\mathcal{F}^*}{k}\right) d\phi^*, \psi \right\rangle \\ &- \left\langle \psi^*, d\left(\mathcal{A} - \frac{\mathcal{F}}{k}\right)\phi \right\rangle - \left\langle d\left(\mathcal{A}^* - \frac{\mathcal{F}^*}{k}\right)\phi^*, \psi \right\rangle \quad , \end{aligned} \tag{2.21}$$

that can be rearranged as follows:

$$\begin{aligned} d\mathcal{L} = &\left\langle \frac{\partial R}{\partial \Sigma}, d\Sigma \right\rangle + \left\langle \frac{\partial R}{\partial \phi} - \left(\mathcal{A}^* - \frac{\mathcal{F}^*}{k}\right)\psi^*, d\phi \right\rangle \\ &+ \left\langle d\phi^*, \frac{\partial R}{\partial \phi^*} - \left(\mathcal{A} - \frac{\mathcal{F}}{k}\right)\psi \right\rangle \\ &- \left\langle \psi^*, d\left(\mathcal{A} - \frac{\mathcal{F}}{k}\right)\phi \right\rangle - \left\langle d\left(\mathcal{A}^* - \frac{\mathcal{F}^*}{k}\right)\phi^*, \psi \right\rangle \quad . \end{aligned} \tag{2.22}$$

In Eq. 2.22 the second and the third term vanish if ψ and ψ^* are chosen such as:

$$\begin{aligned} \left(\mathcal{A} - \frac{\mathcal{F}}{k}\right)\psi &= \frac{\partial R}{\partial \phi^*} \\ \left(\mathcal{A}^* - \frac{\mathcal{F}^*}{k}\right)\psi^* &= \frac{\partial R}{\partial \phi} \end{aligned} \quad . \tag{2.23}$$

Eq. 2.23 admits solution only if $\left\langle \frac{\partial R}{\partial \phi}, \phi \right\rangle = 0$ and $\left\langle \frac{\partial R}{\partial \phi^*}, \phi^* \right\rangle = 0$ but these conditions are automatically satisfied by the condition of R being homogeneous of order zero (Euler's theorem on homogeneous functions). The functions ψ and ψ^* are called forward and adjoint importances and they are not univocally defined by condition 2.23; indeed, for any scalar a and b, we can add $a\phi$ and

$b\phi^*$ respectively, and $\psi + a\phi$ and $\psi^* + b\phi^*$ will still be solution of Eq. 2.23. Thanks to this additional degree of freedom ψ and ψ^* can be selected in such a way that the variation of k in Eq. 2.22 vanish and that translate in imposing the additional condition $\langle \psi^*, \mathcal{F}\phi \rangle = 0$ and $\langle \phi^*, \mathcal{F}\psi \rangle = 0$. To summarize, the sensitivity of any bilinear ratio R homogeneous of order zero can be obtained as follows:

$$\begin{cases} dR = \left\langle \frac{\partial R}{\partial \Sigma}, d\Sigma \right\rangle - \left\langle \psi^*, \left(d\mathcal{A} - \frac{d\mathcal{F}}{k} \right) \phi \right\rangle - \left\langle \left(d\mathcal{A}^* - \frac{d\mathcal{F}^*}{k} \right) \phi^*, \psi \right\rangle \\ \left(\mathcal{A} - \frac{\mathcal{F}}{k} \right) \psi = \frac{\partial R}{\partial \phi^*} \qquad and \qquad \langle \phi^*, \mathcal{F}\psi \rangle = 0 \\ \left(\mathcal{A}^* - \frac{\mathcal{F}^*}{k} \right) \psi^* = \frac{\partial R}{\partial \phi} \qquad and \qquad \langle \psi^*, \mathcal{F}\phi \rangle = 0 \end{cases} \tag{2.24}$$

2.4 Uncertainty quantification

Sensitivities can be used to propagate the uncertainty related to nuclear data to any given quantity whose sensitivity can be computed with the previous methods. To do so, a dispersion matrix has to be used. A dispersion matrix is a positive definite matrix containing variance and covariance data related to the multigroup nuclear data used by the neutronic code. If $\mathbf{D}$ is such a dispersion matrix, the element D_{ij}, where the indices represent a unique combination of reaction r, energy group g and isotope n, is equal to:

- D_{ij} = variance(σ_i) , if $i = j$
- D_{ij} = covariance(σ_i,σ_j), if $i \neq j$

Several dispersion matrices exist but in this study the COMAC-V2.0 matrix has been used [15]. To express the uncertainty in a compact form it is convenient to define the sensitivity vector, that is specific to each given quantity R, and whose element S_i are defined in the following way:

$$S_i(R) = \frac{dR}{R} \Big/ \frac{d\sigma_i}{\sigma_i} \quad . \tag{2.25}$$

Having defined the covariance matrix and sensitivity vector, the uncertanty ϵ associated to a given quantity R can be obtained with the so called sandwich formula that is:

$$\epsilon(R) = \sqrt{S^T(R)\mathbf{D}S(R)} \quad , \tag{2.26}$$

where the superscript T is used to denote the transpose vector.

Application of this technique will be shown in chapter 4.

2.5 Implementation in APOLLO3

At the beginning of this thesis APOLLO3 already had a perturbation module able to perform standard perturbation theory calculations that allow to compute sensitivity vectors for the reactivity. Its implementation, however, was in a preliminary state and its use was limited by an important computation

time needed to compute integrals. This work contributed to the optimization of SPT and to the implementation of GPT that has been done from scratch [9, 16]. Due to the industrial nature of APOLLO3, its structure and the implementations done during this thesis can't be fully detailed; this section, however, describe the main steps made in order to obtain the sensitivity vector and the main ideas behind the implementation that has been done.

2.5.1 SPT

Forward and adjoint fluxes are computed with the MINARET solver. Those fluxes are then stored in the so called fields that are data structures composed by a mesh and data for each element of the mesh [17]. Fields can have several levels so that each data can be a field by itself.

To make an example we describe the typical field associated to an S_N flux:

- The first level is the one associated to the energy mesh, and it has as many elements as the number of energy groups used in the calculation. The data contained in each entry is the field describing the flux for that particular energy group.
- The second level is the direction level and it has as many elements as the direction used to discretize the angular variable (e.g. S_4 calculation has 24 directions). The data contained in each entry is the field associated with the flux value on the spatial mesh for the specific energy group and direction.
- The third level is the spatial level and it has as many elements as the spatial mesh. The data contained in each entry is a float associated to the average flux value.

During the conversion of the flux from the numerical structure used by the solver to the one of the fields several operations are done:

- The finite element flux is integrated over the spatial meshes to obtain its mean value. This is an approximation but allows to reduce the memory occupation.
- Angular flux is projected over the spherical harmonics so to have the moments of the flux. This is the flux that is actually used to compute neutron scattering.
- Two fields, the S_N one and the one projected over the spherical harmonics, are provided as output for each computed field.

Since the Boltzmann equation can be perturbed in one of its three operators:

- Change in the total operator
- Change in the scattering operator
- Change in the production operator

any possible perturbation can be expressed as a linear combination of those three types of perturbation.

A sensitivity vector for a typical SPT calculation can contain up to 100.000 elements, each of which represent a perturbation just described. Therefore, an efficient implementation of these products, is a necessary condition to practical application.

The strategy that has been chosen to achieve this efficient implementation, is to perform those products in two steps:

- At first the adjoint and forward fields are multiplied and integrated on the geometrical variables from which nuclear data are not dependent and the results are stored in a specific field.
- Finally, those fields are combined with the nuclear data to obtain the sensitivity.

Since the variable dependence is peculiar to each operator the first step has to be repeated three times for each specific operator.

Total scalar product

The aim is to compute a scalar product of the following form:

$$\langle \phi^*, d\mathcal{T}\phi \rangle = \oint_{4\pi} d\hat{\Omega} \int_{\infty} dE \int_{V} d\vec{r}\ \phi^*(\hat{\Omega}, E, \vec{r})\ d\Sigma_t(E, \vec{r})\ \phi(\hat{\Omega}, E, \vec{r}) \quad . \tag{2.27}$$

where $d\Sigma_t$ represents a possible variation of the total cross section.

Due to the numerical representation of the fluxes in APOLLO3 this integral can be be computed as follows:

$$\langle \phi^*, d\mathcal{T}\phi \rangle \approx \sum_g \sum_d \sum_s W_s[s] W_d[d] \phi^*[g][d][s] d\Sigma_t[g][s] \phi[g][d][s] \tag{2.28}$$

where s is used to denote the spatial mesh, d the discrete direction and g the energy group; W_s represent the weight associated to each spatial mesh (the volume of the mesh) and W_d the weight associated to each direction (depending on the different quadratures that could be employed). $\phi^*[g][d][s]$ represents the average S_N flux for each spatial mesh and the square parenthesis have been employed to remark the discrete nature of these field with respect of the continuous ones.

Since $\mathcal{T}$ does not depend on d the first step is to compute the scalar products between the adjoint and the forward flux, including all the weights, keeping the dependence on the spatial mesh and the energy groups. Therefore a new field has been defined as follows:

$$\langle \phi^* \phi \rangle [g][s] \approx \langle \phi^*, \delta(g)\delta(s)\phi \rangle \approx \sum_d W_s[s] W_d[d] \phi^*[g][d][s] \phi[g][d][s]. \tag{2.29}$$

Eq. 2.29, although it has the same computational cost of Eq. 2.28, since it access to different memory slots, can be parallelised. This parallelisation

strategy has been implemented during this work using OpenMP [18]. Also a new way of handling the weights, W_s and W_d, has been introduced to reduce cache missing, that is a phenomena that occurs when there are accesses to non continuous memory chunks and that considerably slows down the calculations [19]. Those weight, presenting only one dimension, are rearranged in a memory efficient way before looping over the indices according to the order encountered during the loops.

Once the field in Eq. 2.29 is defined any scalar product involving an operator with the same structure of the total one, can be efficiently computed as follows:

$$\langle \phi^*, d\mathcal{T}\phi \rangle \approx \sum_g \sum_s \langle \phi^* \phi \rangle [g][s] d\Sigma_t[g][s] \tag{2.30}$$

Production scalar product

For the production operator similar considerations can be made. First of all, it can be noted how the production operator depends only on the scalar flux (flux integrated over all the directions). This is an important simplification since it permits to neglect the direction dimension. Using the capital letter to denote the flux moments of order l, m ($\Phi^{l,m}$) and being the scalar flux equal to the moment of order 0,0, the scalar product that has to be computed is of the following form:

$$\left\langle \Phi^{*0,0}, d\mathcal{F}\Phi^{0,0} \right\rangle = \int_V d\vec{r} \int_\infty dE\ \Phi^{*0,0}(E,\vec{r}) \int_\infty dE'\ d\left[\frac{\chi}{4\pi}\ \nu\Sigma_f\right](E,E',\vec{r})\ \Phi^{0,0}(E',\vec{r}) \tag{2.31}$$

where all the nuclear data, and their dependencies, have been grouped together.

Representing the numerical version of the harmonics of the flux as follows:

$$\Phi^{l,m} \approx \Phi[g][l][m][s] \tag{2.32}$$

where, g is used to represent the energy group, l and m the spherical harmonic's order and s the spatial mesh, also the scalar product involving a production operator can be expressed in its numerical representation as follows:

$$\langle \Phi^*, d\mathcal{F}\Phi \rangle \approx \sum_{gp} \sum_g \sum_s W_s[s] \Phi^*[gp][0][0][s] d\left[\frac{\chi}{4\pi}\ \nu\Sigma_f\right][gp][g][s] \Phi[g][0][0][s] \tag{2.33}$$

where, similarly, gp and g are used to denoted the energy group of the adjoint and forward field respectively, s the index of spatial meshes and W_s is used for the weight (volume) of each spatial mesh.

Also here, a new field has been introduced, defined as follows:

$$\langle \Phi^* \Phi \rangle [gp][g][s] \approx \left\langle \Phi^{*0,0}, \delta(gp)\delta(g)\delta(s)\Phi^{0,0} \right\rangle \approx W_s[s] \Phi^*[gp][0][0][s] \Phi[g][0][0][s], \tag{2.34}$$

Also in this case, as opposite with the one step implementation, we could benefits of the parallelization during the computation of this field and of the memory optimization coming from a proper rearrangement of W_s.

The final scalar product can be computed as follows:

$$\langle \Phi^*, d\mathcal{F}\Phi \rangle \approx \sum_{gp} \sum_{g} \sum_{s} d \left[\frac{\chi}{4\pi} \nu\Sigma_f \right] [gp][g][s] \langle \Phi^*\Phi \rangle [gp][g][s] \tag{2.35}$$

Scattering scalar product

For the scattering operator a similar strategy has been adopted. The scalar product that has to be computed is of the following type:

$$\langle \phi^*, d\mathcal{S}\phi \rangle = \int_V d\vec{r} \oint_{4\pi} d\hat{\Omega} \int_\infty dE\ \phi^*(\hat{\Omega}, E, \vec{r}) \int_\infty dE' \oint_{4\pi} d\hat{\Omega}'\ \Sigma_s(\hat{\Omega}\cdot\hat{\Omega}', E \leftarrow E', \vec{r})\ \phi(\hat{\Omega}', E', \vec{r}) \tag{2.36}$$

Using the cross-section developed in Legendre polynomials and the moment of the fluxes, the scattering scalar product can be obtained numerically as follows:

$$\langle \phi^*, d\mathcal{S}\phi \rangle = \sum_{gp} \sum_{g} \sum_{l} \sum_{m} \sum_{s} W_s[s] W_l[l] \Phi^*[gp][l][m][s] d\Sigma_s[gp][g][l][s] \Phi[g][l][m][s] \tag{2.37}$$

where, as before, where, g and gp are used to represent the energy groups, l and m the spherical harmonic's order, s the spatial mesh, W_s the weight (volume) of each spatial mesh, W_l the normalization coefficient of each Legendre order and $\Sigma_s[gp][g][l][s]$ is the discrete version of the scattering cross-section $\Sigma_s^l(E \leftarrow E', \vec{r})$.

The new field introduced in this case is of the following form:

$$\langle \Phi^*\Phi \rangle [gp][g][l][s] \approx \sum_m \left\langle \Phi^{*l,m}, \delta(gp)\delta(g)\delta(l)\delta(s)\Phi^{l,m} \right\rangle \approx \sum_m W_s[s] \Phi^*[gp][l][m][s] \Phi[g][l][m][s] \tag{2.38}$$

Also in this case the calculation of this field has been parallelized and the weights have be rearranged to have an efficient memory access.

The final scalar product can be computed as follows:

$$\langle \phi^*, d\mathcal{S}\phi \rangle = \sum_{gp} \sum_{g} \sum_{l} \sum_{m} \sum_{s} d\Sigma_s[gp][g][l][s] \langle \Phi^*\Phi \rangle [gp][g][l][s] \tag{2.39}$$

Results

To provide the orders of magnitude of the resource requirements for the quantities described in this sections we present the typical resource required for the main steps described so far. The test case is a full core calculation of a fast neutron reactor with 33 energy groups, 36 directions, using approximately 300.000 spatial meshes and finite elements of the first order. The calculation is performed using 24 processors and the sensitivity vector has about 5000 elements.

The results are shown in Table 2.1 where in the column "Before" and "After" are presented the characteristic memory occupation and computation time of the different tasks described so far, before and after the developments done during this work: the operations listed in the first four lines have not been affected by those developments but are reported to provide the order of magnitude of the whole calculation.

Table 2.1 – Memory occupation and computation type of the main task in a SPT calculation

	Before		After	
	Memory	Time	Memory	Time
Forward Flux calculation	16 GB	2 h	16 GB	2 h
Adjoint Flux calculation	16 GB	2 h	16 GB	2 h
Forward Field creation	4 GB	10 s	4 GB	10 s
Adjoint Field creation	4 GB	10 s	4 GB	10 s
Total scalar prod.	<1 GB	20 s	<1 GB	1 s
Production scalar prod.	<1 GB	700 s	<1 GB	2 s
Scattering scalar prod.	<1 GB	1500 s	<1 GB	2 s
Sensitivity calculation	<1 GB	1800 s	<1 GB	5 s

2.5.2 GPT

GPT, to compute sensitivity vectors to quantities different from reactivity, has been implemented in APOLLO3 during this work. As mentioned in section 2.3 to perform a GPT calculation it is necessary to compute forward and adjoint importances and select a specific solution. Importances are obtained through source calculations where the production operator has been divided by the k-effective obtained during the flux calculation. Sources are $\frac{\partial R}{\partial \phi}$ and $\frac{\partial R}{\partial \phi^*}$ and are computed automatically by the perturbation module according to the quantity of interest that has been provided as input. At present the possible quantities of interest that can be analysed are:

- Any linear ratio of capture reaction rates
- Any linear ratio of fission reaction rates
- A bilinear ratio representing the effective delayed neutron fraction (that will be described in the next chapter)

The main issue preventing the analysis of other bilinear quantities it that, for many of them, the terms $\frac{\partial R}{\partial \phi}$ and $\frac{\partial R}{\partial \phi^*}$ can be anisotropic and currently our solvers are not able to handle those kinds of problems.

Concerning the selection of the specific solution, although it can be done at the end of the calculation, to ensure stability, the conditions $\langle \psi^*, \mathcal{F}\phi \rangle = 0$ and $\langle \phi^*, \mathcal{F}\psi \rangle = 0$ are imposed in each outer iteration. This process is known as filtering. MINARET, that already had this feature for the adjoint calculation, has been modified to allow for this possibility for the forward one. Once the importances have been obtained, the scalar products described in the previous section, are computed between the forward flux and the adjoint importance and between the adjoint flux and the direct importance. This lead to a doubling of the scalar products that have to be computed and of their memory requirements. Being those relatively cheep to compute, both in terms of memory and time (Tab. 2.1), the most expensive operations are the calculation of the additional importances. Importances can be obtained approximately at the

same cost of the normal fluxes, leading to GPT calculations that are, overall, almost twice as memory and time demanding as SPT calculations.

Thanks to these tools, it is possible to accurately analyze several parameters and in particular, those that are relevant for the kinetic behavior of a nuclear reactor, that will be presented in the following chapter.

Chapter 3

Reduced Order Models in Reactor Kinetics

Contents

This chapter presents a discussion of the main simplified models (usually called reduced order models) that can be applied to the study of reactor kinetics with a focus on the ones adopted in this work and their implementation in the code at our disposal. Section 3.1 makes a brief overview of the main simplified methods available in reactor kinetics. Section 3.2 focuses on nuclear data that are related with the kinetic behavior of the reactor and on their implementation in APOLLO3. Sections 3.3 and 3.4 describe briefly the implementation of the two methods adopted for the studies conducted during this work.

3.1 Overview of Reactor Kinetics Methods

In section 1.2 we estimated with an example the order of magnitude of the computational cost of a typical calculation with brute force discretization. Even

with all the techniques described in the same section, a steady state calculation takes between tens of minutes to a few hours. Adding another dimension as the time variable without any particular simplification is therefore non-affordable with the present computational capabilities.

Most of the methods employed to overcome this problem rely on a flux factorization that has been proposed by Henry [20]:

$$\begin{cases} \phi(\hat{\Omega}, E, \vec{r}, t) = \psi(\hat{\Omega}, E, \vec{r}, t)T(t) \\ \left\langle \phi^* \frac{1}{v} \psi \right\rangle = c \end{cases} \tag{3.1}$$

where ψ is known as the shape function and T is known as the amplitude. The idea behind this factorization is that the shape function (ψ) and the scalar amplitude (T) evolve on different time scales. Thanks to this, being the shape the most expensive part to obtain, decoupling the different time scales allows to compute with different frequencies the two quantities leading to potentially good results with much smaller computation time. This factorization, to be uniquely defined, needs a normalization condition that usually is done using the adjoint flux. The reason is that using the normalization condition in Eq. 3.1 implies that the amplitude is governed by the point kinetic equations that will be discussed in the following section.

3.1.1 Point Kinetics

The point kinetics (PK) equations were proposed initially by Fermi by means of physical considerations [21] but can be obtained rigorously introducing the factorization of the flux in Eq. 3.1, multiplying the time dependent Boltzmann equation by a weight function (usually the adjoint flux) and integrating on all variables except time [20]. The equations obtained at the end are the following ones:

$$\begin{cases} \frac{dT}{dt} = \frac{\rho - \beta}{\Lambda} T(t) + \sum_i \lambda_i c_i(t) \\ \frac{dc_i}{dt} = -\lambda_i c_i(t) + \frac{\beta_i}{\Lambda} T(t) \end{cases}, \tag{3.2}$$

where T is the total amplitude of the flux and the other parameters can be found in Table 3.1.

As we can see, Eq. (3.2) is a system of ordinary differential equations (ODE). From the computational point of view, although being a stiff problem, the solution of these equations is not a critical task and this problem can be tackled with good accuracy and small computation time [22, 23].

The main issue left is the computation of the kinetic parameters that can be obtained as in Table 3.1. Even though any weight function could be used, the standard practice is to use the initial adjoint flux due to its physical meaning (section 2.1 and [13]) and mathematical properties. No approximation would have been introduced if the forward flux used in the formulas in Table 3.1 were the time depended flux ϕ. However, since all the coefficients are obtained through a ratio of fluxes, and therefore do not depend on the flux amplitude, the

$$\rho = \frac{\langle \phi^*(\mathcal{F}-\mathcal{A})\phi \rangle}{\langle \phi^* \mathcal{F} \phi \rangle} \qquad \Lambda = \frac{\left\langle \phi^* \frac{1}{v} \phi \right\rangle}{\langle \phi^* \mathcal{F} \phi \rangle} \qquad \beta_i = \frac{\langle \phi^* \mathcal{F}_{di} \phi \rangle}{\langle \phi^* \mathcal{F} \phi \rangle}$$

$$\beta = \textstyle\sum_i \beta_i \qquad c_i = \dfrac{\left\langle \phi^* \frac{\chi_i^d}{4\pi} C_i \right\rangle}{\left\langle \phi^* \frac{1}{v} \phi \right\rangle}$$

Table 3.1 – Point kinetics parameters

standard way to proceed is to use always the forward flux of the critical problem associated with the initial configuration, therefore neglecting any shape change (PK approximation). In conclusion, to implement this method it is enough to compute the critical forward (Eq. 1.14) and adjoint fluxes (Eq. 2.10) and use them to compute kinetic parameters.

Inhour equation

Since the focus of this work is the analysis of the neutronic response of a generic system, this section discusses a bit more the physical meaning of the main coefficients in Table 3.1 and which are the typical behaviours after a step change that can be modeled by PK.

Λ is usually referred as the mean neutron generation lifetime and it represents the average duration of a neutron generation. The parameter β, that is usually called β-effective, is the effective fraction of delayed neutrons over the total fission neutrons produced; effective means that, being weighed by the adjoint flux, it represents the delayed fraction of neutrons that actually participate to the chain reaction and it is not simply the ratio of the delayed neutron produced over the total ones. This parameter, from now on, will be always call β-effective to distinguish it from the β that is usually the ratio of delayed neutrons over the total ones [1].

To see how these parameters affect the system behaviour, consider a system where those parameters are constant. In that case the system obeys to PK equations and the solution for T and c_i will be a linear combination of exponential functions.

$$\begin{aligned} T(t) &= Te^{\omega t} \\ c_i(t) &= c_i e^{\omega t} \end{aligned} \tag{3.3}$$

Notice that the PK problem can be expressed in compact form as follows:

$$\frac{d}{dt} \begin{pmatrix} T \\ \vdots \\ c_i \\ \vdots \end{pmatrix} = \mathcal{M} \begin{pmatrix} T \\ \vdots \\ c_i \\ \vdots \end{pmatrix} \qquad , \tag{3.4}$$

and in the constant coefficient case, the Eq. 3.4 reduces to:

$$(\mathcal{M} - \omega I)\, V = 0 \tag{3.5}$$

where I is the identity matrix and therefore ω plays the role of the eigenvalue.

If solutions in Eq. 3.3 are plugged in the Eq. 3.2 and the system is solved for ρ, we find the possible ω's must obey the Inhour Equation or Nordheim Equation [1]:

$$\rho = \omega \left(\Lambda + \sum_i \frac{\beta_i}{\omega + \lambda_1} \right) \quad . \tag{3.6}$$

Eq. 3.6 represents the relation between ω, that can be seen as the system characteristic time, and the reactivity. The plot resulting from Eq. 3.6 can

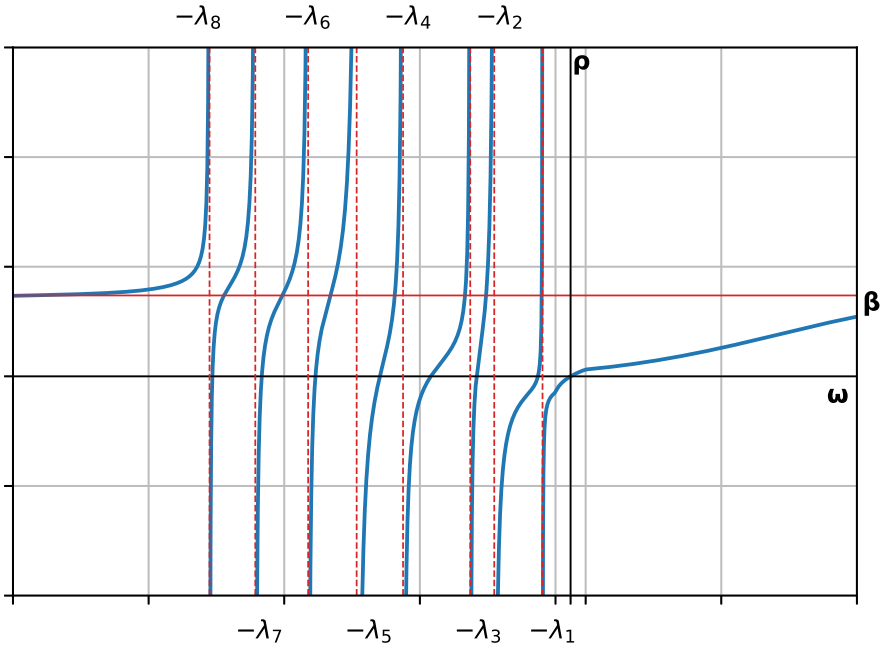

Figure 3.1 – Inhour equation

be seen in Fig. 3.1 with a symmetric logarithmic x axes. The vertical dashed lines represent the decay constant of the various precursor families and the horizontal red line represent $\rho = \beta$-effective. Eq. 3.1, for any given ρ, has nine roots $\omega_8 < ... < \omega_1 < \omega_0$; this can be proved by the fact that the inhour equation has an oblique asymptote $\rho = \Lambda\omega + \beta$ and that:

$$\frac{d\rho}{d\omega} = \Lambda + \sum_i \frac{\beta_i \lambda_i}{(\lambda_i + \omega)^2} > 0 \tag{3.7}$$

From Fig. 3.1 it can be seen how, seven of these roots $(\omega_1, ..., \omega_7)$ are always between the various decay constant and that when the system is subcritical

($\rho < 0$) the ω_0 is always negative, meaning that the total amplitude will decrease with time.

For $\rho < \beta$, ω_8 is quite far from the others. This eigenvalue is usually referred as the prompt eigenvalue and it is the one describing the response of the prompt neutrons. To understand why imagine a configuration at equilibrium at t=0; this implies that $\rho = 0$ and that all the time derivatives in Eq. 3.2 are equal to zero. In this condition we have that:

$$\lambda_i c_i(0) = \frac{\beta_i(0)}{\Lambda} T(0) \quad . \tag{3.8}$$

Let's introduce a perturbation ($\rho < \beta$). In this case $|\omega_8| >> |\lambda_i|$ and therefore λ_i can be neglected in the Eq. 3.6 leading to the following relation:

$$\omega_8 \approx \frac{\rho - \beta}{\Lambda} \tag{3.9}$$

Due the big discrepancies between ω_8 and the others eigenvalues is reasonable to assume that at first, the system evolves quickly, without a significant decay of the initial precursors. To obtain the amplitude of this change it is reasonable to neglect the time derivatives and compute the amplitude of the system with precursor still in the initial condition. This phenomenon is known as prompt jump (PJ) and its amplitude can be computed substituting condition 3.8 in Eq. 3.2, neglecting time derivatives, obtaining the following relation:

$$\frac{T(PJ)}{T(0)} = \frac{\beta}{\beta - \rho} \quad . \tag{3.10}$$

3.1.2 Multipoint kinetics

The Multipoint kinetics (MPK) approach also consists in dealing with a zero-dimensional model but, instead of using just one point as in the previous method, we split the reactor in different zones and we use a point for each. The consequence of this modeling is that the ODE describing the evolution of each region will be coupled with the others. How to describe this coupling will depend on which version of the multi-point-kinetics method we are using.

Avery's model

The first version of MPK has been proposed by Avery [24] using mainly physical considerations. In this case, we define the partial forward and adjoint fluxes of each region as follows:

$$\mathcal{A}\phi_j = \frac{1}{k_{eff}} \mathcal{F}_j \phi \qquad \mathcal{A}^* \phi_j^* = \frac{1}{k_{eff}} \mathcal{F}_j^* \phi^* \quad , \tag{3.11}$$

both of them are defined over the whole reactor but with a source term obtained by restricting the multiplication operator to region j and applying it to the total flux computed previously (and therefore already known). In this case, if we

$$k_{jk} = \frac{\langle \mathcal{F}_j \phi \rangle \langle \phi^* \mathcal{F}_j \phi_k \rangle}{\langle \mathcal{F}_k \phi \rangle \langle \phi^* \mathcal{F}_j \phi \rangle} k_{eff} \qquad k^d_{jk,i} = \frac{\langle \mathcal{F}_j \phi \rangle \langle \phi^* \mathcal{F}_{dik} \phi \rangle}{\langle \mathcal{F}_{ik} \phi \rangle \langle \phi^* \mathcal{F}_j \phi \rangle} k_{eff}$$

$$l_{jk} = \frac{\left\langle \phi^*_j \frac{1}{v} \phi_k \right\rangle}{\langle \phi^* \mathcal{F}_j \phi_k \rangle} k_{eff} \qquad S_{jk} = \frac{\langle \mathcal{F}_j \phi \rangle \langle \phi^* \mathcal{F}_j \phi_k \rangle}{\langle \phi^* \mathcal{F}_j \phi \rangle}$$

$$\beta_{jk} = \frac{\left\langle \phi^*_j \mathcal{F}_{dk} \phi \right\rangle}{\left\langle \phi^*_j \mathcal{F}_k \phi \right\rangle} \qquad \beta_{ki} = \frac{\langle \mathcal{F}_{dik} \phi \rangle}{\langle \mathcal{F}_k \phi \rangle} \qquad C_{ki} = \left\langle \frac{\chi^d_i}{4\pi} C_i \right\rangle_k$$

Table 3.2 – Avery's MPK parameters

split the reactor in n regions, we have n^2 equations for the evolution of the neutron population and n times the number of precursor families equations for the precursor concentrations. The resulting system is the following

$$\begin{cases} l_{jk} \frac{dS_{jk}}{dt} = k_{jk}(1-\beta_{jk}) \sum_m S_{km} - S_{jk} + \sum_i k^d_{jk,i} \lambda_i C_{ki} \\ \frac{dC_{ki}}{dt} = -\lambda_i C_{ki} + \beta_{ki} \sum_m S_{km} \end{cases} , \tag{3.12}$$

where each parameter can be expressed as in Table 3.2, again with the approximation that the time-dependent fluxes are replaced with the static ones.

In this model, the partial neutron populations S_{jk} represent neutrons produced in region j by neutrons born in region k and we have an equation for each of them.

Kobayashi's model

The Kobayashi version of MPK has been derived more recently focusing more on a mathematical rigorous approach to the problem [25]. The resulting importances used as weight functions are closer to the Green function definition and are defined as follows:

$$\mathcal{A}^* G_j = \nu \Sigma_{fj} \qquad , \tag{3.13}$$

where the partial importance (G_j) here is computed by using as a source the total production cross section restricted to region j, without using any flux.

The resulting system of equations is:

$$\begin{cases} l_j \frac{dS_j}{dt} = \sum_k k_{jk}(1-\beta_{jk}) S_k - S_j + \sum_i \lambda_i \sum_k k^d_{ijk} C_{ki} \\ \frac{dC_{ki}}{dt} = -\lambda_i C_{ki} + \beta_{ik} S_k \end{cases} , \tag{3.14}$$

where the unknown neutron populations S are the populations of each region independently from where the neutrons which generate them were coming. Therefore the resulting system has fewer equations for the population evolution (as many as the number of regions) but the same amount for the precursors concentrations. Parameters can be computed as in Table 3.3, once again, static fluxes are used instead of dynamic ones.

$$k_{jk} = \frac{\langle G_j \mathcal{F}_k \phi \rangle}{\langle \mathcal{F}_k \phi \rangle} \qquad k^d_{ijk} = \frac{\langle G_j \mathcal{F}_{dik} \phi \rangle}{\langle \mathcal{F}_{dik} \phi \rangle} \qquad l_j = \frac{\left\langle G_j \frac{1}{v} \phi \right\rangle}{\langle \mathcal{F}_j \phi \rangle} \qquad \beta_{jk} = \frac{\langle G_j \mathcal{F}_{dk} \phi \rangle}{\langle G_j \mathcal{F}_k \phi \rangle}$$

$$\beta_{ij} = \frac{\langle \mathcal{F}_{dij} \phi \rangle}{\langle \mathcal{F}_j \phi \rangle} \qquad S_j = \langle \mathcal{F}_j \phi \rangle \qquad C_{ki} = \left\langle \frac{\chi^d_i}{4\pi} C_i \right\rangle_k$$

Table 3.3 – Kobayashi's MPK parameters

Comments

The main differences among the methods described so far are in the weight functions. PK uses the adjoint flux that is a measure of the importance of neutrons relative to their capability to participate in the chain reaction [13]. Avery's MPK uses a partial version of forward and adjoint fluxes (Eq. 3.11) that add to total the respective fluxes used in PK. Kobayashi's importances instead can be seen as the capability of the neutron to reproduce neutrons, but at the next generation only, not over the total chain reaction [22]. The calculation of all of these importance functions has been implemented in APOLLO3 during this thesis. It is important to notice that those calculations are calculations with a given source but without the production operator. This deeply simplifies the calculation, reducing the computation time, since outer iterations are not needed in those calculations.

It is important to notice also that all the methods described so far can be expressed in the compact form:

$$\frac{dS}{dt} = \mathcal{M} S \qquad , \tag{3.15}$$

where the size of vector S and of matrix $\mathcal{M}$ depends on the method we are using; in particular, if S is vector of length n, $\mathcal{M}$ is a $n \times n$ square matrix. In our case, since we are using the JEFF 3.1.1 nuclear data library, we use 8 precursor families [26]. Therefore for PK the S vector has 9 elements (8 for the precursor families and one for the neutron population). For Kobayashi's MPK, if the number of regions in which we are subdividing our reactor is n, the S vector has $9n$ elements, n for the neutron populations, and $8n$ for the precursors (8 components in each region). For Avery's MPK, S has $(8+n)n$ elements, n^2 for the neutron populations, and $8n$ for the precursors. The study of the eigenvalues of $\mathcal{M}$ can provide useful information about the transient, in a similar way as for PK, as it will be shown in chapter 5. Finally we would like to define the prompt sub-matrix as the square matrix that we obtain from the total one ($\mathcal{M}$) by eliminating lines and columns concerning precursors. This matrix will be the one associated to a model in which precursors do not exist. To clarify this definition we make the example for the associated model in the Kobayashi's case:

$$l_j \frac{dS_j}{dt} = \sum_k k_{jk}(1-\beta_{jk}) S_k - S_j \qquad . \tag{3.16}$$

The comparison between the eigenvalues of the prompt sub-matrix and those of the total one can help us to identify the source of the different behaviors.

3.1.3 Quasi-Static methods

The family of methods that are under the name of quasi-static rely directly on Henry's factorization (Eq. 3.1). The idea behind these methods is to define two different time scales, one for the shape and one for the amplitude, and to deal with them using different time discretizations. The aim is to tackle the stiff behavior of Boltzmann equation only by dealing with the amplitude, that is cheap to compute, using high order methods or small time steps, while dealing with the shape on a coarser time resolution. The way the amplitude and the shape affect each others can be computed numerically in different ways and therefore different variants of the quasi static methods exist.

The simplest one is the adiabatic method. Basically it states that all the time derivatives in the Boltzmann equations are zero and that the amplitude evolution does not affect the shape. The shape is obtained by a steady state calculation, that can be done, at most, any time that there is a change in the core. The amplitude evolution is obtained by means of a point kinetic model. PK parameters can be updated once the new flux is computed and they can be interpolated between one value and the other, however this method is not able to catch fast spatial effects and this adiabatic assumption is mostly used for depletion calculations.

Higher accuracy versions of the quasi static methods are the improved quasi static method (IQM) and the predictor-corrector quasi static method (PCQM). In the first one, we plug the Henry factorization (3.1) in the Boltzmann equation and we solve for the shape, in this way we obtain an integro-differential equation that is the following:

$$\frac{1}{v}\cdot\frac{\partial\psi}{\partial t} = -\left(\mathcal{A}-\mathcal{F}_p+\frac{1}{vT}\frac{dT}{dt}\right)\psi+\frac{1}{4\pi}\frac{1}{T}\sum_i \chi_i\lambda_i C_i \tag{3.17}$$

Here the amplitude (T) is supposed to be known. We can therefore, starting from a known initial configuration, compute the point kinetic parameters, compute the evolution of the amplitude, use it to compute the shape and so on. However since the normalization conditions (second Eq. 3.1) has to be respected, and it is conserved by the Eq. 3.17 only if the exact amplitude is used, additional iterations are done between the shape and the amplitude calculations, using the new shape to recompute the point kinetics parameters until convergence.

In the PCQM we use directly the Boltzmann equation and we compute the flux at each shape time step. Then, by imposing the normalization condition, we extract the shape, we compute the kinetic parameters and by computing the amplitude evolution we correct the flux normalization. This leads to a linear

method as can be seen in the following plot showing the flowcharts of the two methods.

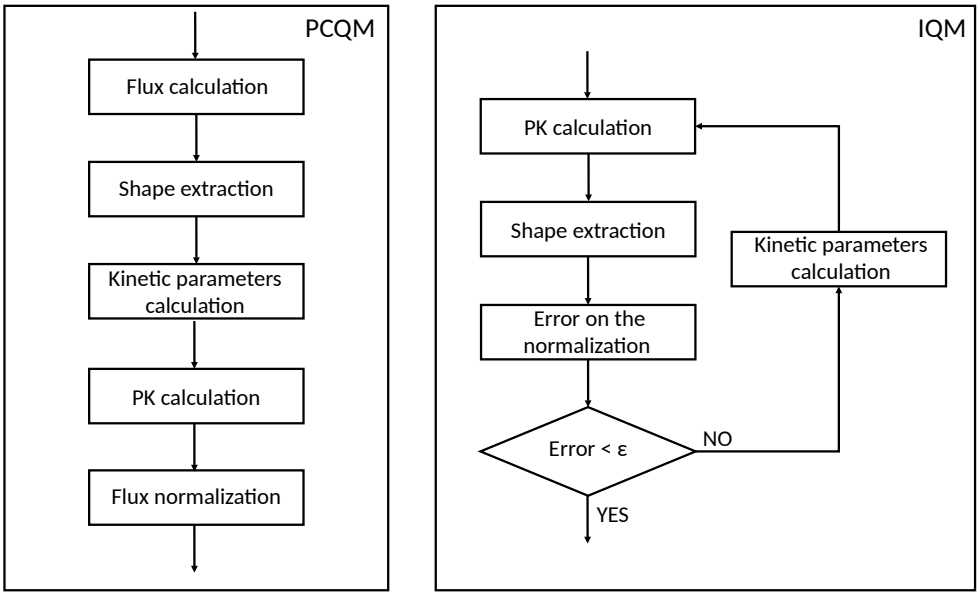

Figure 3.2 – Flow chart of the two methods

It is worth mentioning that with both methods the choice of the size of the time steps, both amplitude and shape ones, is free and can be done arbitrarly. The amplitude time step, used to solve a stiff ordinary differential equation, is more constrained since, usually, numerical stability problems arise, however plenty of literature is available regarding this kind of problems (both about stability and optimization). The choice of the shape time step instead is usually dictated by experience and guided with a posteriori evaluations, except for very recent propositions [27].

3.1.4 Direct Method

The direct method consists in solving the time dependent transport equation by means of direct discretization of the time variable without any further assumption. To approximate the time derivative usually the implicit Euler scheme is chosen:

$$\frac{1}{v} \cdot \frac{\phi^{n+1} - \phi^{n}}{\Delta t} = -\left(\mathcal{A} - \mathcal{F}_p\right)\phi^{n+1} + \frac{1}{4\pi}\sum_i \chi_i \lambda_i C_i^{n+1} \tag{3.18}$$

where the index n is the time step number and $\Delta t = t_{n+1} - t_n$

The implicit Euler method is usually preferred due to the fact that the transport equation is stiff in time and explicit methods do not assure stability but in some cases, using small time step, a Crank Nicolson method can be also used. In the direct method no correction is applied to the flux level and to catch fast transient behavior we are forced to use very short time-steps. Considering

that in fast reactors the typical mean neutron generation time is of the order of 0.5 μs, using a time step of that order will lead to not-affordable simulations almost in any realistic situation. However this method can be used to validate the previous ones in devoted benchmarks.

3.2 Delayed Nuclear Data

As already anticipated in section 1.2, cross-section processing is constituted by several steps and in each of them a representative flux is used to condense those cross-sections to be used in the following one. Except for a recent proposition [28], multi group cross sections that would be used in time dependent calculations are produced by using a flux computed by a steady state calculation. Steady state calculations are usually done using the k-mode approximation and therefore, to describe the fission operator, need only the total χ and the total ν. For this reason, so far, APOLLO3 permits to process only those data during lattice calculation and delayed data, that are necessary only during time dependent calculation, have been included only very recently. Even with the very last development, delayed nuclear data can be processed by the lattice side of the code only to produce global kinetic properties for each materials, therefore loosing any dependence from the single isotopes. Since this was considered a limitation that was not compatible with the aim of this work, we have implemented an alternative procedure to keep those dependencies on the core side.

Before describing how those data have been implemented in APOLLO3, it is better to detail a bit more the different models that can be adopted for the precursors families. The physics that these models aim to describe is that when a nucleus fissions it emits neutrons and fission products. Some of those fission products can then undergo a beta decay emitting a neutron; that neutron is called delayed neutron and the decaying isotope is called precursor. Unfortunately, not all nuclear properties of all precursors are sufficiently well known, or known with a reasonable accuracy to allow for a satisfactory modeling of this process; instead what is done is that this process is measured by means of integral experiments and data are fitted with precursors families that are a set of precursors sharing similar decay constants. Defining the criteria to constrain the choice of families is an open debate and two main propositions exist [26]:

- Using 6 precursors families whose properties depend on the fissioning system, as in the American nuclear library ENDF.
- Using 8 precursors families whose properties are independent from the fissioning system, as in the European nuclear library JEFF.

The nuclear data library currently used at CEA is JEFF 3.1.1, that has 8 precursor families. The model adopted in this library is that each precursor family has a fixed decay constant independently from the fissioning system (Table 3.4), and, in this particular version of the JEFF library, also the spectra of the precursor families are independent from the isotope which generates the precursor.

Table 3.4 – Set of half-lives recommended by the WPEC-SG6

Group	**Prec.**	**Prec.** $T_{1/2}$ **[s]**	**Group** $T_{1/2}$ **[s]**
1	^{87}Br	55.6	55.6
2	^{137}I	24.5	24.5
3	^{88}Br	16.3	16.3
4	^{138}I	6.46	5.21
	^{93}Rb	5.93	
	^{89}Br	4.38	
5	^{94}Rb	2.76	2.37
	^{139}I	2.30	
	^{85}As	2.08	
	^{98m}Y	2.00	
6	^{93}Kr	1.29	1.04
	^{144}Cs	1.00	
	^{140}I	0.86	
7	^{91}Br	0.542	0.424
	^{97}Rb	0.384	
8	^{96}Rb	0.203	0.195
	^{97}Rb	0.170	

An extensive discussion of the model adopted and of the decaying constant can be found in [29]. Having properties that are defined independently from the fissioning isotope allows to handle those data without any homogenization or averaging procedure, simplifying their processing.

3.2.1 χ_d

Delayed fission spectra are in general poorly known [30] and their reevaluation is currently under consideration by several institutions [29, 30]. As a matter of example, in the following plots the spectra of the various precursors families are represented; it is worth noticing that, with respect of the prompt fission ones, those spectra are mostly located at considerably smaller energies.

In the multi group approximation, fission spectra are simply condensed on the energy mesh:

$$\chi_g = \int_{E_{g+1}}^{E_g} \chi(E)dE \qquad and \qquad \sum_g \chi_g = 1 \quad , \tag{3.19}$$

so their processing is almost straightforward in the JEFF 3.1.1 case.

3.2.2 ν_d

For this work, it has been decided to provide delayed data directly to the core side of the code after a simple preprocessing. The aim is to preserve the delayed neutron production rate. In order to do so, since the total neutron production

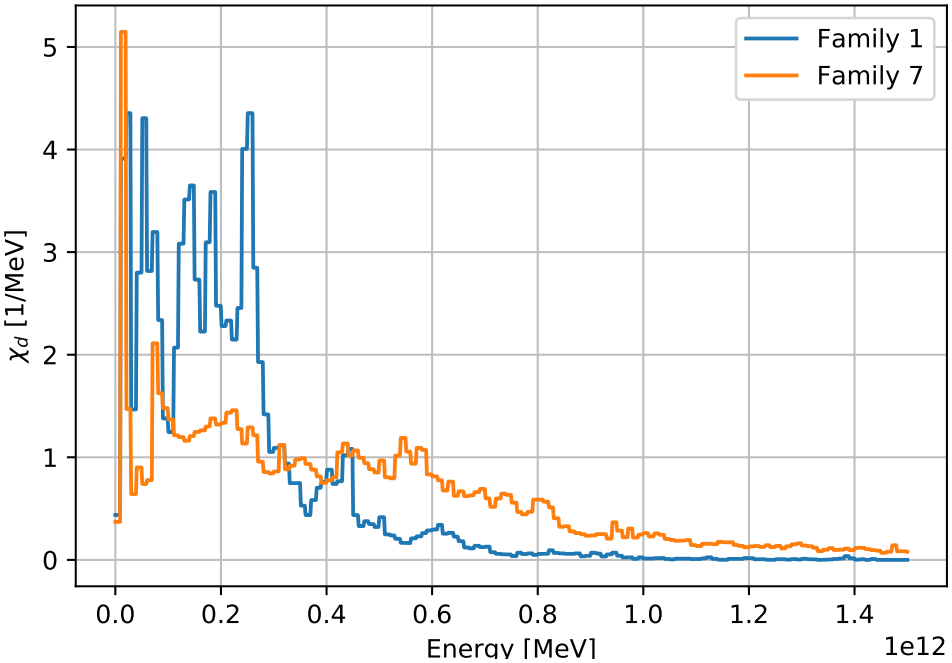

Figure 3.3 – χ_d energy dependence of the precursor families 1 and 7 in JEFF 3.1.1

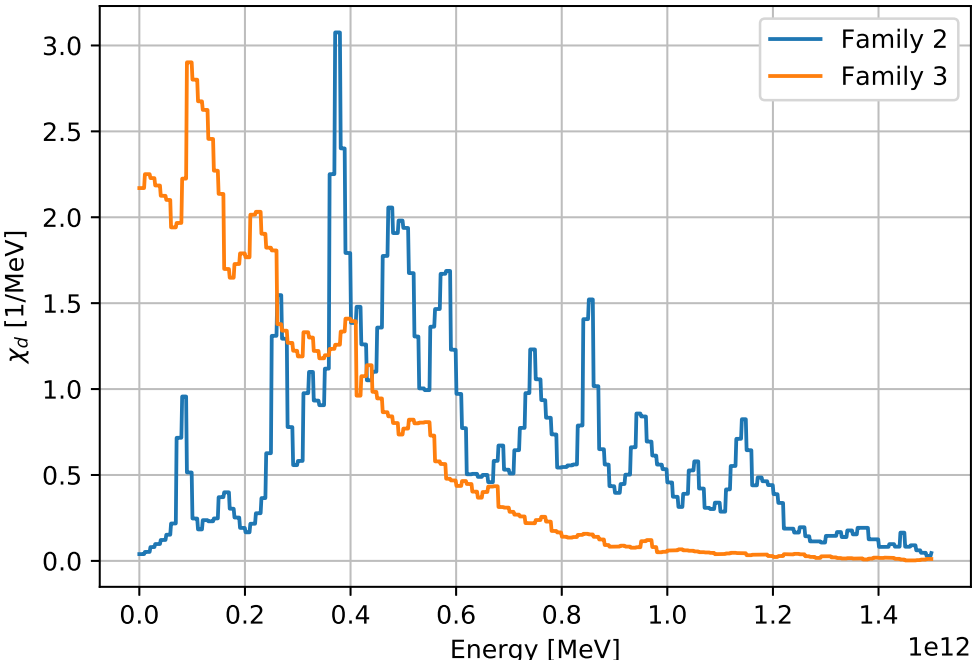

Figure 3.4 – χ_d energy dependence of the precursor families 2 and 3 in JEFF 3.1.1

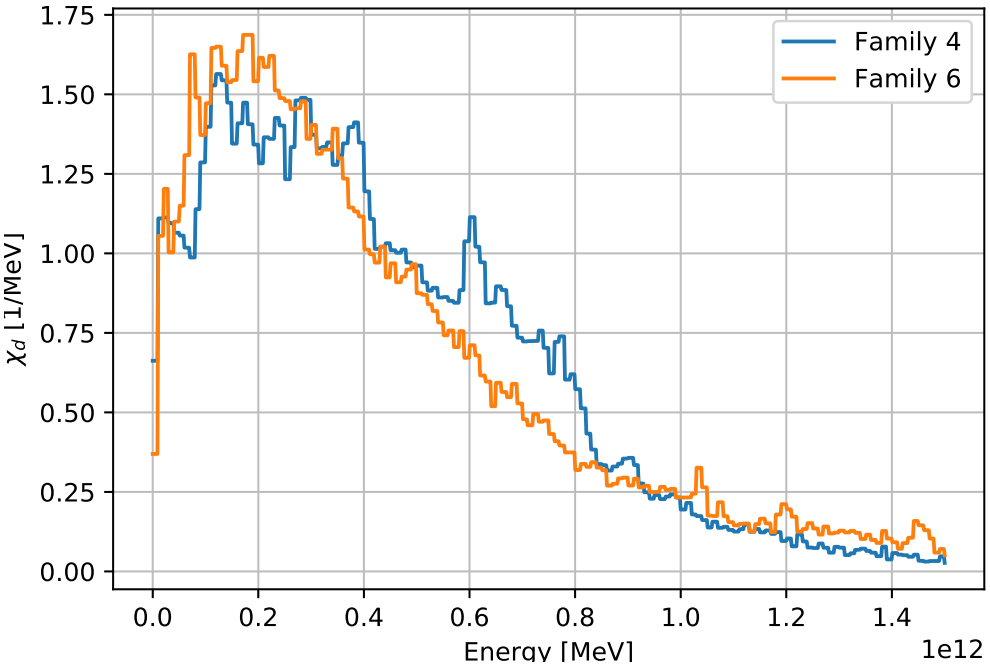

Figure 3.5 – χ_d energy dependence of the precursor families 4 and 6 in JEFF 3.1.1

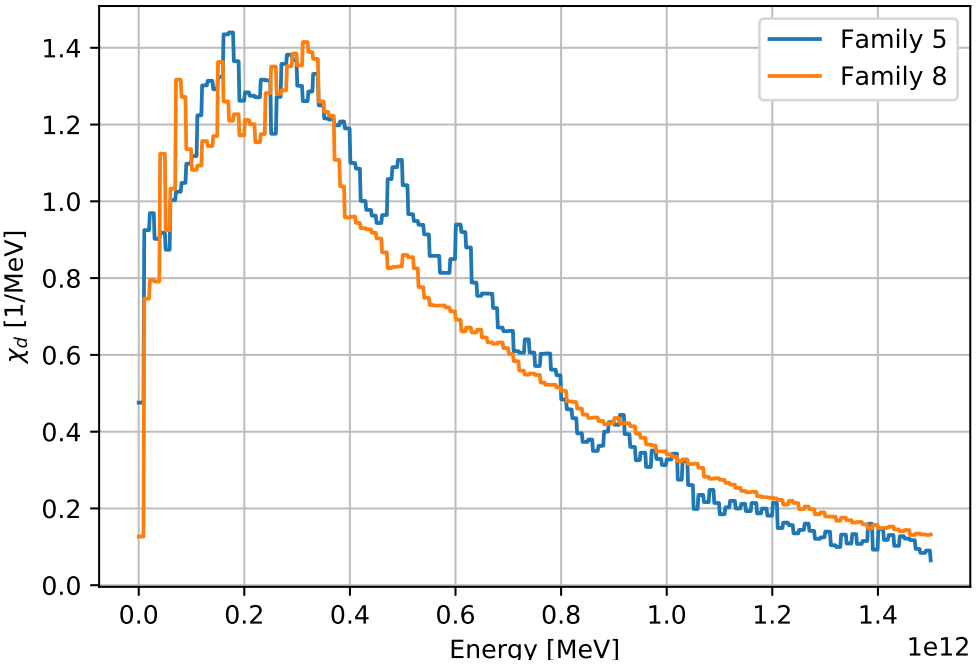

Figure 3.6 – χ_d energy dependence of the precursor families 5 and 8 in JEFF 3.1.1

rate is a fundamental quantity that goes through all the different steps of the calculation scheme and that is accurately validated, the delayed emission rate can be derived starting from the total one. Due to the identity:

$$\nu_d \Sigma_f \phi = \frac{\nu_d}{\nu} \nu \Sigma_f \phi = \beta \nu \Sigma_f \phi \quad , \tag{3.20}$$

for each energy group the following relation hold:

$$min(\beta) \int_{E_{g+1}}^{E_g} dE\ \nu \Sigma_f \phi \leq \int_{E_{g+1}}^{E_g} dE\ \nu_d \Sigma_f \phi \leq max(\beta) \int_{E_{g+1}}^{E_g} dE\ \nu \Sigma_f \phi \quad . \tag{3.21}$$

While the fission cross-section Σ_f has a complex energy dependence, ν and ν_d have a much smoother behaviour. An extensive analysis of those data can be

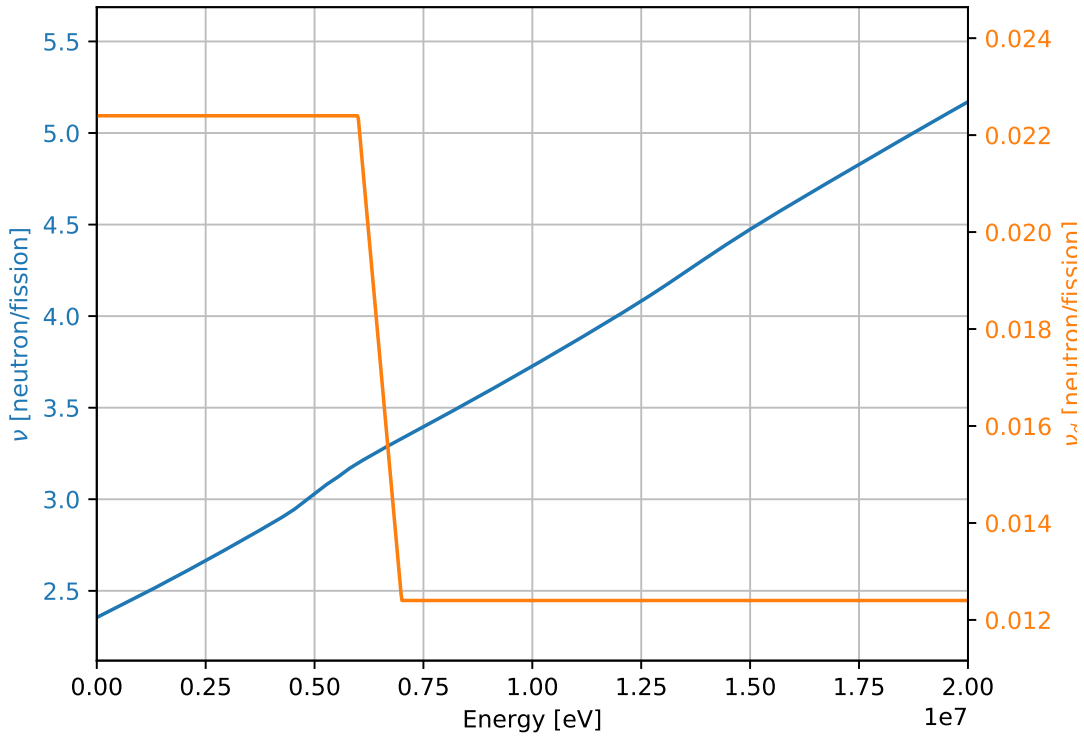

Figure 3.7 – ν and ν_d energy dependence of ^{236}U (JEFF 3.1.1)

found in [29] and the present situation can be summarized as follows: for most of the isotopes, ν has an almost linear energy dependence, while ν_D is constant up to about 5 MeV (energy of the neutron inducing fission) where it has an important drop; an example can be seen in Fig. 3.7 regarding ^{236}U. For the main isotopes the energy dependence has been evaluated with higher precision [29] and the global behaviour, while presenting the same qualitative behaviour, has a more complicated energy dependence, see Fig 3.8 for the case of ^{235}U.

To understand how these data can be condensed according to the multigroup formalism, nuclear data are integrated over an (usually narrow) energy mesh

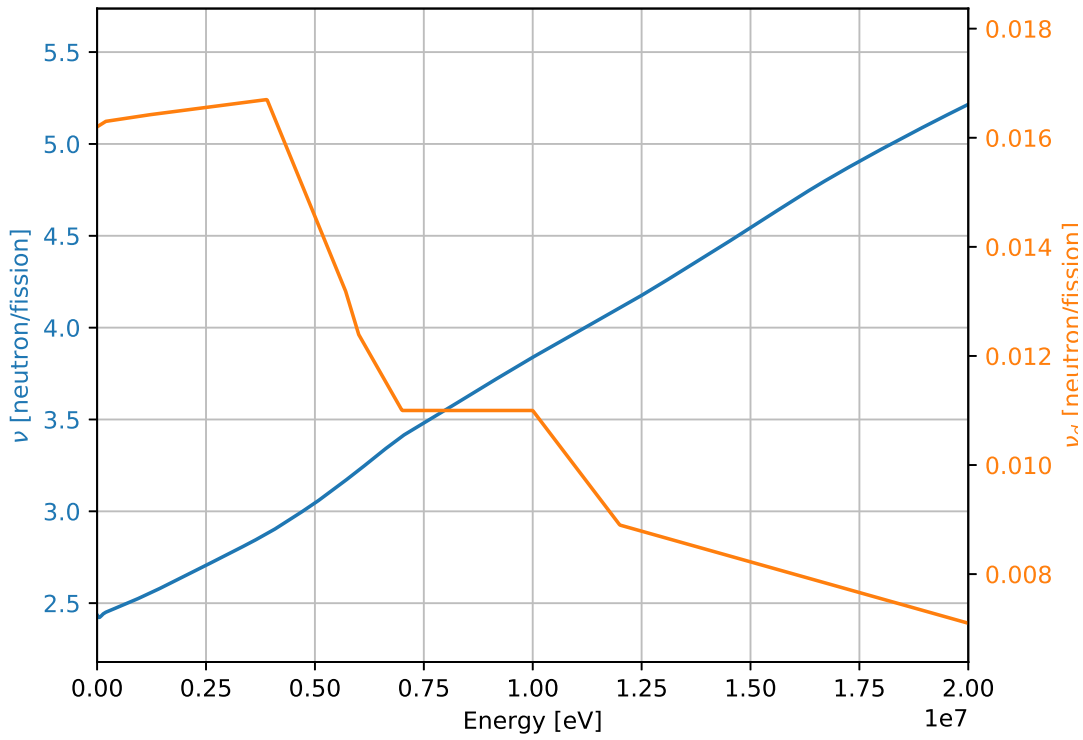

Figure 3.8 – ν and ν_d energy dependence of ^{235}U (JEFF 3.1.1)

with a representative flux. A popular weight flux is the iwt=4 option of the GROUPR module of NJOY [7] that can be decomposed in the following 3 components:

- A Boltzmann thermal spectrum
- A $1/E$ slowing down part
- A fission spectrum

To see what is the energy variation of this representative flux and of the delayed neutron fraction $\beta = \nu_d/\nu$ (not to be confused with the β-effective defined previously) we can look at Fig. 3.9 where they are plotted on the same semi-logarithmic energy axis. β being almost constant at very low energy, the region including the thermal bump has not been plotted. The vertical dashed lines represent the bounds of the 33 groups energy mesh that is usually employed for fast reactor calculations and the region beyond 1 MeV is zoomed at to show more precisely the stiff changes that occur at high energy. As can be seen, β is almost constant up to the most energetic groups, therefore any weight flux will have a very small impact on the multigroup beta value and its effect on the total calculation. Focusing on energies larger than 1 MeV, it can be observed that the stiff decrease of the beta happens at energies that are larger than the mean fission energy; this is also an energy range where there are no resonances.

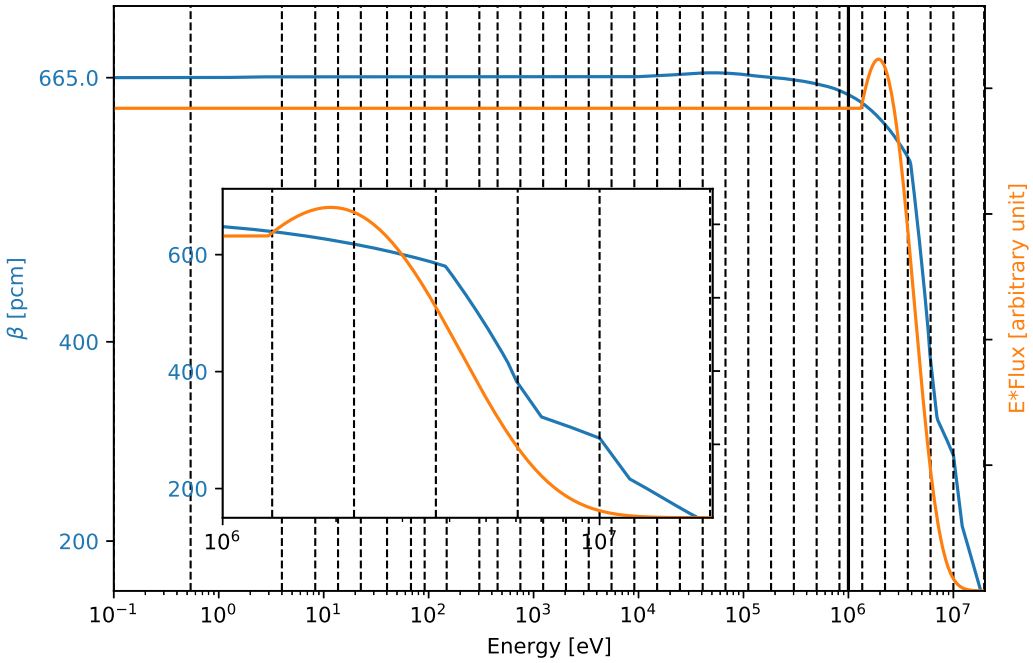

Figure 3.9 – β energy dependence of ^{235}U

For all these reasons a representative fission spectrum can be considered a good "in group" approximation of the actual flux and can be used to produce the multigroup beta for each isotope, directly on a coarser mesh.

Multi group betas have been produced for the main energy meshes for all the isotopes in the library JEFF 3.1.1 presenting delayed nuclear data. These isotopes are:

- ^{227}Th, ^{229}Th, ^{232}Th.
- ^{231}Pa.
- ^{232}U, ^{233}U, ^{234}U, ^{235}U, ^{236}U, ^{237}U, ^{238}U.
- ^{237}Np, ^{238}Np.
- ^{238}Pu, ^{239}Pu, ^{240}Pu, ^{241}Pu, ^{242}Pu.
- ^{241}Am, ^{242}Am, ^{243}Am.
- ^{242}Cm, ^{243}Cm, ^{244}Cm, ^{245}Cm, ^{246}Cm, ^{248}Cm.
- ^{249}Cf, ^{251}Cf.
- ^{254}Es.

3.3 Point Kinetics Implementation

Due to the several similarities with perturbation theory, the calculation of kinetic parameters has been implemented within the perturbation module of APOLLO3 [31]. Thanks to the optimization of the scalar products described in section 2.2, all the parameters needed for PK can be computed extremely efficiently once the forward and the adjoint fluxes are available. The main development has been a python interface to provide delayed nuclear data to the code in order to create the needed operators in a way consistent with the data structure of APOLLO3 [16]. While the data processed and used during this work belongs to the JEFF 3.1.1 library, the interface created can be used also with other data structures (e.g. delayed fission spectra depending on the fissioning isotope). Once all the parameters are computed, they are provided by APOLLO3 as output in a python environment; thanks to this, the system of ODE can be defined outside of APOLLO3 and can be solved in python. We developed python functions that take these parameters as input and define the system of ODE in matrix form. To this end, during this work, the scipy library [32] available in python has been used; it includes both ODE and linear algebra modules that can be used to perform a broad range of different analyses. The main functions used during this work have been:

- scipy.integrate.ode has been used for numerical integration of the system of ODE. The functions implemented are a wrapping of the ODEPACK library developed in FORTRAN and automatically recognize stiff problems. They are deeply optimized and have extremely good performance from the computational point of view [33].
- scipy.linalg.eig has been used to extract eigenvalues and eigenvector of the ODE matrices [34] (matrix $\mathcal{M}$ defined in section 3.1).

3.4 Multipoint Kinetics Implementation

The implementation of MPK has been done within the pertubation module of APOLLO3 to benefit from the various feature described so far. That implementation strategy has been chosen to be as consistent as possible with the one adopted for PK so to have easy comparison among the various methods. The main differences with PK is the need to define the various regions and to compute the importances related to each of those. The region selection is done independently from the MPK variant. The user, during the definition of the geometry, uses the region name property to tag differently the various regions; then, before proceeding with the MPK calculation, provides the number of regions and the list of region names belonging to each of them. Once the calculation starts the system automatically computes the forward and adjoint flux and the various importances related to the regions. The output of the calculation are the MPK parameters, provided as output in python. The system of ODE is defined by means of python's functions that take those output as input and the integration strategy is the same as the one used for PK.

3.4.1 Avery

As anticipated in section 3.1.2, importances are easier to compute with respect to the forward and adjoint flux. To provide an order of magnitude, using the same reference case as before (SFR core with 33 energy groups and 300.000 spatial meshes) the calculation of one flux takes about 2h while the calculation of an importance takes about 10 min. In Avery's MPK both forward and adjoint importances have to be computed. The coefficients appearing in Avery's MPK are obtained by scalar products between all the combinations of those importances. Due to the fact that those importances are fast to compute, and since memory is our main bottleneck, we implemented the algorithm in the following way:

- Forward and adjoint fluxes are computed and stored in memory.
- A first loop over the MPK regions (index j) is performed, where the adjoint importance relative to the region is computed.
- A nested loop is performed again over MPK regions (index k), where the forward importance relative to the region is computed.
- All the needed scalar products involving adjoint importance j and forward importance k are done, those products are then combined with the various operators to compute the needed coefficients and those are stored in matrices.
- Moving to the next region, importances are overwritten to save memory.
- At the end of the calculation all the coefficients are combined together to compute the MPK parameters.

If n is the number of regions, this implementation computes n times the same forward importance but at least avoids the need to store n importances, as each of them occupies the same amount of memory as a normal flux (for the reference case, it is 4 GB)

3.4.2 Kobayashi

Kobayashi's MPK has only adjoint importances and therefore its implementation is easier. Only one loop is done over the regions, importances are computed and used to obtain the various coefficients and then are overwritten to save memory.

Chapter 4

Kinetic Parameters

Contents

This chapter presents two sets of results about point kinetic parameters with a special focus on the beta effective. The purpose is to demonstrate the potential of the methods discussed so far. Section 4.1 presents the results about the ASTRID core, that is a fast neutron reactor, while section 4.2 presents the results about EPICURE that is a thermal core. These systems have been chosen to represent two situations as different as possible and as such to cover a wide range of applications. For both, a few elements about the validation are discussed at first and then the β-effective is analysed in terms of individual contributions and of dependence on nuclear data.

4.1 ASTRID

The first system that has been analysed is an ASTRID core. ASTRID is the acronym of Advanced Sodium Technological Reactor for Industrial Demonstration and was supposed to be the first prototype of a SFR of the 4^{th} generation in France. Among the several peculiarities ASTRID has an heterogeneous axial composition that permit to this core to have a negative global sodium void coefficient; for this reason this type of core is usually referred to with the acronym CFV (from the french Coeur à Faible reactivite de Vidange that means low void effect core). The ASTRID project went through different design phases but,

for what concerns this work, the two versions that have been analysed are the CFV V1 [35] and the CFV Basic Design (BD) 16/10 [6]. The reason we chose to model two different version is that the ASTRID CFV V1 has been used in a recent work [22] using MPK and computing coefficients with ERANOS [36], and we decided to use the same configuration to have an initial reference. The choice to model the BD 16/10, instead, is due to the fact that for this core an extensive work to characterize it from the neutronic point of view has been recently done [6] and therefore we could benefit from existing models that have been accurately validated. In fact, in order to have a low void effect the system presents an heterogeneous axial structure that, in case of sodium void, enhances neutron leakage leading to an overall negative effect on the reactivity. This heterogeneity induces axial effects that, in order to have a faithful description, have to be modeled also during the lattice step, where usually 2D approximations are used. The definition of a proper calculation scheme for this type of reactor has been the core of a recent work [6]. An example of the ASTRID CFV V1 geometry can be seen in Fig. 4.1. To have an idea of the dimensions, the lattice pitch is 17.17 cm. The main difference with the BD 16/10 is in the Pu isotopic composition of the fuel and in the reflector, whose main component is steel for the CFV V1 and MgO for the BD 16/10.

4.1.1 Validation

The first step to model a reactor transient is to compute the effective delayed fraction (β) and the mean neutron generation time (Λ) as are described in section 3.1. To help the reader we recall their expressions:

$$\Lambda = \frac{\left\langle \phi^* \frac{1}{v} \phi \right\rangle}{\langle \phi^* \mathcal{F} \phi \rangle} \qquad \beta = \frac{\langle \phi^* \mathcal{F}_d \phi \rangle}{\langle \phi^* \mathcal{F} \phi \rangle} \tag{4.1}$$

To validate the PK implementation in APOLLO3 those quantities have been computed for the ASTRID BD 16/10 and then compared against those obtained by a Monte Carlo calculation performed with the TRIPOLI4 code [37], using the iterated fission probability method (IFP) [38].

Due to the size of this reactor and the necessity to compute both the forward and the adjoint flux, the main limitation for this kind of calculation is the memory occupation.

To overcome this issue we decided not to model the Radial neutron shield (outer grey zone in Fig. 4.1). This choice, while reducing the memory consumption, affects mainly the results on the mean neutron generation time. The reason is that in the reflector, neutrons are considerably slowed down, with a somewhat low absorption rate, so that the contribution of the peripheral part of the flux to the $\left\langle \phi^* \frac{1}{v} \phi \right\rangle$ term is relatively important; neglecting that part can induce an error of the order of a few percent, resulting in a small underestimation of the total Λ. Another known source of underestimation of the value of λ is the use of the velocity associated to the mean energy of the group [39]. This aspect however has not been investigated particularly during this work.

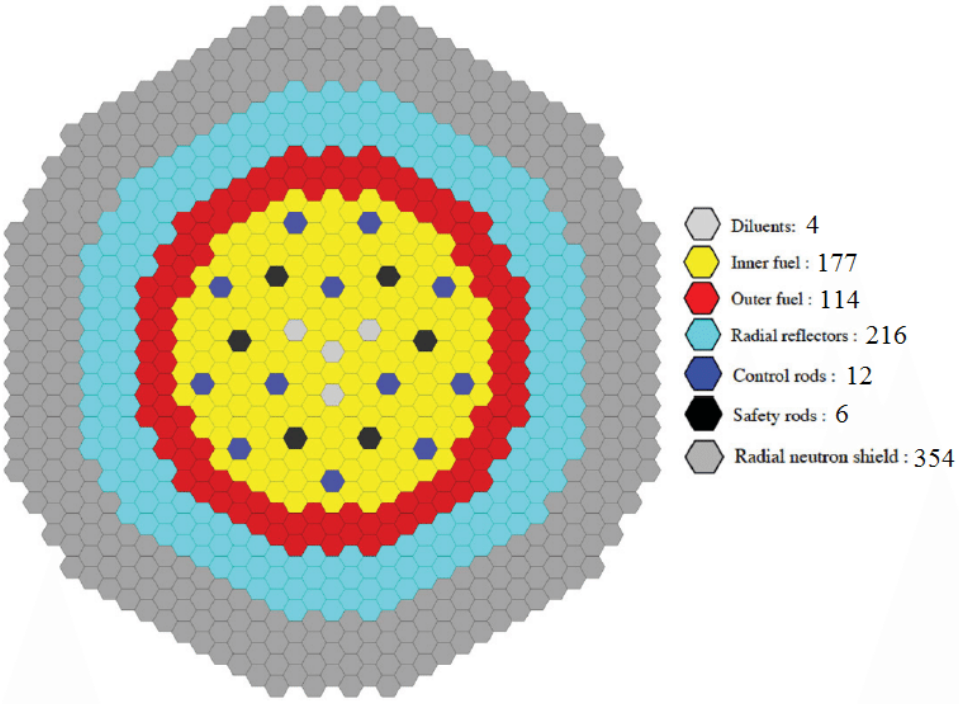

Figure 4.1 – ASTRID CFV V1 core

	TRIPOLI4	APOLLO3	Δ
K_{eff}	1.036026±4pcm	1.03367	235 pcm
Λ	0.6350±0.0014 μs	0.6140 μs	0.021 μs (3%)
β	371±1.6 pcm	370.2 pcm	0.8 pcm (0,2%)
Time	90366 s	1100 s	

Table 4.1 – Kinetic Parameters for ASTRID BD 16/10

The results obtained are summarized in Table 4.1. As can be seen, even if there is a relatively important error on the k-effective, partially due to the normal error of the calculation scheme and partially to the choice not to include the radial shield in the APOLLO3 calculation, the kinetic parameters are well computed. The relative error on Λ with respect of the Monte Carlo reference, even if small, is considerably larger than the one on β. As anticipated before, this is due to two reasons: the first is that neglecting the most external part of the reactor has a small impact on the flux in the core, and therefore on fissions, but neglects also a set of very slow neutrons that, having very small velocity, can have important impact on the generation time; the second one is that in the multigroup formulation, the neutron velocity is chosen to be the one associated to the mean energy of the group, and this has a known impact on this parameter [39]. We think that the main source of error is the multigroup formulation, insight in this direction are provided in the section 4.2.

4.1.2 Results

In this section we provide the results for the ASTRID CFV V1 core [35]. As already mentioned this core has slightly modified concentrations with respect to the design previously discussed but, focusing on the β-effective, this has a small impact. This configuration has a total β-effective equal to 369 pcm. In

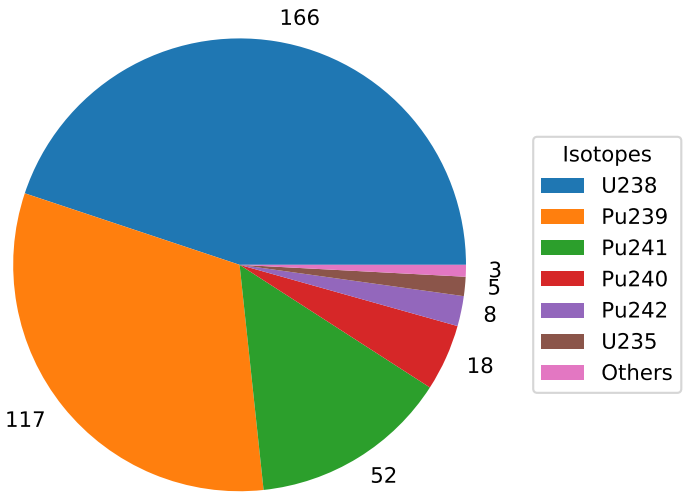

Figure 4.2 – ASTRID β-effective: contribution by nuclide

Fig. 4.2 we can see the various contributions to the β-effective of the main isotopes. As can be seen, the main contributor to β-effective is ^{238}U due to his very high beta (initial plateau at 1985 pcm), it is then followed by the ^{239}Pu that is the main fissile isotope but with a much smaller proper beta (initial plateau at 227 pcm) and the from the other Pu isotopes. To have an idea of the relative fission rates, in this configuration, ^{239}Pu accounts for 65% of the fissions in the system, followed by ^{241}Pu with 12%, by ^{238}U with 11% and then by ^{240}Pu with 7%. As a matter of comparison the initial plateau of ^{240}Pu is at 312 pcm and the one of ^{241}Pu is at 546 pcm.

Looking at sensitivities, the main conclusion is that direct effects are the dominant contributors, as can be seen in Table 4.2. Notice that χ and χ_d do not appear in the table since the total value (the one obtained summing over all the energy range) associated to their sensitivities is equal to the one associated to ν and ν_d by construction. The reader interested in the differences in the energy dependencies can consult the appendix A. In Table 4.2 can be seen how all the ν_{tot} have a negative impact on the β-effective (increasing the denominator) while the ν_{D} have a positive impact (being at the numerator). In this calculation ν_{tot} and ν_{d} are considered being independent one from the other

Table 4.2 – **Sensitivities (in %/%) of β-effective for the ASTRID CFV V1.**

Isotope	Capture	Fission	Elastic	Inelastic	NXN	ν_{tot}	ν_d
^{16}O	2.16 e-3	-	-2.16 e-2	-3.85 e-5	-1.21 e-9	-	-
^{23}Na	1.33 e-4	-	-1.72 e-2	-5.64 e-3	-3.76 e-7	-	-
^{50}Cr	4.48 e-5	-	-3.09 e-4	-2.20 e-4	-4.28 e-9	-	-
^{52}Cr	-6.31 e-6	-	-3.90 e-3	-4.04 e-3	-1.39 e-6	-	-
^{54}Fe	8.33 e-4	-	-2.15 e-3	-1.80 e-3	-5.78 e-7	-	-
^{56}Fe	3.04 e-4	-	-1.96 e-2	-2.97 e-2	-1.71 e-5	-	-
^{57}Fe	-7.38 e-5	-	-5.60 e-4	-8.78 e-4	-8.74 e-6	-	-
^{58}Ni	1.61 e-3	-	-1.85 e-3	-1.83 e-3	-6.21 e-8	-	-
^{235}U	-1.00 e-4	7.64 e-3	-2.13 e-5	-7.00 e-5	-3.10 e-6	-6.10 e-3	1.37 e-2
^{238}U	-1.73 e-2	**2.55 e-1**	-1.25 e-2	-5.78 e-2	-1.89 e-3	**-2.27 e-1**	**4.48 e-1**
^{238}Pu	-2.60 e-4	-1.22 e-2	-8.87 e-5	-1.16 e-4	-3.18 e-6	-2.16 e-2	7.62 e-3
^{239}Pu	-6.85 e-3	**-1.80 e-1**	-1.47 e-3	-2.96 e-3	-8.71 e-5	**-5.24 e-1**	**3.18 e-1**
^{240}Pu	-2.34 e-3	-4.38 e-2	-7.33 e-4	-1.73 e-3	-2.75 e-5	**-1.04 e-1**	4.75 e-2
^{241}Pu	-4.38 e-4	5.95 e-2	-2.06 e-4	-4.21 e-4	-5.44 e-5	-8.37 e-2	**1.41 e-1**
^{242}Pu	-7.30 e-4	-1.38 e-3	-2.55 e-4	-6.98 e-4	-1.79 e-5	-2.64 e-2	2.14 e-2
^{241}Am	-4.35 e-4	-3.51 e-3	-3.29 e-5	-5.57 e-5	-5.15 e-7	-4.90 e-3	7.80 e-4

and therefore the (small) effect that an increase of ν_d has on ν_{tot} is neglected.

The two main isotopes to which the β-effective is sensitive are ^{238}U and ^{239}Pu as can be also understood by looking at the different isotope contributions (Fig 4.2). In particular the Fission cross section has a positive contribution for ^{238}U and a negative one for ^{239}Pu. This can be explained by looking at the β-effective as an average of the beta of different isotopes and since ^{238}U has a beta that is more than seven times larger than the one of ^{239}Pu, changes in their relative contribution affect the β-effective with opposite signs.

The main indirect contributions come from the elastic and inelastic scattering. One thing that can be noted is that all those contributions are negative. Looking at the energy decomposition of those contributions (available in appendix A) it can be seen that they aren't always negative but that the dominant part, for all isotopes, comes from the energy groups just above 1 MeV; this is likely to be due to the fission threshold of ^{238}U and to its very large beta. The reason is that slowing down neutrons into an energy region where they can't induce fission on ^{238}U has a negative impact for the β-effective.

For what concerns uncertainty, the various contributions can be found in Table 4.3. As can be seen, the two main contributions, as can be expected, come from ^{238}U and ^{239}Pu. In particular, for both, the dominant source of uncertainty is ν_d. This is due to the poor knowledge of this parameter and to the high sensitivity associated. The high uncertainty characterizing ν_d affects all the isotopes, and due to its direct contribution and high sensitivity, the total value associated to ν_d constitutes around 94% of the total beta uncertainty (88% of the total variance). The second major contribution comes from the fission cross section (7% of the total variance), and in particular for the less fissile isotopes, as the ^{238}U and the ^{240}Pu, for which the fission cross has higher uncertainty.

Table 4.3 – **Uncertainty propagation (in pcm) of beta effective for the ASTRID CFV V1 core. Negative values stand for imaginary values, i.e. negative contributions to the overall variance.**

Isotope	Capture	Fission	Elastic	Inelastic	NXN	ν_{tot}	ν_d	χ	TOTAL
^{16}O	0.06	-	0.09	0.00	-	-	-	-	0.11
^{23}Na	0.00	-	0.04	0.03	-	-	-	-	0.05
^{50}Cr	0.01	-	0.00	0.00	-	-	-	-	0.01
^{52}Cr	0.00	-	0.00	0.01	-	-	-	-	0.01
^{54}Fe	0.01	-	0.01	0.01	-	-	-	-	0.02
^{56}Fe	0.02	-	0.06	0.09	-	-	-	-	0.12
^{57}Fe	0.00	-	0.00	0.00	-	-	-	-	0.01
^{58}Ni	0.03	-	0.00	0.00	-	-	-	-	0.03
^{235}U	0.00	0.00	-0.00	0.00	0.00	-0.00	0.04	0.00	0.04
^{238}U	0.12	0.48	-0.06	-0.09	0.04	-0.02	**1.50**	0.01	**1.58**
^{238}Pu	0.00	0.01	0.00	0.00	0.00	0.06	0.11	0.09	0.15
^{239}Pu	0.02	0.07	-0.01	-0.02	-0.01	0.06	**1.32**	0.34	**1.36**
^{240}Pu	-0.04	0.32	-0.00	0.02	0.01	0.01	0.23	0.05	0.40
^{241}Pu	0.02	0.04	0.00	0.01	0.00	0.02	0.70	0.22	0.74
^{242}Pu	0.01	0.00	0.00	0.01	0.00	0.01	0.20	0.02	0.21
^{241}Am	0.00	0.00	-0.00	0.00	0.00	0.01	0.01	0.00	0.01
TOTAL	0.13	0.59	0.11	0.03	0.04	0.08	**2.14**	0.42	**2.27**

It is important to notice that no contribution from delayed spectra has been included. The reason is that for these data, at present, no covariance matrices are available. While recent work provided an estimation of the total effect using reasonable assumptions to guess their value [40], due to the recent effort to measure those data [30], we preferred not to include them in our estimation and to wait for their measured values and associated uncertainties.

4.2 EPICURE

The second system analysed is an EPICURE UM17x17 core, for which a reanalysis with modern tools is on progress at CEA Cadarache. EPICURE UM17x17 is an experimental program held in the EOLE facility at CEA Cadarache in the 90's [41]. The EPICURE UM17x17 configuration is composed of a central 17x17 MOX-7% pins surrounded by 3.7% U-235 enriched UO2 pins, with a lattice pitch of 1.26 cm.

The reason why this system has been chosen is because of its geometry composed of 289 MOX fuel pins and 1351 UOX fuel pins, thus presenting an unusual beta-effective. To model this reactor the usual two-step approach has been used. On the lattice side, a 2D section representing cells, cladding and moderator has been modeled without the vessel (Figure 4.3a). The JEFF-3.1.1 nuclear data library has been used to perform a 281 energy groups calculation, using the IDT solver from APOLLO3 [10]. Cross-sections are then homogenized for the core-level calculation according to the geometry in Figure 4.3b and condensed from 281 to 26 energy groups.

(a) pin by pin (b) homogenized

Figure 4.3 – IDT 2D geometries modeling

On the core side the homogenized 2D geometry in Fig. 4.4 has been used. Unlike the previous case, this configuration represents a thermal reactor (for which leakage is less important than in fast neutron reactor) and it has an axially homogeneous geometry; thanks to that, using a 2D geometry permits to reduce the resource demanding of a calculation without impacting considerably the modeling accuracy. Fluxes and importances calculations are performed with the MINARET Sn solver from APOLLO3 [12], using 25388 triangular meshes. With these options, the calculation for the core step takes about 20 minutes on 32 cores and 4 GB of RAM.

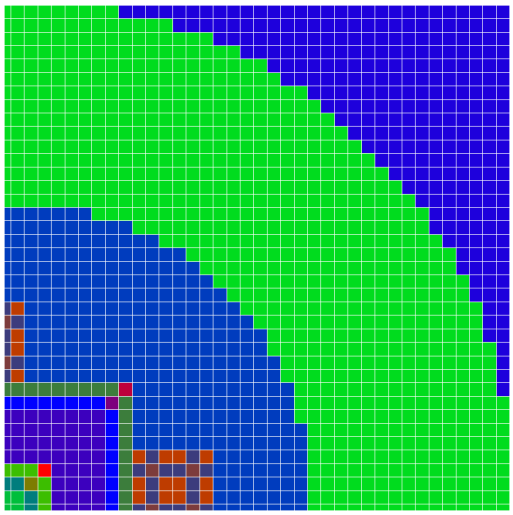

Figure 4.4 – MINARET 2D geometry

4.2.1 Validation

Thanks to the possibility to model the core through a 2D calculation requiring only 4GB of RAM, several different options have been tested, including a

	TRIPOLI4	IDT	MINARET 26G	MINARET 281G
K_{eff}	1.048557±2.2pcm	1.04678	1.04712	1.04655
Λ	18.62487±0.003 μs	-	17.73 μs	18.36
β	648.6 ± 0.8 pcm	-	647.1 pcm	648.7 pcm

Table 4.4 – Kinetic Parameters for EPICURE

core calculation with 281 energy groups; moreover, thanks to the recent effort to accurately model this experiment, the calculations are validated against a TRIPOLI4® [37] one, done on the same configuration (2D). The results obtained in the different steps, including the k-effective obtained in the IDT calculation, are listed in the Table 4.4.

On this configuration several tests have been done, the main two that will be presented are the effect of the weight flux on the final result and the comparison of the sensitivity calculation against direct calculations with the perturbed cross sections.

Concerning the effect of the weight flux, the beta has been computed with delayed nuclear data obtained with the procedure described in section 3.2 and with the same procedure but using a flat flux, therefore simple condensation. The results is that with 26 energy groups we obtain a beta of 647.1 pcm using a representative flux and of 640.7 pcm using a flat one. The same calculation can be done with 281 energy groups for which we obtained 648.7 pcm with a representative flux and 648.5 pcm with a flat one. Those results are consistent with the expectations and confirm that using a representative weight flux could mitigate with good results the fact of not processing delayed data through the two-step approach, i.e. in the lattice step.

In Table 4.4 can be seen the effect that the number of energy groups used in the calculation have on the Λ. Moving from 281 to 26 energy groups the error goes from 1.3% to 5% with respect the reference calculation (TRIPOLI). These values are compatible with the error shown for the ASTRID case and seem to support the fact that the energy mesh is the main source of error (i.e. neglecting the radial shield has a minor impact).

The calculation of sensitivities, that will be presented in the next section, is validated against direct calculations made by changing some input data. A sample of data, chosen to be representative of different possible behaviours, is increased by 1% and the calculation is run again. The chosen sample is:

- the capture cross-section of ^{238}U between 34 and 76 meV (energy group 24)
- the capture cross-section of ^{238}U between 4 eV and 52 eV (energy group 12)
- the capture cross-section of ^{235}U between 34 and 76 meV (energy group 24).

- the fission cross-section of ^{235}U between 10 and 34 meV (energy group 25)
- the ν_D of ^{235}U between 34 and 76 meV (energy group 24).

In all these cases the relative error between the predicted effect on the beta effective and the obtained perturbation is below 1%. To test the robustness of our implementation, we studied also a simplified model of a fast reactor with 6 energy groups. We checked the contribution by energy group and we tested capture, elastic, inelastic scattering and delayed data of ^{238}U, elastic scattering of ^{16}O, fission cross-section and delayed data of ^{235}U and in all the cases we found deviation from the predicted behavior to be within 1%.

4.2.2 Results

The results are summarized in two tables and we present only the results for the isotopes contributing to more than 1.0 e-4 to the total uncertainty on the beta effective. The contribution to the beta effective of the various isotopes can be

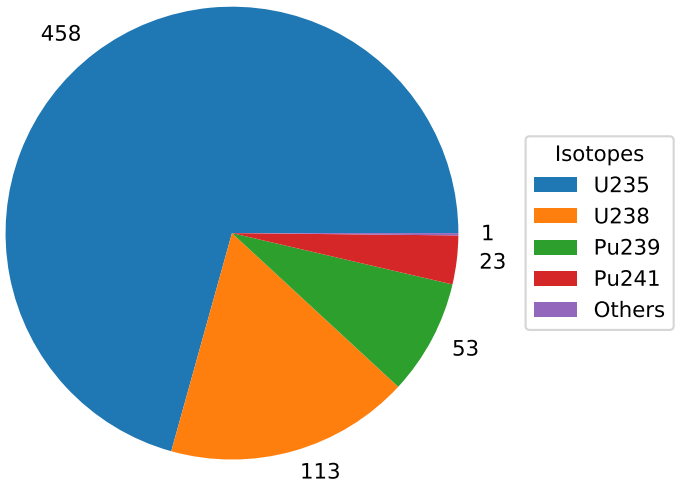

Figure 4.5 – Epicure

seen in Fig. 4.5; the main one is ^{235}U since it is the main fissile isotope and has a relatively high beta (initial plateau at 665 pcm), followed by ^{238}U and ^{239}Pu for which the same arguments as in the ASTRID case are valid: although ^{239}Pu contributes more to the fission rate than ^{238}U, the huge differences between in their delayed fraction (initial plateau at 1985 pcm for ^{238}U and at 227 pcm for ^{239}Pu) makes ^{238}U a more important contributor. To have a comparison of the

Table 4.5 – **Sensitivities (in %/%) of beta effective for the Epicure UM17x17 experiment.**

Isotope	Capture	Elastic	Inelastic	NXN	Fission	ν_{tot}	ν_d
^{1}H	-1.46 e-2	-8.51 e-2	-	-	-	-	-
^{16}O	2.30 e-3	-2.40 e-2	-3.38 e-4	-2.35 e-6	-	-	-
^{90}Zr	1.25 e-4	-2.62 e-3	-3.13 e-3	-3.93 e-6	-	-	-
^{91}Zr	-2.07 e-4	-5.23 e-4	-9.65 e-4	-1.80 e-5	-	-	-
^{92}Zr	6.04 e-6	-7.20 e-4	-1.69 e-3	-2.03 e-5	-	-	-
^{94}Zr	4.72 e-5	-7.16 e-4	-1.76 e-3	-3.36 e-5	-	-	-
^{235}U	-3.31 e-2	-1.41 e-4	-5.56 e-4	-3.07 e-5	**1.07 e-1**	**-4.39 e-1**	**7.06 e-1**
^{238}U	-2.94 e-3	-5.78 e-3	-3.29 e-2	-1.73 e-3	6.47 e-2	**-1.30 e-1**	**1.74 e-1**
^{239}Pu	6.46 e-2	-4.76 e-5	-2.21 e-4	-1.09 e-5	**-1.51 e-1**	**-3.58 e-1**	8.24 e-2
^{240}Pu	4.48 e-2	-1.91 e-5	-1.16 e-4	-3.20 e-6	-3.25 e-3	-5.25 e-3	1.02 e-3
^{241}Pu	6.94 e-3	-5.95 e-6	-3.17 e-5	-6.48 e-6	-8.40 e-3	-6.33 e-2	3.48 e-2
^{242}Pu	5.08 e-3	-8.94 e-6	-3.16 e-5	-1.53 e-6	-4.18 e-4	-9.49 e-4	3.61 e-4
^{241}Am	1.09 e-2	-2.18 e-6	-1.72 e-5	-1.75 e-7	-6.81 e-4	-9.60 e-4	8.93 e-5

different contributions to the fission rate, ^{235}U accounts for 75% of the fissions, followed by ^{239}Pu with 16% and then by ^{238}U with 6%.

For what concern sensitivities, as in the previous case, the main conclusion is that direct effects are the dominant contributors as can be seen in Table 4.5. Also in this case all ν_{tot} have a negative impact on the beta (increasing the denominator) while the ν_D has a positive impact (being at the numerator).

We can notice that the main isotopes contributing to the sensitivity of the beta effective are ^{235}U with a positive effect through the fission cross-section and ^{239}Pu with a negative sensitivity on the fission cross-section. This can be explained, as before: in a mixed UOX-MOX system the β-effective is an average of the beta of the main fissioning isotopes and since the beta of ^{235}U is more than three times larger of the one of ^{239}Pu, an increasing the relative fission rate of ^{235}U has a positive effect on the beta. Among the indirect effects, we can observe non-negligible effects from the capture of isotopes present at high concentration, such as ^{1}H, ^{16}O, U and Pu, the elastic scattering of ^{1}H and ^{16}O and the inelastic scattering of ^{238}U. However, all these indirect contributions are at most of the order of 10^{-2} %/% and one order of magnitude smaller than the direct ones. Regarding the elastic and inelastic scattering, all the effects are negative. By looking at the energy distribution of sensitivity we can see, as before, that the main contribution comes from the energy groups above 1 MeV (appendix B). Even if in this case the relative importance of ^{238}U is smaller compared to the ASTRID case, above this energy, the contribution to the beta effective from the fissions of ^{238}U are an important part of the total beta. This explains why increasing the scattering and therefore decreasing the energy of neutrons below the ^{238}U threshold has a negative impact on the beta. The sensitivities to the spectrum, total and delayed, are not listed in the table (4.5) since, as before, their total value is the same as the total value of the ν, total and delayed, and therefore can be read from there; however it has a different energy distribution that has been used for the uncertainty calculation and can

Table 4.6 – **Uncertainty propagation (in %) of beta effective for the Epicure UM17x17 experiment. Negative values stand for imaginary values, i.e. negative contributions to the overall variance.**

Isotope	Capture	Elastic	Inelastic	NXN	Fission	ν_{tot}	ν_d	χ	TOTAL
^{1}H	0.04	0.14	0.00	0.00	-	-	-	-	0.15
^{16}O	0.05	0.08	0.00	0.00	-	-	-	-	0.10
^{90}Zr	0.00	0.01	0.02	0.00	-	-	-	-	0.02
^{91}Zr	0.00	0.00	0.01	0.00	-	-	-	-	0.01
^{92}Zr	0.00	0.01	0.01	0.00	-	-	-	-	0.01
^{94}Zr	0.00	0.01	0.01	0.00	-	-	-	-	0.01
^{235}U	0.04	0.00	0.00	0.00	0.04	-0.07	**2.23**	0.11	**2.23**
^{238}U	0.01	0.00	0.15	0.04	0.02	0.04	0.57	0.04	0.60
^{239}Pu	0.10	0.00	0.00	0.00	0.13	-0.04	0.50	0.16	0.55
^{240}Pu	0.07	0.00	0.00	0.00	0.02	0.00	0.00	0.00	0.08
^{241}Pu	0.02	0.00	0.00	0.00	0.01	0.03	0.17	0.10	0.20
^{242}Pu	0.06	0.00	0.00	0.00	0.00	0.00	0.00	0.00	0.06
^{241}Am	0.03	0.00	0.00	0.00	0.00	0.00	0.00	0.00	0.03
TOTAL	0.16	0.16	0.16	0.04	0.14	-0.06	**2.36**	0.22	**2.39**

be found in appendix B.

The results show what was already anticipated from the sensitivities: that the indirect contributions are negligible with respect to the direct ones. In particular, the ν_D having an higher uncertainty with respect to the ν_{tot}, is the main source of uncertainty (97.5% of the global variance, with a major contribution from ^{235}U: 87% of the global variance). Among the indirect contributions, elastic scattering of ^{1}H and inelastic scattering of ^{238}U are the main contributors, but with contributions to the global variance less than 0.3 %, i.e. practically negligible. Also in this case, covariance matrices for delayed spectra are not available at this moment and therefore are neglected. This is probably an important source of underestimation since sensitivities to delayed spectra are of the same order of the ones to the ν_d and delayed spectra are poorly known [40]. We can indeed expect that their inclusion in uncertainty calculation can lead to a non-negligible increase of the total uncertainty computed in this work.

4.3 Conclusions and perspectives

This chapter has shown how the techniques described in Chapter 2 can be applied to characterize the kinetic parameters described in section 3. The discussion has been mainly focused on the β-effective to demonstrate how those methods can be used to provide physical insight about the properties of a system. The configurations used in this chapter are chosen to be as different as possible, in order to prove the validity of the methods on a wide range of cases.

Concerning the β-effective the main conclusion is that it is mainly sensitive to nuclear data involved directly in its calculation and less to the indirect contributions. The uncertainties propagated from nuclear data show a similar

dependence.

The main physical consideration that can be extrapolated from the interpretation of those sensitivities is that the β-effective, being a weighted average of the β of the isotopes participating to the chain reaction, depends mainly on the relative contribution of those isotopes. The relative contribution is mainly due to design choices (e.g. material composition), but looking for general considerations that can be inferred by nuclear data, we can see an always negative correlation with the β-effective value and any scattering cross-section (elastic,inelastic or nxn). The explanation to this is that, being ^{238}U the isotope with the highest β, and having a fission threshold at 1 MeV, any slowing down of the neutrons reduces the weight of this isotope and this has a negative impact on this parameter.

One of the perspectives of this work is to apply the same methodology to study the mean generation life time (Λ). One of the reasons that prevented those results to be presented in this work is that to apply GPT to the study of Λ, importances have to be computed using an anisotropic source, a problem that our solver is not able to handle yet. Another issue is that Λ does not depend on delayed nuclear data but has a dependence on the neutron velocity. This dependence, so far, has been implemented rigidly by using always the velocity associated to a kind of "mean energy" of the group. This limitation has a known impact on the accuracy of the results [39] and therefore different choices have to be considered (e.g. velocity preprocessing). Finally the possibility to extend this kind of analysis to the coefficients used in MPK can be considered.

Chapter 5

Transient Analysis

Contents

This chapter discusses three different transients analysed with the techniques presented in chapter 3. The transients chosen serve as examples to discuss the similarities and the differences of those methods, representing situations with different peculiarities. Section 5.1 presents the results relative to a typical transient of an instantaneous rod extraction. In section 5.2 a case with zones much different from each other is considered to highlight the differences that could occur by using different modeling techniques. In section 5.3 an experimental case is reproduced using some of those methods to demonstrate their potential.

5.1 ASTRID

The first transient modeled takes place in the ASTRID CFV V1 core [35] already described in Section 4.1. The transient we analyzed is a step change where the red-circled rod in region 1 (see Fig. 5.1) is instantaneously removed from the core. The same transient has been recently analyzed in [22] with the ECCO/ERANOS code [36]. Since this core has a $2\pi/3$ rotational symmetry, for the application of the MPK we chose three symmetric regions as shown in Fig. 5.1, as was done in the [22].

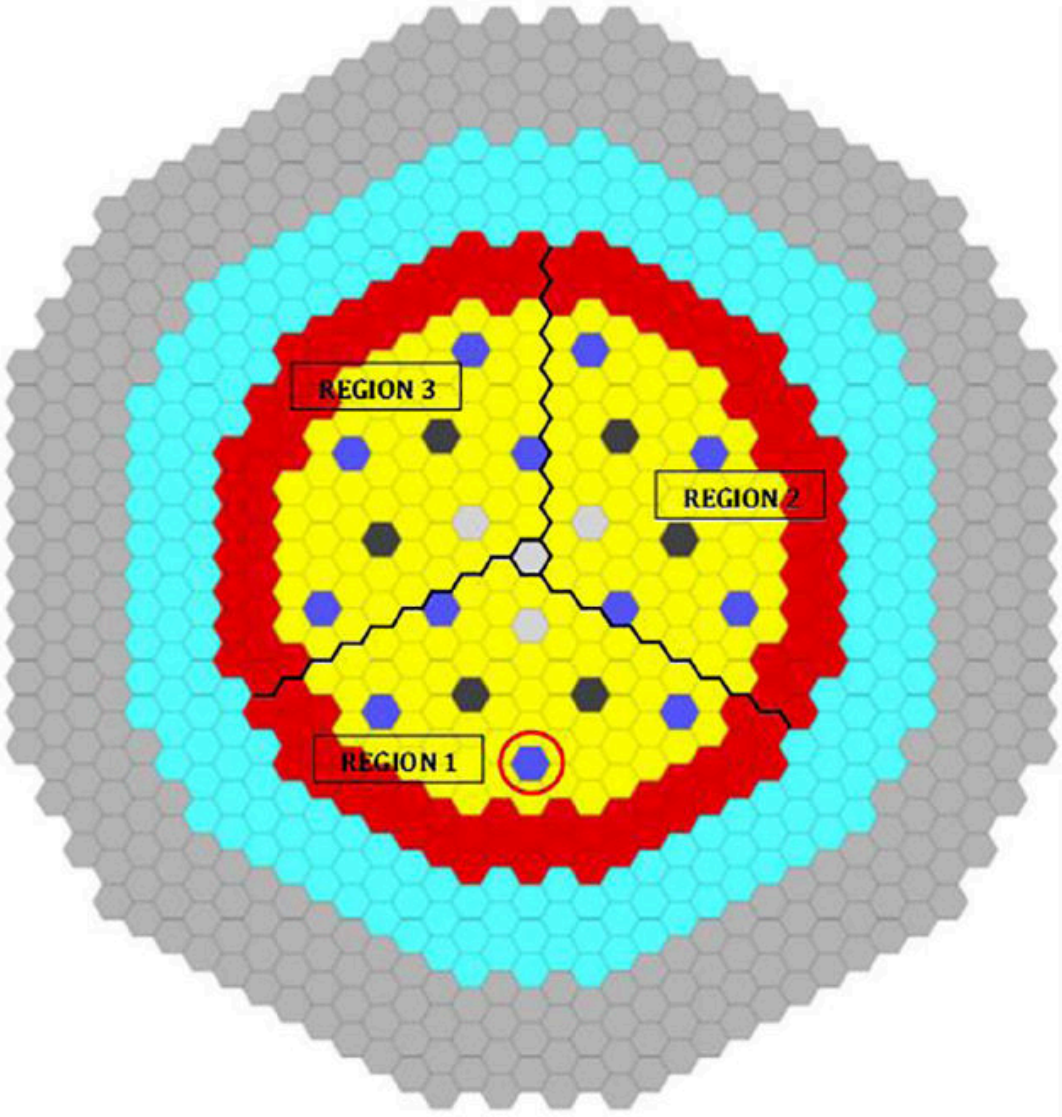

Figure 5.1 – ASTRID CFV-V1 - Color code: Yellow: inner fuel - Red: outer fuel - Light blue: reflector - Grey: shielding - Dark blue and black: control rods - White: inert sub-assemblies

The reactivity injected is ρ=349pcm and, since the β is equal to 369 pcm, the system remains below prompt criticality but with a small margin.

5.1.1 Results

We present three sets of results, one for PK and two for MPK (one for Avery's model and one for Kobayashi's model). The total population evolution, sum of the populations over the three regions) is plotted in Fig. 5.2.

As can be seen there is no major difference between the various modeling techniques for what concerns the total population.

Looking at the population repartition (Fig. 5.3), a quick change in the neutron

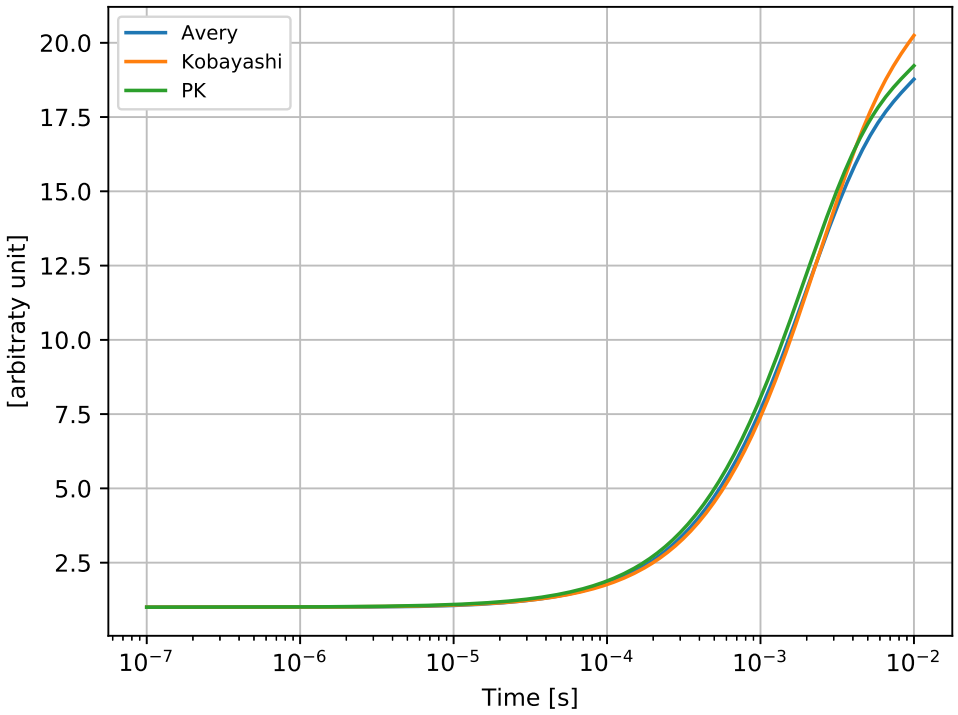

Figure 5.2 – Total neutron population evolution - ASTRID model

population distribution, taking place before the prompt jump, can be seen in both MPK models. This redistribution of the individual neutron populations, however, has no effect on the evolution of the total one and, therefore, PK remains a good approximation as far we are not interested in local values.

For what concerns the asymptotic behavior (Fig. 5.4) no major differences exist among the various models. We believe that the existing minor discrepancies can be explained by numerical error during the coefficient calculation and by the use of the k-eigenvalue instead of the ω one.

Looking at the eigenvalues of the transition matrix $\mathcal{M}$ (see section 3.1.2), plotted in Fig. 5.5, we can see how some eigenvalues cluster around the opposites of the decay constants of precursor families [42]. Those values are 7 for PK (as the number of families minus one) and 23 for Kobayashi and Avery (as the number of families times the number of regions, minus one). For PK this can be understood by looking at the inhour equation plot (Fig 3.1 in section 3.1) where it can be seen how the roots are in between the vertical asymptotes located at $\omega = -\lambda_i$, except for the two external ones. We notice also a single positive eigenvalue (the dominant one) with a similar value for all the models (with the biggest discrepancy, between PK and Kobayashi's MPK being about 8%). On top of these values, representing the effects that precursors have on the system, and that are common between PK and MPK, there are sets of eigenvalues, negative and with large absolute values, enabling shape changes

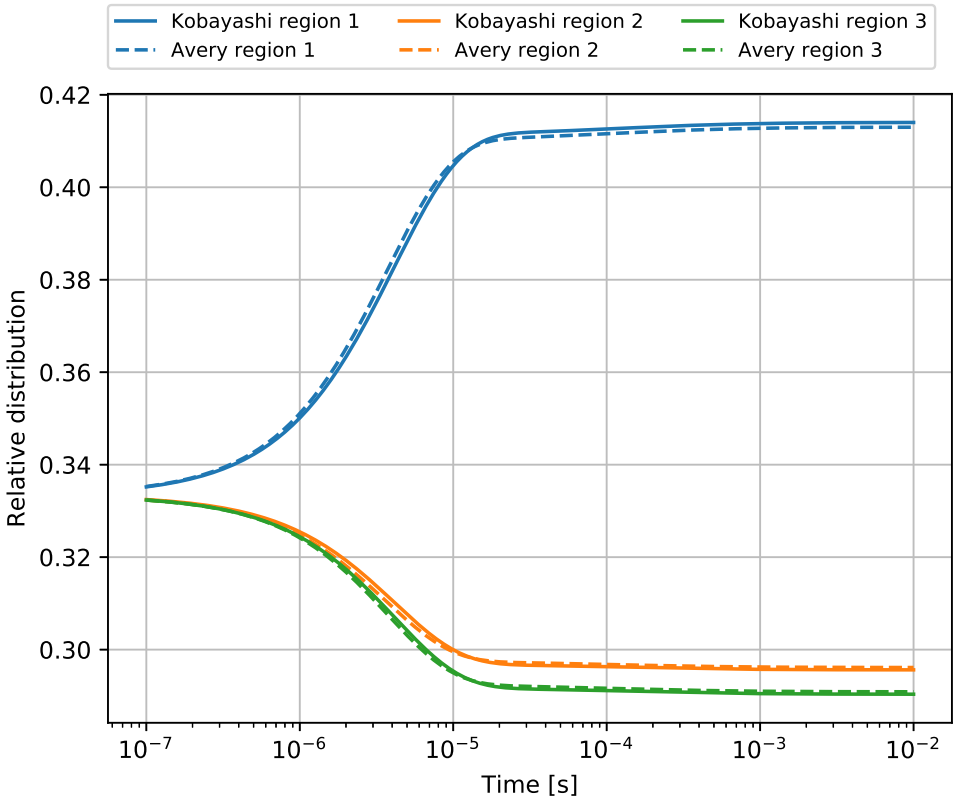

Figure 5.3 – Relative neutron population evolution - ASTRID model

on a very short timescale. The one between -10^3 and -10^2 s^{-1} is common between PK and and MPK and is the one related to the prompt jump. All the others are related to relative population changes (that we will call shape changes) and are peculiar to MPK. For all the MPK models, if we compare these eigenvalues (those $< -10^2$ s^{-1}) with the ones we obtain from the prompt sub-matrix (defined is section 3.1.2 as the matrix describing the system without precursors) we notice that we get very closely the same eigenvalues (maximum relative error below 10^{-8}), except for the "prompt jump" eigenvalue for which we have a relative error of 2%. This seems to show that, as eigenvalues get closer to the regions occupied by those due to precursors, those starts to interfere and the system can't be seen as a composition of prompt and delayed effect anymore.

5.2 Coupled Fast-Thermal reactor

The second system modeled is a simplified 1D model of a coupled fast-thermal coupled reactor. Although being an extremely simplified configuration, this model aims at having short computation time while retaining enough heterogeneity to highlight the differences among the modeling techniques presented so far. The slab is divided into 6 regions as can be seen in Fig. 5.6 where reflection condition is applied to the left boundary and vacuum condition to

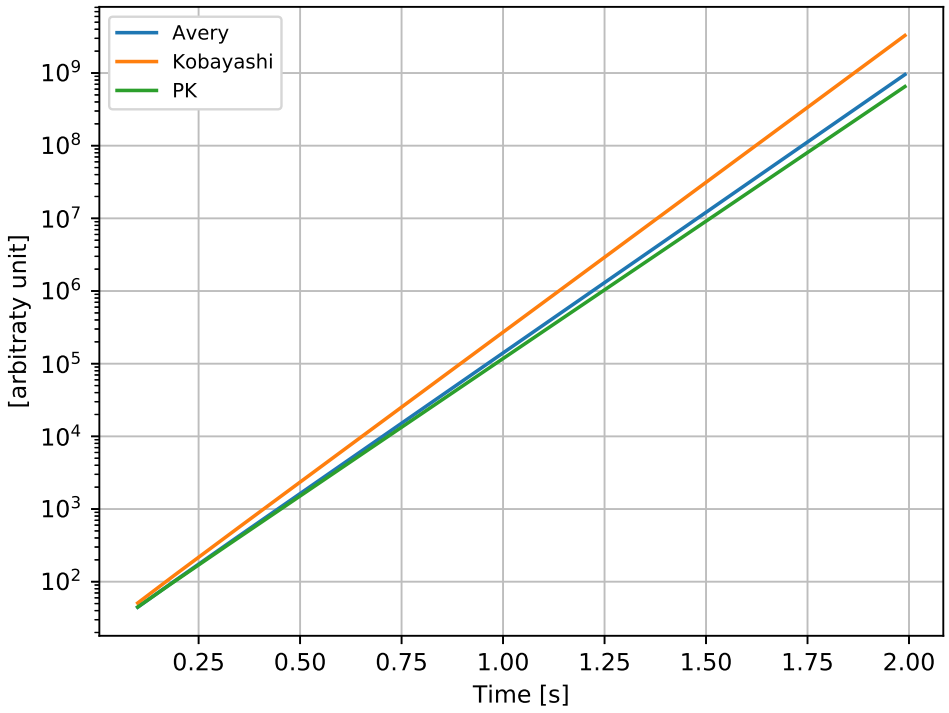

Figure 5.4 – Asymptotic neutron population behavior - ASTRID model

the right one; from left to right there is a central fast zone (Fast, F), a filter to absorb thermal neutrons (Absorber, A), a natural uranium transition zone (Buffer, B), an enriched uranium plate (Converter, C), a thermal zone (Thermal, T) and a water reflector (Water, W).

The material used for the fast zone is the cell used in the ERMINE V program of the MINERVE experimental reactor, in the center of the ZONA-1 core [43]. This cell is composed of 6 MOx rodlets, 2 natural UOx rodlets, and 8 sodium rodlets, combined in a 2 inch square. The filter to absorb thermal neutrons is made up of natural B_4C rodlets and the natural uranium in the transition zone is in the form of UO_2 rodlets. The UO_2 rodlets in region C are enriched at 30% in ^{235}U and the UO_2 rodlets in the thermal zone are arranged in a 26 cm square lattice and have 3.7% enrichment in ^{235}U. Water is present only in the thermal zone and in the reflector. All the materials have been homogenized by ECCO/ERANOS [36] and provided to APOLLO3® using a 33 group energy mesh (more detail can be found in [44, 45]).

The basic idea behind this configuration is that the absorber, the buffer and the converter help to decouple the fast zone from the thermal one, as most of the fissions take place in these two latter zones.

We can then introduce a perturbation, removing the absorber and the converter. In this way, we change the kinetic parameters of the reactor keep-

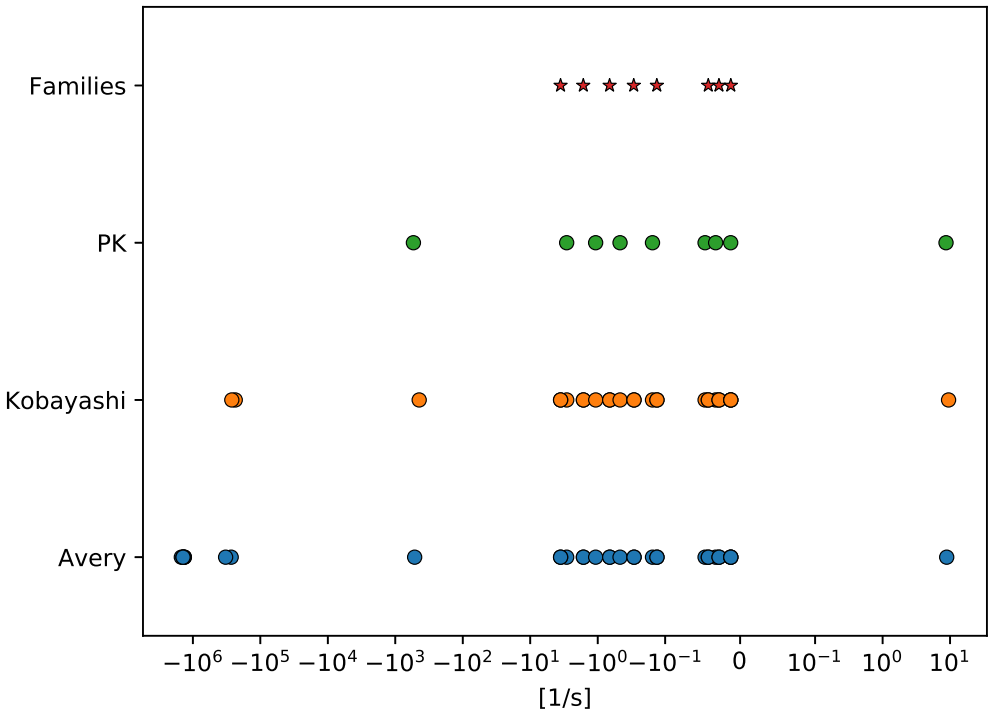

Figure 5.5 – Eigenvalues of the ASTRID model

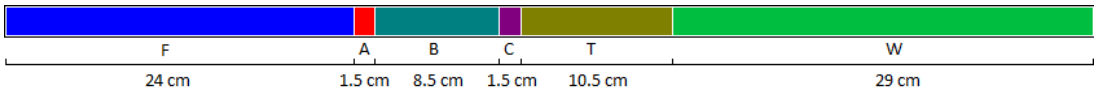

Figure 5.6 – 1D model of a coupled fast-termal reactor

ing the reactivity insertion positive but below prompt criticality (β=586pcm and ρ=284pcm). In order to do so we artificially replace the material in the converter zone (enriched uranium) with the one in the buffer zone (natural uranium) and remove 92% of the ^{10}B in the absorber zone.

In order to keep the transient simple and to focus on the neutronics, we simulate an instantaneous change without considering thermal feedback. The system is supposed to be at t=0 in steady state in the nominal configuration and to shift instantaneously to the perturbed configuration. In order to have a steady state system at t=0, we divide artificially all the coupling matrices by the k-effective of the nominal configuration, that is 1.11706.

5.2.1 Results

For this configuration, we present five sets of results. One set is obtained by applying PK, and four are obtained by applying MPK. For MPK we have 2 sets using four regions (one with Kobayashi's and one with Avery's models), one for each homogeneous fissile zone (that are F, B, C and T in Fig. 5.6) and

PK (k_{eff})	1.11706
Kobayashi (k_{jk})	$\begin{bmatrix} 0.88923 & 0.29334 & 0.15291 & 0.05134 \\ 0.03203 & 0.12125 & 0.07372 & 0.02288 \\ 0.12134 & 0.28680 & 0.38487 & 0.19834 \\ 0.16048 & 0.41637 & 0.56683 & 0.77045 \end{bmatrix}$
Avery (k_{jk})	$\begin{bmatrix} 0.89357 & 0.28779 & 0.15006 & 0.05032 \\ 0.03211 & 0.12127 & 0.07364 & 0.02286 \\ 0.12139 & 0.28695 & 0.38502 & 0.19824 \\ 0.16864 & 0.43211 & 0.58580 & 0.75710 \end{bmatrix}$

Table 5.1 – k_{eff} and k_{jk} of the nominal configuration (before division by k_{eff})

two sets using 6 regions (one with Kobayashi's and with one Avery's models), where we split in half the 2 main fissile regions that are F and T.

As an example, we present the main kinetic parameters and coupling matrices we obtained for the nominal case.

The k_{eff} and k_{jk} are listed in Table 5.1, mean generation time and its MPK generalizations are in Table 5.2, beta effective and β_{jk} in Table 5.3. A first observation can immediately be made on the data presented in Table 5.1, the dominant eigenvalue of both k_{jk} matrices is equal to k_{eff}, as it should be by construction. This is a first verification of our implementation and shows how, in MPK, the k_{jk} matrix has a role similar to the one that the scalar k_{eff} has in PK. Regarding the data in Table 5.2 they represent the mean neutron generation life times. These data are mainly sensitive to the neutron spectrum and show how the spectrum gets softer moving towards the thermal zone (last line). We can also observe that, looking at the Avery's l_{jk}, discriminating the various regions where neutrons are generated (different columns represent different departing regions) has limited effects with respect to the importance that has the region where the neutrons end (different lines represent different ending regions).

Finally, looking at data in Table 5.3 we can see how the delayed neutron fraction has a very heterogeneous distribution, mainly depending on where neutrons are produced (therefore presenting similar values along each column). The main exception is the second line, representing the neutrons ending in the natural uranium zone (zone B in Fig. 5.6), that have considerably smaller effective delayed fraction with respect to neutrons born from same regions (therefore being in the same column) but ending in a different one. This can be explained by the fact that delayed neutrons are produced with considerably

PK (Λ) [μs]	9.9915
Kobayashi (l_j) [μs]	$\begin{bmatrix} 0.3125 \\ 0.4241 \\ 3.7227 \\ 28.232 \end{bmatrix}$
Avery (l_{jk}) [μs]	$\begin{bmatrix} 0.2465 & 0.3491 & 0.3935 & 0.4495 \\ 0.2938 & 0.1370 & 0.2646 & 0.6829 \\ 2.8120 & 2.5776 & 2.4007 & 4.2755 \\ 17.8861 & 18.8878 & 19.1796 & 25.4637 \end{bmatrix}$

Table 5.2 – Λ, l_j and l_{jk} of the nominal configuration

PK (β_{eff}) [pcm]	586.9
Kobayashi (β_{jk}) [pcm]	$\begin{bmatrix} 332.4 & 1097.1 & 497.3 & 299.2 \\ 119.3 & 289.9 & 170.0 & 194.4 \\ 339.8 & 1486.3 & 776.3 & 715.0 \\ 304.2 & 1371.8 & 727.6 & 807.3 \end{bmatrix}$
Avery (β_{jk}) [pcm]	$\begin{bmatrix} 332.7 & 1097.1 & 496.7 & 298.4 \\ 119.2 & 289.9 & 170.0 & 194.3 \\ 339.8 & 1486.1 & 776.2 & 714.7 \\ 307.7 & 1390.7 & 738.7 & 809.4 \end{bmatrix}$

Table 5.3 – β_{eff} and β_{jk} of the nominal configuration

smaller energies, and therefore have less probability to induce fission in the buffer region containing mainly ^{238}U, that has a fission threshold at 1 MeV.

The first quantity on which we would like to focus on is the total neutron population evolution during the transient, that can be seen in Fig. 5.7.

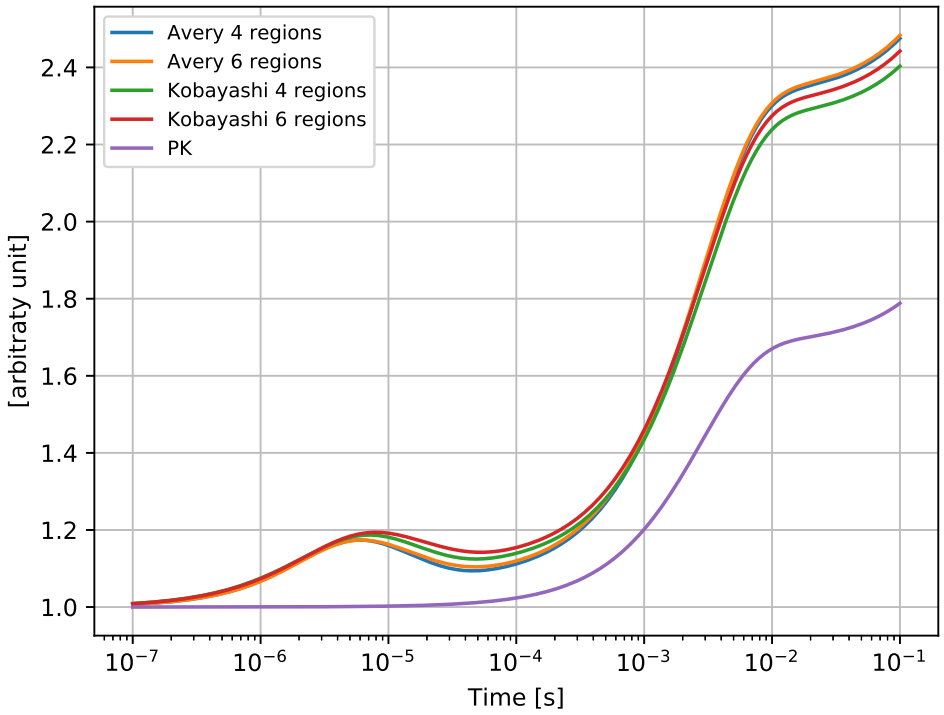

Figure 5.7 – Total neutron population evolution - 1D model

This time, on a short time scale, there is a huge difference between the results obtained with PK and those obtained with MPK, while all the MPK cases provide similar results. In particular, all the MPK curves have a bump before $10^{-5}s$ that is completely absent in the PK one. After that, there is the classical prompt jump that, however, in the MPK cases has a bigger amplitude. Looking at the differences among the various MPK, subdividing the main regions has virtually no effect on the Avery modeling and leads to a slight increase of the total neutron population modeled by Kobayashi MPK. Compared to Avery, Kobayashi has a slightly bigger population before the prompt jump and slightly smaller afterwards. As commented in the previous case, these minor differences can be due to numerical errors and probably shouldn't be interpreted as physical features of the models.

Looking at Fig. 5.8 we can see the relative distribution of the neutron population in the various regions. We can notice how the redistribution of the neutron population takes place at the same time as the first bump in the total population evolution and is almost complete before the prompt jump. We can

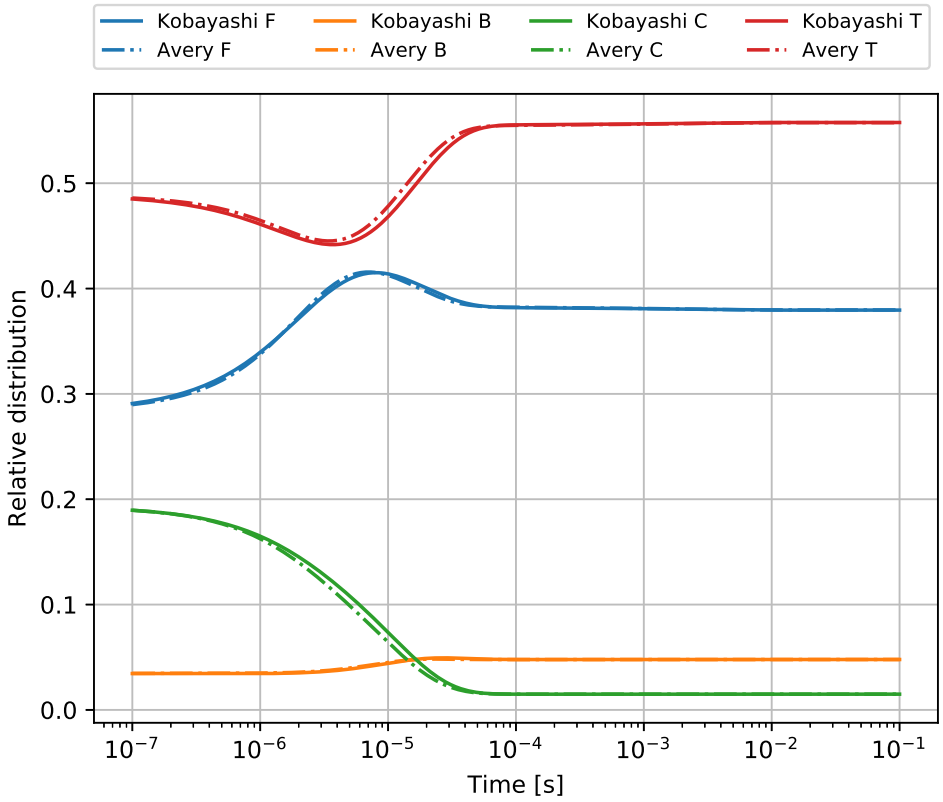

Figure 5.8 – Relative neutron population evolution - 1D model

also notice that no major difference appears between Kobayashi's and Avery's models.

Concerning the long time scale, all models present a coherent exponential behavior with Kobayashi's model having a slightly different time constant with respect to the other results and that changes slightly with the further subdivision of the main fissile zones. This effect, even though of second order, could be due to the approximations made (e.g. the use of the k-modes instead of the ω-modes to compute the MPK coefficients) and should be further investigated.

To conclude, we can look at the eigenvalues of the problem in the different models, plotted in Fig. 5.10 where, on the horizontal axis we have the real part of the eigenvalues on a symmetric log scale. We have to remark that all the eigenvalues are real, except for Avery's MPK with 6 regions that has 10 complex eigenvalues (5 couples of complex conjugates); in all the cases however the real part is much larger than the imaginary part, meaning that the damping effect is dominant with respect to the oscillating behavior and therefore we focus only on real parts.

In the first line we plotted the decay constant of each precursor family, so to show how some of the various eigenvalues cluster around the eight $(-\lambda_i)$ with a multiplicity equal to the region number (as already discussed by Henry [42] and in the previous section). As expected, in all cases, we have one positive

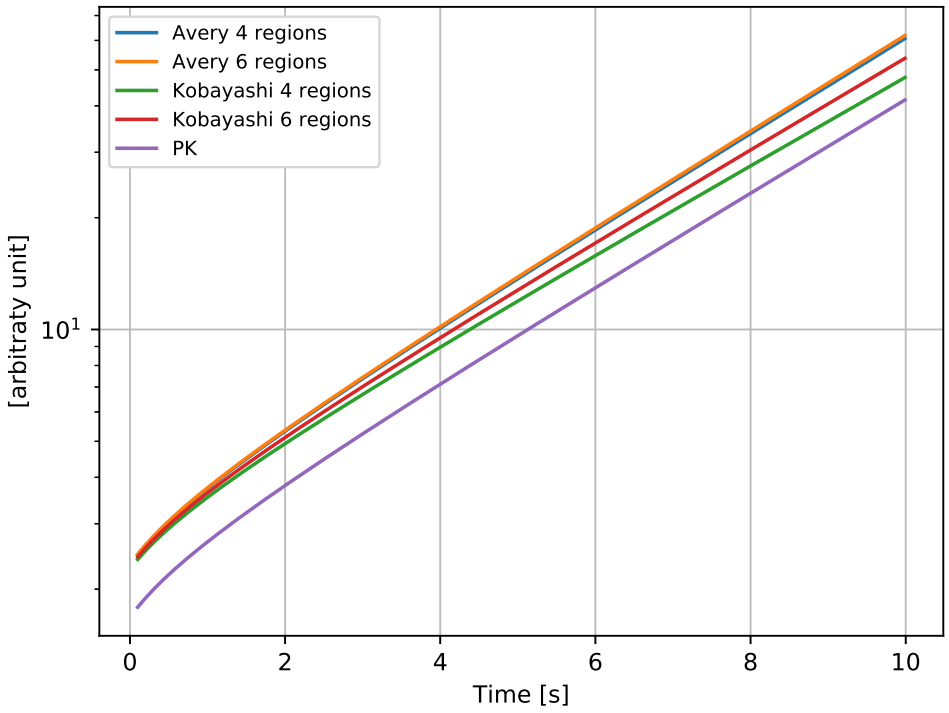

Figure 5.9 – Asymptotic neutron population behavior - 1D model

eigenvalue with similar value for all the methods (with the biggest discrepancy being between Avery's and Kobayashi's models and of about 7%). As before, there are several eigenvalues on a very short timescale. All of those are equal to the ones obtained from the relative prompt sub-matrix (maximum relative error below 10^{-8}), except for the one relative to the prompt jump (the one appearing also in PK); In all the models, the relative difference between the promt eigenvalue obtained from the full matrix and from the prompt one is around 0.3%. Looking at the different times scale, it can be seen how the bump noticed in Fig. (5.7), that occurs at 10^{-6} s, is mainly due to the prompt behavior of the system.

5.3 MUSE

The MUSE-4 experiment has been carried out at the MASURCA nuclear facility at CEA Cadarache. The purpose of the this program was to operate a fast subcritical core coupled with a neutron source to simulate an ADS reactor [46].

In Fig. 5.11 a cross-cut of the geometry of the MUSE core can be seen with the various materials that are present in the configuration that has been studied. To model this system a set of three homogenized materials (lead, fuel and reflector) have been condensed with the ECCO/ERANOS code [36] on

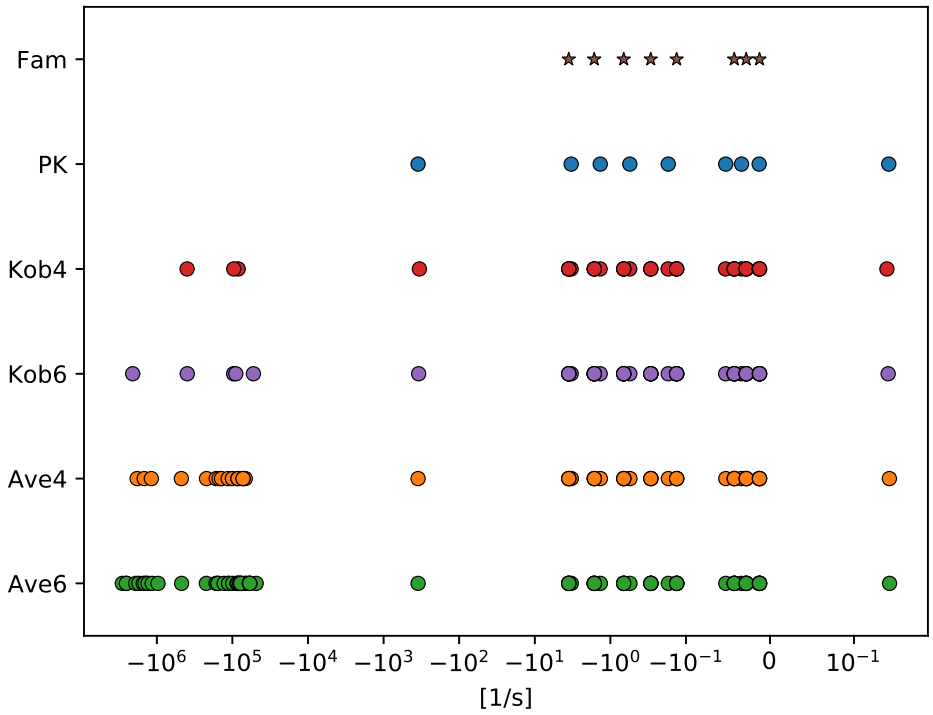

Figure 5.10 – Eigenvalues of the 1D model

the usual 33 group energy mesh. The geometry produced for the APOLLO3 calculation can be seen in Fig. 5.12; to further reduce the memory requirement only one fourth of the horizontal cut of reactor has been modeled and the reflection condition is applied to the lower and left boundaries of the shown plane; also axially the reactor is considered symmetric and only half has been used in the calculation, leading to the modeling of just one eight of the whole geometry. Without pretending to reproduce the exact geometry the square of the APOLLO3 geometry shown in Fig. 5.12 has a side of 5.3 cm, therefore half of the squares in Fig 5.11. In the APOLLO3 geometry, moving from the center towards the outer part we have (region numbers correspond to the MPK description of the system):

- Lead (violet)
- Lead (dark green)
- Fuel - Region 1 (light green)
- Fuel - Region 2 (dark green)
- Fuel - Region 3 (blue)
- Fuel - Region 4 (light green)
- Reflector - (blue)

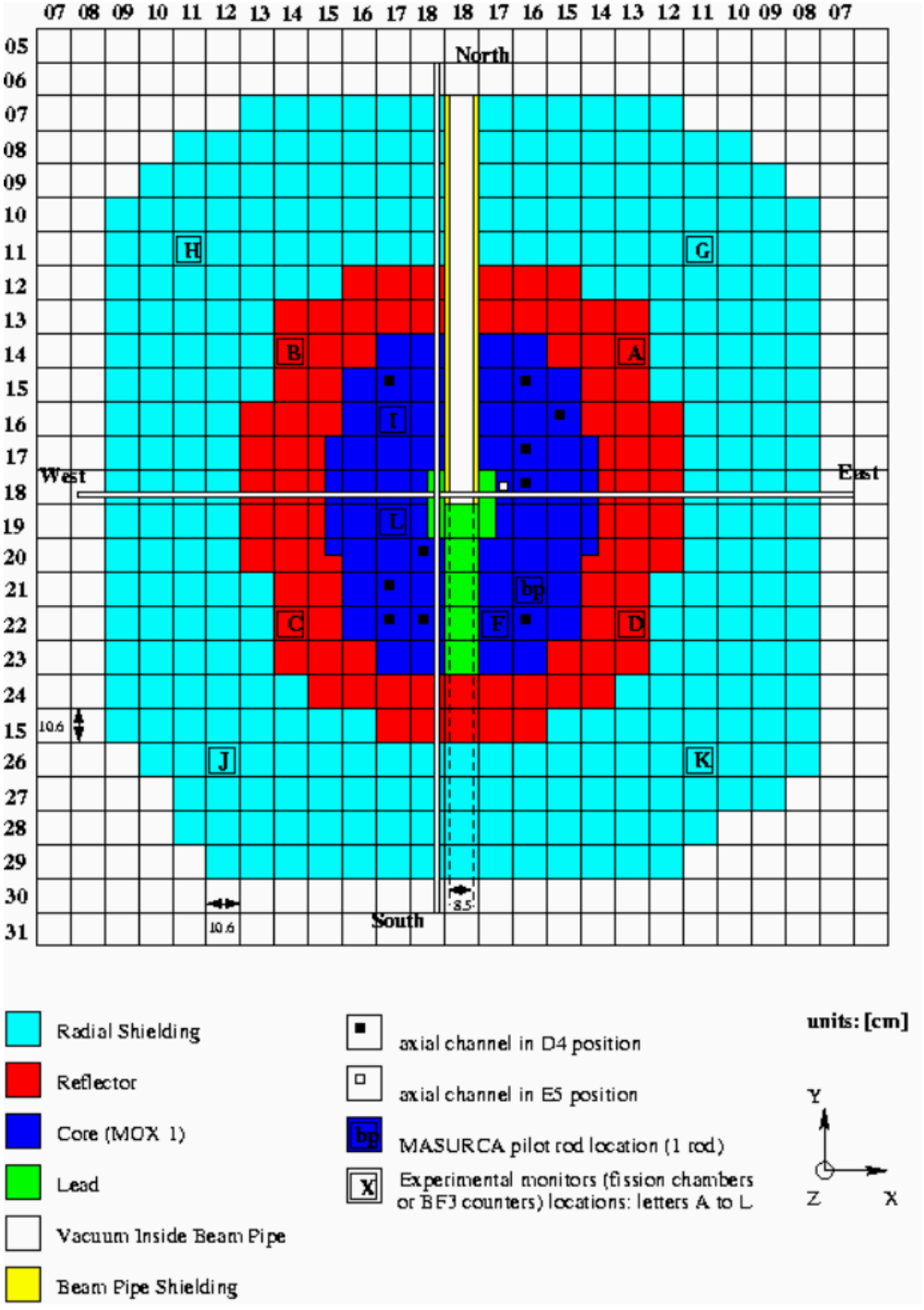

Figure 5.11 – Horizontal section of the experimental configuration - MUSE

- Fission chamber - Region 5 (the small brown square)
- Neutron shield - (red)

Reflector and neutron shield have been modeled using the same material and the fission chamber has been modeled using the same material used for the fuel.

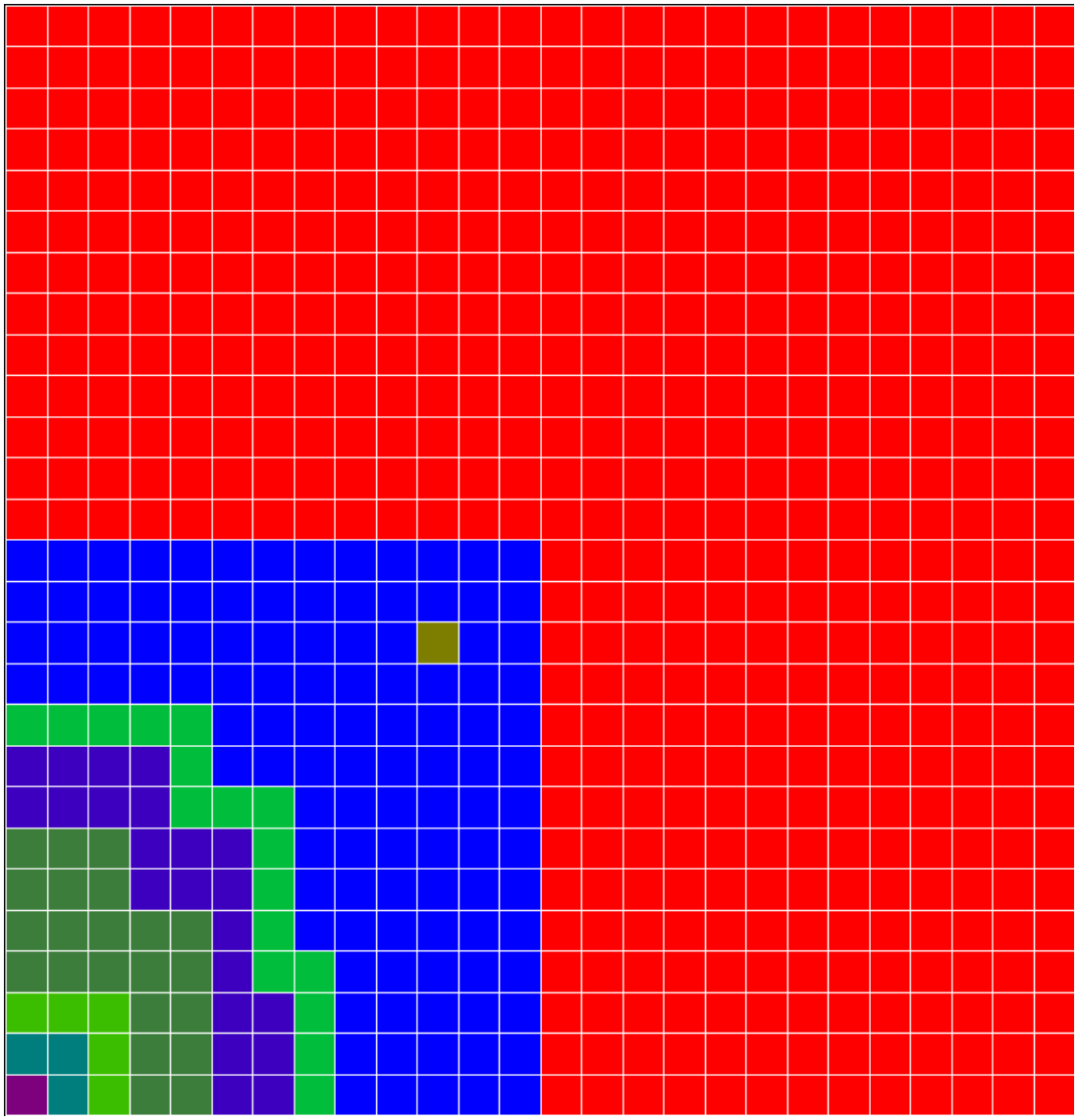

Figure 5.12 – MUSE - APOLLO3 geometry

Axially the geometry has been deeply simplified, using only seven planes, the regions are kept concentric but the core has been modeled as a prism. The total height (50.7 cm $\times$ 2) and the active one (29.5 cm $\times$ 2) have been adjusted to exploit all the memory at our disposal (64 GB) and to reproduce the k-effective of the configuration we are studying (k-effective = 0.97). While this can be a considerable deviation from the real geometry, for the purpose of this study it can be considered to be acceptable. We modeled this system using Kobayashi's MPK with 5 regions, numbered as in the previous list. Further information about the experimental configuration can be found in the final report of the MUSE program where the configuration that is being discussed is called SC2 [46].

5.3.1 Results

The transient reproduced during the experiment is a neutron injection by means of a source during 0.5 μs and then the source is cut off and the system is left to evolve naturally. Since the source is located in the central lead zone, we reproduced this transient by forcing a source term only in the first region, the closest to the lead zone. The system is modeled only using the Kobayashi's formalism since in the Avery's one, S_{jk} represents the neutrons going from a region to another and therefore the same approach can't be used. The results

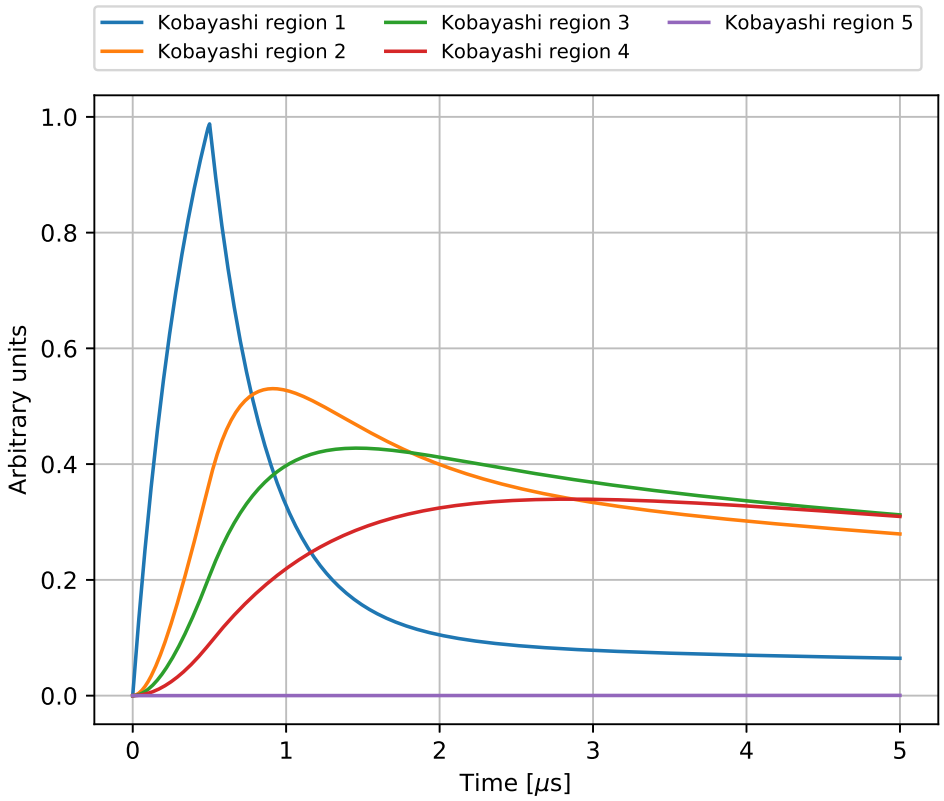

Figure 5.13 – Neutron population evolution over the first 5 μs - MUSE

for the first 5 μs are shown in Fig 5.13 on a natural scale. The delays among the various regions are clearly visible. The initial peak, due to the source located in the region 1, vanishes within a few μs and the exponential decrease is rapidly established.

Looking at the neutron population in the various regions, over the first 100 μs on a semi-logarithmic scale (Fig. 5.14) we can notice how, even though the decrease has the same slope in all the regions, in the fifth (that is the fission chamber in the reflector) it is considerably delayed and smoothed.

To demonstrate the potential of MPK, in Fig. 5.15 we can see the data measured during the experiment and those obtained thanks to a Monte Carlo simulation [46]. Those data are in good agreement until 125 μs (with the initial pulse at around 20 μs) and, after that, the simulated data start to deviate

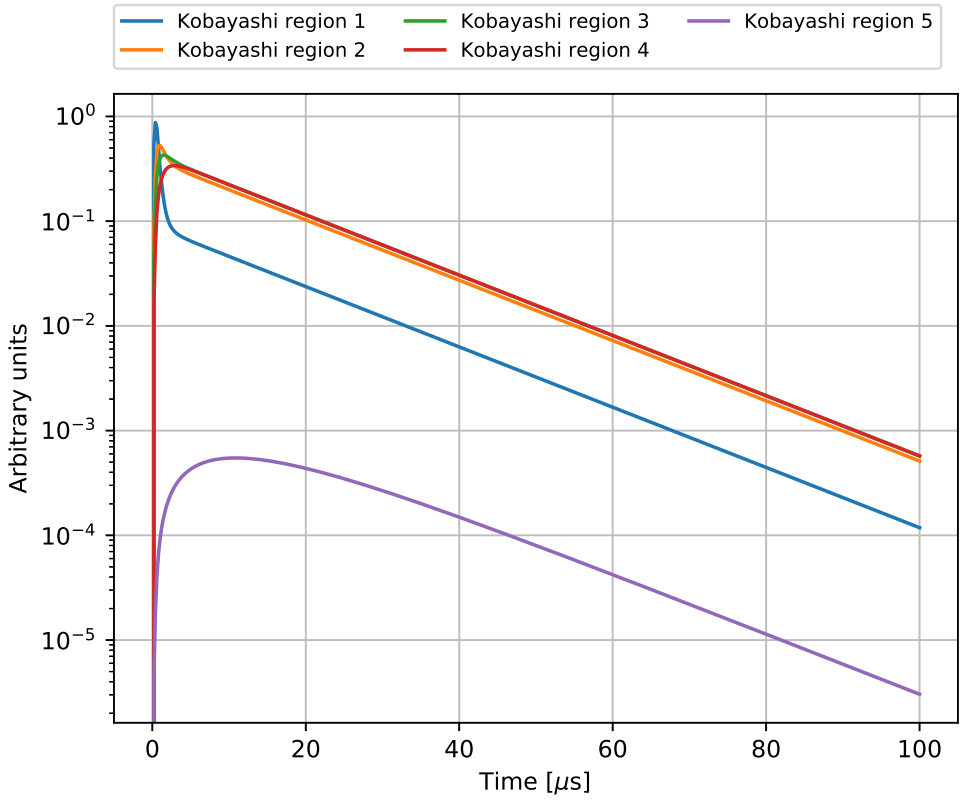

Figure 5.14 – Neutron population evolution over the first 100 μs - MUSE

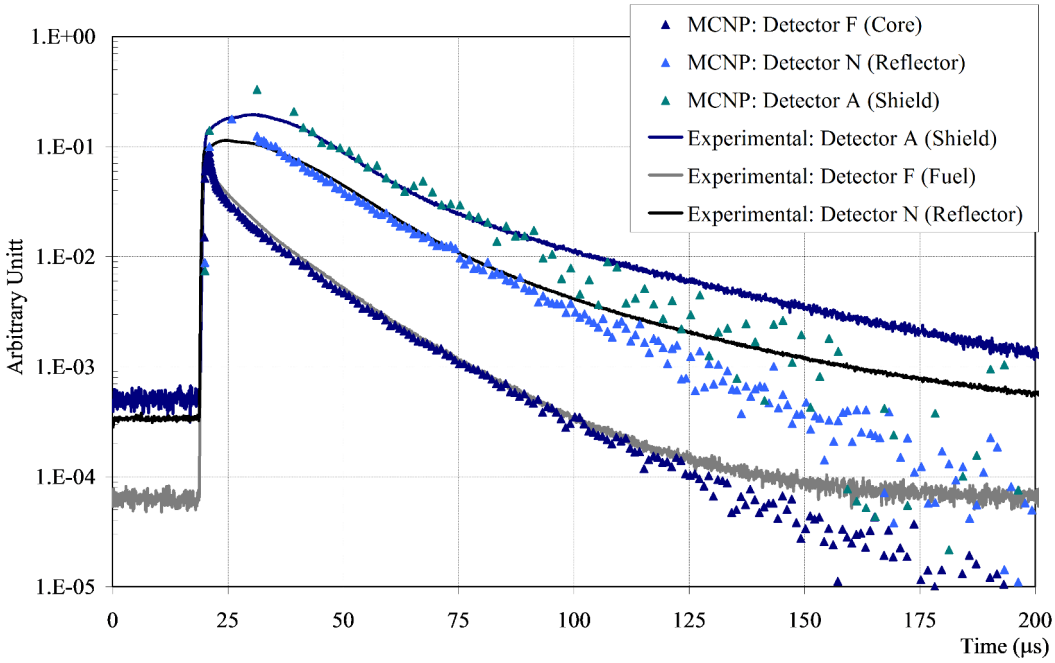

Figure 5.15 – Experimental data and Monte Carlo simulation - MUSE

from the measured ones. We can also notice how the dispersion of the simulated data, due to their Monte Carlo nature, increase during the transient. Notice

that, after the prompt response, the system evolves driven by precursors decay; therefore the discrepancy between experimental data and simulated ones is likely to be due to the fact that existing precursors populations before the source step are not properly modeled. Another indication in this direction is provided by the experimental data before the source injection (Fig. 5.15 before 20 μs). It can be noticed how the starting level of the signal in the detectors is a non-zero value. The prompt response measured by the detectors ends on the values measured before the source while simulated data goes below that level. The probable explanation can be that, while all the calculations are done starting without precursors, the typical experiment is performed by repeating source pulses (shorter than 1 μs) with 1 kHz frequency for about 3h; the experimental data plotted in Fig. 5.15 are the result of the sum of all of those pulses. Therefore it is reasonable to assume that, even if the background is measured before the experiment, those transients repeated over time lead to a build up of precursors that could affect the final part of the prompt transient.

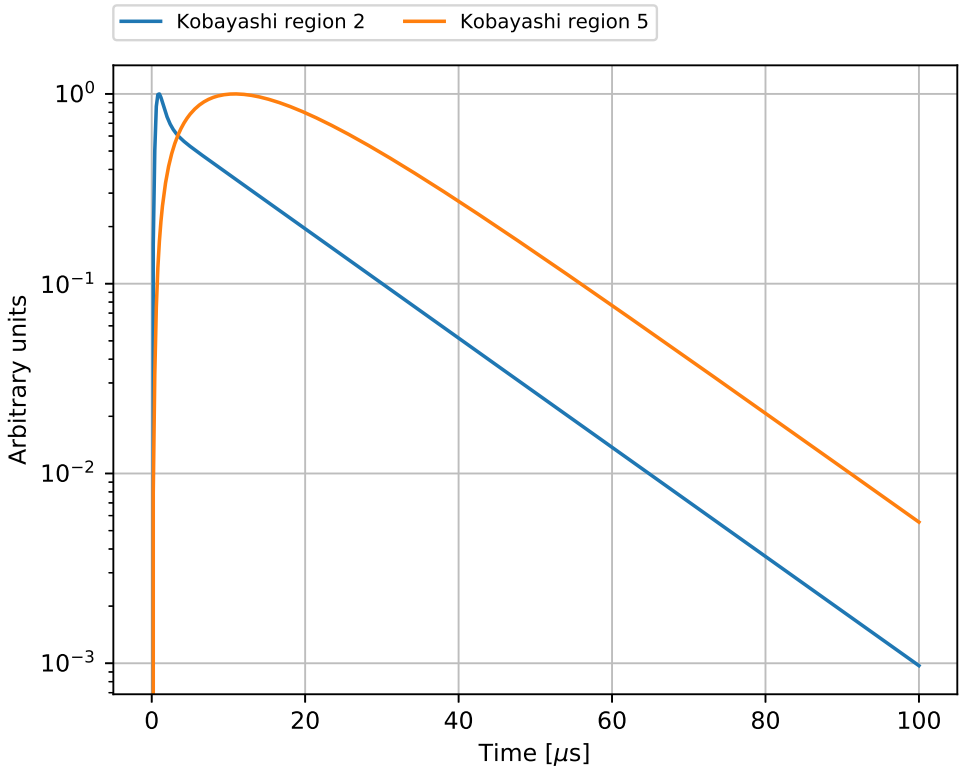

Figure 5.16 – Neutron population evolution over the first 100 μs normalized to 1 - MUSE

While the report relies on Monte Carlo simulation due to the incapability of PK to reproduce this phenomena, it can be seen in Fig. 5.16 how MPK results, normalized consistently with the experimental data, reproduce spatial effects, both the initial spike in the core and the delay of the maximum in the reflector.

As matter of comparison the total amplitude evolution modeled with PK and

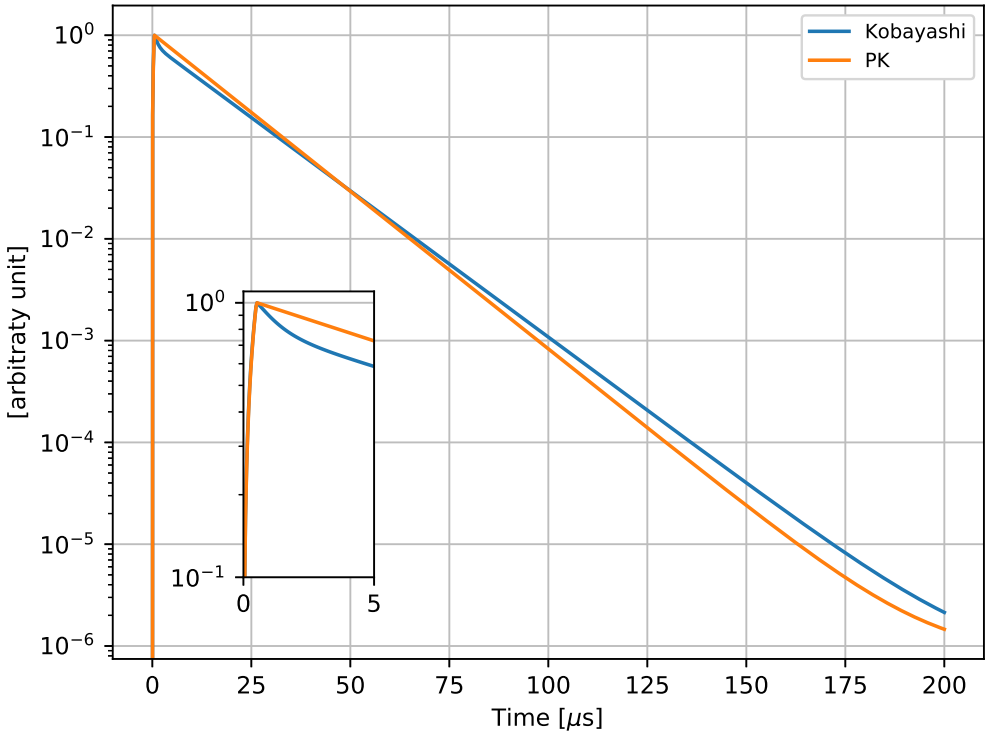

Figure 5.17 – Total neutron population evolution, PK vs MPK - MUSE

MPK can be seen in Fig. 5.18. The PK parameters obtained for this configuration are a β-effective of 332.8 pcm and a Λ of 0,47 μs and, as already mentioned, the k-effective of the modeled configuration is equal to 0.97. The whole set of kinetic parameters, including Kobayashi's one can be found in appendix E.1.

Finally, looking at the eigenvalues, even for this situation where no positive eigenvalue exists, the same behaviour of the previous case is found: some eigenvalues cluster around the opposite of the precursor families decay constants, the others are almost equal to the ones of the prompt sub-matrix. Again, all the eigenvalues specific to MPK, appear on shorter time scale. The main difference between this case and the previous two is that this case is sub-critical and the system is very far from critically (k-effective=0.97). For this reasons the eigenvalues linked to precursors are closer to the decay constants and there are eight of them, in contrast with the previous case were there are only seven. This can be understood by looking at the inhour equation plot and realizing that, being very sub-critical, we are moving towards the lower part of the asymptots.

5.4 Conclusions and perspectives

This chapter has shown how some of the methods described in Chapter 3 (PK and MPK) can be applied to model reactor transient and to characterize

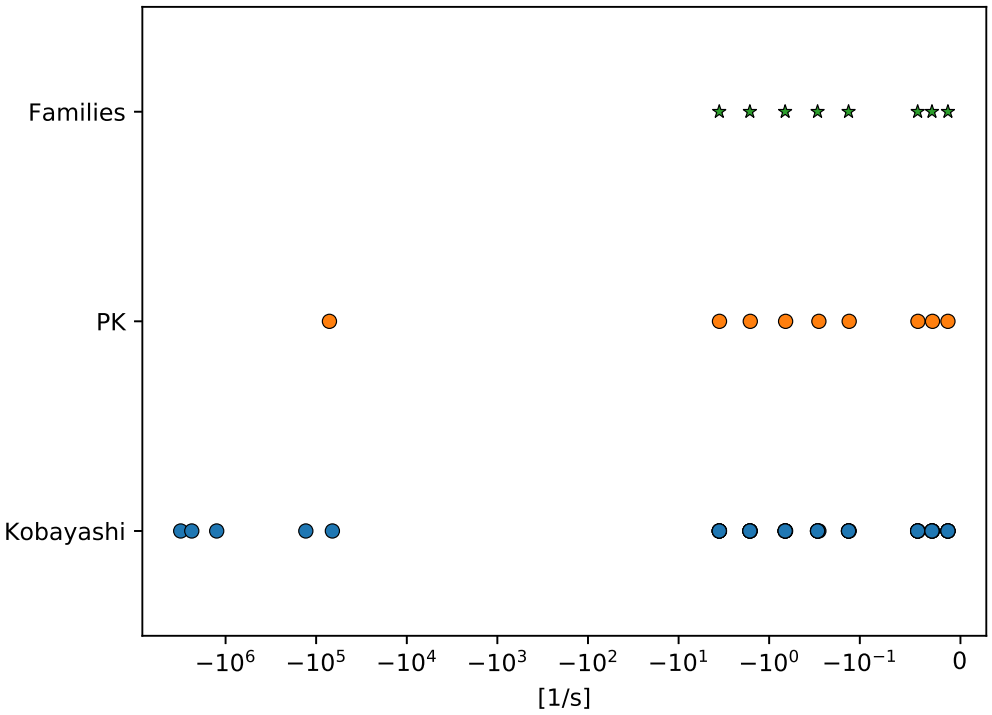

Figure 5.18 – Eigenvalues of the MUSE model

the neutronic response of various systems. The transients analysed have been chosen in order to gradually highlight and stress the differences between PK and MPK.

The results show how, depending from the situation, MPK can lead to important improvement in the system modeling managing to capture phenomena that PK is not able to account for. So far, no relevant difference is found in the results obtained by applying the Avery's and Kobayashi's variant of MPK, but further investigation is necessary to draw conclusions in this direction. At present Avery's formalism present additional cost that seems not to be motivated by any particular advantage with respect of the Kobayashi's one.

Concerning the perspectives of this work we believe that it could be interesting to repeat the same analyses presented in this chapter by using the ω-modes instead of the k ones. This could mitigate the differences in the asymptotic behaviours described by the two versions of MPK. Another interesting aspect could be the use of a subcritical flux, obtained by a source problem, to recompute the coefficients used for the MUSE case. Unfortunately, at present the code at our disposal does not allow for this possibility and some developments are required. Regarding the MUSE case, the reconstruction of the irradiation history of the pulsed source could explain the deviation in the terminal part between experimental and simulated data, but further analysis of the experimental part is required. Another interesting field of research could be the

introduction of a source in the Avery's formalism; although it is still unclear how to do it, this could potentially highlight some differences with Kobayashi's version of MPK (thanks to the different structure of generation time) clarifying their potential.

Chapter 6

Conclusion

6.1 Main conclusions

The kinetic behaviour of a nuclear reactor is governed by phenomena taking place on different time scales. Due to this, kinetic calculations are among the most resource demanding task in reactor physics, and usually result in being not affordable even with the most advanced super computers.

It is common practice to overcome this issue by using simplified models; one of the most popular is PK that models the reactor as it were point-like. Unfortunately models of this kind are not able to capture spatial effects that can affect global quantities, as the total neutron population and therefore the reactor power.

One of the objectives of this work was the evaluation of the alternatives available to overcome this limitation. Among the various candidates available in the literature, we considered that MPK can be a natural evolution of PK while keeping reasonable resource demanding.

The capability to compute the coefficients necessary to apply these two methods have been implemented in the APOLLO3 code under development at CEA. The APOLLO3 implementation has been validated using reference calculations, typically using Monte Carlo simulations, and the results obtained thanks to this work have been found to be in good agreement with the reference ones.

During this work, the analytic capabilities of APOLLO3 have been extended to apply GPT, meaning the capability to compute the sensitivity vector of bilinear ratios to nuclear data. Since most of the coefficients needed to apply reduced-order kinetic methods are expressed by bilinear ratios, this technique can be a useful tool to characterize the kinetic behavior of a system.

A particular effort has been devoted to characterize the β-effective, that is one of the governing parameters of PK. The analyses have been performed for two systems, a thermal and a fast one, chosen to represent a sound basis of representative cases. The results obtained have many similarities, despite the

different nature of the cases analysed. For both system we found that ^{238}U has an important impact on the effective delayed fraction, both through its direct and indirect effects. The direct contribution comes directly from the fact that ^{238}U, having the larger nuclear β among the isotopes often encountered in a typical reactor, gives large contribution to the β-effective even if it represents a small percentage of the relative fission rate. The indirect contribution comes from the fact that, since ^{238}U has a fission threshold around 1 MeV, any scattering reaction that tends to move neutrons below that energy have negative impact on β-effective. Regarding specificities of the results on the β-effective of the two systems, the thermal system has a β-effective (648 pcm) considerably larger than the one of the fast neutron one (369 pcm). This is mainly due to the fact that in the first case, the main fissioning isotope (^{235}U) has a β considerably larger of the one of the main fissioning isotope in the fast case (^{239}Pu). Regarding the mean neutron generation time the value associated to the thermal system ($\approx 18\ \mu s$) is considerably larger than for the fast one ($\approx 0.63\ \mu s$), as expected.

Concerning the differences between PK and MPK, in the first case analysed, an instantaneous rod ejection in the ASTRID SFR, PK and MPK provide similar results for what concerns the total neutron population. Our interpretation is that, since the MPK models have quite homogeneous kinetic properties, PK is a good approximation. It is nevertheless observed that, when using MPK, the adjustment in the neutron shape takes place on a very short time scales and before the prompt jump.

The second case analysed, a coupled fast-thermal reactor, demonstrates how, in such heterogeneous systems, the assumption implied by PK (reactor modeled by a point using global kinetic properties) prevents to model fast phenomena that lead to global effects on the total neutron populations. Those effects, on the contrary, are modeled similarly by both the MPK variants that have been implemented during this work.

The MUSE case allows to test our implementations allowing for a qualitative comparison with experimental data. The analysis shown how these fast effects actually take place and can be captured by MPK.

6.2 Perspectives

Concerning the GPT the main perspective is to perform a similar analysis on the mean neutron generation time (Λ), a parameter for which we can expect higher sensitivity to indirect effects. The main limitation which prevented us to perform those analysis during this work have been the necessity to use an anisotropic source, that our code can not handle at the moment. This kind of study could clarify the effect the multigroup approximation (on the choice of the group neutron velocity) has on this parameter and how to mitigate it.

Concerning MPK methods, the main perspectives are the calculation of the kinetic coefficients they require using different shapes. These could be com-

puted using fluxes obtained by ω-eigenvalue problems or by source calculations according to the specific case.

It would be interesting also to stress the differences between Avery's and Kobayashi's versions of MPK. Indeed while the first allows to distinguish the generation lifetime by the regions where the neutrons are born (in addition to the regions where they induce fission), the second is considerably cheaper to compute (it does not require direct importances). Unfortunately during this work we could not find any case in which this is a relevant feature but we can not exclude that those cases exist.

Finally, specifically to the MUSE experiment, it would be interesting to retrieve experimental data and compare them directly to a simulation. This can be done after reconstructing the system history that could allow to model the existing precursor population. We expect that this could explain that deviation from simulated data to the experimental ones that can be seen in Fig. 5.15 after 100 μs.

Bibliography

[1] A. F. Henry. *Nuclear-Reactor Analysis*. MIT Press, 1975.

[2] S. Glasstone. *Principles of nuclear reactor engineering*. van Nostrand, 1955.

[3] E.E. Lewis and W.F. Miller. *Computational methods of neutron transport*. American Nuclear Society, 1984.

[4] A. Hébert. *Applied reactor physics*. Presses internationales Polytechnique, 2009.

[5] G. Birkhoff and R. S. Varga. Reactor criticality and nonnegative matrices. *Journal of the Society for Industrial and Applied Mathematics*, 6(4):354–377, 1958.

[6] B. Faure. *Development of Neutronic Calculation Schemes for Heterogeneous Sodium-Cooled Nuclear Cores in the APOLLO3 Code. Application to the ASTRID Prototype* . PhD thesis, CEA Cadarache, 13115 Saint-Paul-Lez-Durance ; Aix Marseille Université, October 2019.

[7] R.E. MacFarlane and A.C. Kahler. Methods for processing ENDF/B-VII with NJOY. *Nuclear Data Sheets*, 111(12):2739 – 2890, 2010. Nuclear Reaction Data.

[8] D. Schneider, F. Dolci, F. Gabriel, J.-M. Palau, M. Guillo, and B. Pothet. APOLLO3: CEA/DEN deterministic multi-purpose code for reactor physics analysis. In *Proc. Int. Conf. PHYSOR 2016*, Sun Valley, Idaho, United States, 2016. American Nuclear Society.

[9] P. Archier, A. Calloo, G. Valocchi, Faure B., and J.-M. Palau. Development and verification of perturbative methods in the APOLLO3 code: Sensitivity analysis and uncertainty quantification applied to pressurized-water and sodium fast reactors. In *Proceedings of M&C 2019*, Portland, Oregon, United States, 2019.

[10] J.-M. Palau et al. Recent progress in the V&V of the French APOLLO3 code: 3D full core analysis of the UH1.2 integral experiment using IDT method of characteristics. In *Proceedings of the PHYSOR 2018 Conference*, Cancun, Mexico, 2018.

[11] B. Faure, P. Archier, J.-F. Vidal, J.-M. Palau, and L. Buiron. Neutronic calculation of an axially heterogeneous ASTRID fuel assembly with APOLLO3: Analysis of biases and foreseen improvements. *Annals of Nuclear Energy*, 115:88–104, 2018.

[12] J.Y. Moller, J.-J. Lautard, and D. Schneider. MINARET, a deterministic neutron transport solver for nuclear core calculations. In *Proc. Int. Conf. on Mathematics and Computati onal Methods Applied to Nuclear Science and Engineering (M&C2011)*. American Nuclear Society, 2011.

[13] L.N. Usachev. Equation for the importance of neutrons, reactor kinetics and the theory of perturbations. In *Proc. 1st UN Int. Conf. on the Peaceful Uses of Atomic Energy, Geneva, Switzerland, Aug. 8-12, 1955*, volume 5, pages 503–510, 1956.

[14] A Gandini. A generalized perturbation method for bi-linear functionals of the real and adjoint neutron fluxes. *Journal of Nuclear Energy*, 21(10):755–765, 1967.

[15] P. Archier, C. De Saint Jean, G. Noguère, et al. Comac: Nuclear data covariance matrices library for nuclear reactor applications. In *Proceedings of PHYSOR 2014*, Kyoto, Japan, 2014.

[16] G. Valocchi, P. Archier, and J. Tommasi. Beta effective sensitivity to nuclear data within the APOLLO3 neutronic platform. In *Proc. Int. Conf. PHYSOR 2020*, Cambridge, England, 2020. American Nuclear Society.

[17] P. Archier, C. De Saint Jean, V. Pascal, and J. Tommasi. Spécifications d'un environnement générique pour réaliser des calculs de perturbations, de sensibilités et d'incertitudes avec le code APOLLO3. Technical report, NT DER/SPRC/LEPh/NT/14-207 IND A, 2014.

[18] L. Dagum and R. Menon. OpenMP: an industry standard API for shared-memory programming. *Computational Science & Engineering, IEEE*, 5(1):46–55, 1998.

[19] Introduction to HPC scientific programming: tools and techniques. `https://hpc-forge.cineca.it/files/CoursesDev/public/2014/Introduction_to_HPC_Scientific_Programming:_tools_and_techniques/Bologna/`.

[20] A.F. Henry. The application of reactor kinetics to the analysis of experiments. *Nuclear Science and Engineering*, 3(1):52–70, 1958.

[21] E. Fermi. Problem of time dependence of the reaction rate: effect of delayed neutrons emission. Technical report, Report CP-291, Notes on Lecture of October 1942.

[22] J. Tommasi and G. Palmiotti. Verification of iterative matrix solutions for multipoint kinetics equations. *Annals of Nuclear Energy*, 124:357–371, 2019.

[23] B.D. Ganapol. A highly accurate algorithm for the solution of the point kinetics equations. *Annals of Nuclear Energy*, 62:564 – 571, 2013.

[24] R. Avery. Theory of coupled reactors. *Proc. 2nd UN Int. Conf. Peaceful Uses of Atomic Energy, United Nations*, 12:182, 1958.

[25] K. Kobayashi. Rigorous derivation of multi-point reactor kinetics equations with explicit dependence on perturbation. *Journal of Nuclear Science and Technology*, 29(2):110–120, 1992.

[26] G. Rudstem, P. Finck, A. Filip, A. D'Angelo, and R.D. McKnight. Delayed neutron data for the major actinides. vol. 6. *Nuclear Energy Agency Report NEA/WPEC-6*, 2002.

[27] D. Caron, S. Dulla, and P. Ravetto. Adaptive time step selection in the quasi-static methods of nuclear reactor dynamics. *Annals of Nuclear Energy*, 105:266–281, 2017.

[28] K. Dugan, I. Zmijarevic, and R. Sanchez. Cross-section homogenization for reactivity-induced transient calculations. *Journal of Computational and Theoretical Transport*, 45(6):425–441, 2016.

[29] D. Foligno. *New evaluation of delayed-neutron data and associated covariances*. Theses, CEA Cadarache, 13115 Saint-Paul-Lez-Durance, Aix Marseille Université, CNRS, Centrale Marseille, ED 353 Sciences pour l'ingénieur, mécanique, physique, micro et nanoélectronique, October 2019.

[30] V.M. Piksaikin, A.S. Egorov, A.A. Goverdovski, D.E. Gremyachkin, and K.V. Mitrofanov. High resolution measurements of time-dependent integral delayed neutron spectra from thermal neutron induced fission of 235u. *Annals of Nuclear Energy*, 102:408 – 421, 2017.

[31] P. Archier and V. Pascal. Implémentation et validation d'un module générique de calcul de perturbation dans APOLLO3. Application avec les solveurs MINARET et PASTIS. Technical report, NT DER/SPRC/LEPh 16-201 IND A, 2016.

[32] P. Virtanen et al. Scipy 1.0-Fundamental Algorithms for Scientific Computing in Python. *CoRR*, abs/1907.10121, 2019.

[33] L. Petzold. Automatic selection of methods for solving stiff and nonstiff systems of ordinary differential equations. *SIAM journal on scientific and statistical computing*, 4(1):136–148, 1983.

[34] G. Strang. *Linear algebra and its applications*. Academic Press, 1976.

[35] F. Varaine, P. Marsault, M. S. Chenaud, B. Bernardin, A. Conti, P. Sciora, C. Venard, B. Fontaine, N. Devictor, L. Martin, A. C. Scholer, and D. Verrier. Pre-conceptual design study of ASTRID core. In *ICAPP '12: 2012 International Congress on Advances in Nuclear Power Plants*, Chicago, Illinois, United States, 2012.

[36] J.-M. Ruggieri, J. Tommasi, J.-F. Lebrat, S. Christophe, D. Plisson-Rieunier, C. De Saint Jean, G. Rimpault, and J.-C. Sublet. ERANOS 2.1 : International code system for GEN IV fast reactor analysis. In *ICAPP 2006: International Congress on Advances in Nuclear Power Plants 2006*, Reno, Nevada, United States, 2006.

[37] E. Brun, F. Damian, C.M. Diop, E. Dumonteil, F.X. Hugot, C. Jouanne, Y.K. Lee, F. Malvagi, A. Mazzolo, O. Petit, J.C. Trama, T. Visonneau, and A. Zoia. TRIPOLI-4®, CEA, EDF and AREVA reference Monte Carlo code. *Annals of Nuclear Energy*, 82:151 – 160, 2015.

[38] G. Truchet, P. Leconte, A. Santamarina, E. Brun, F. Damian, and A. Zoia. Computing adjoint-weighted kinetics parameters in TRIPOLI-4® by the Iterated Fission Probability method. *Annals of Nuclear Energy*, 85:17–206, 2015.

[39] S. Dulla, P. Ravetto, P. Saracco, W. Borreani, M. Carta, V. Fabrizio, and V. Peluso. Energy models for the evaluation of the effective neutron lifetime. In *Proceedings of the PHYSOR 2018 Conference*, Cancun, Mexico, 2018.

[40] I.-A. Kodeli. Sensitivity and uncertainty in the effective delayed neutron fraction. *Nuclear Instruments and Methods in Physics Research Section A: Accelerators, Spectrometers, Detectors and Associated Equipment*, 715:70 – 78, 2013.

[41] J. Mondot et al. Epicure : an experimental programme devoted to the validation of the calculational tools for plutonium recycling in pwrs. In *Proc. Int. Conf. PHYSOR 90*, Marseille, France, 1990. American Nuclear Society.

[42] A. F. Henry. The application of inhour modes to the description of non-separable reactor transients. *Nuclear Science and Engineering*, 20(3):338–351, 1964.

[43] L. Martin-Deidier. *Mesure intégrale de la capture des produits de fission dans les réacteurs à neutrons rapides*. PhD thesis, 1979.

[44] P. Ros. *Conception neutronique de configurations expérimentales à forte adaptation spectrale en réacteur de puissance nulle pour des applications multi-filières Gen-II,III & IV*. PhD thesis, Micro et nanotechnologies/Microélectronique. Université Grenoble Alpes, 2017. NNT: 2017GREAI045.

[45] P. Ros, P. Leconte, P. Blaise, and J. Di-Salvo. Fast-thermal coupled cores in ZPR revisited: physical specificities and potentialities for ZEPHYR. In *PHYSOR Conference 2016*, Sun Valley, Idaho, United States, 2016.

[46] F. Mellier. The MUSE experiments for sub critical neutronics validation. Technical report, Tech. Rep. June 2005, 5th Euratom Framwork Program, Final Report of the EU-supported project MUSE, 2005.

Annexes

Appendix A

ASTRID sensitivity tables

This appendix contains the tables with the sensitivities of the β-effective for ASTRID case, presented in section 4.1, to the five main isotopes. The main addition to those presented in section 4.1 is in the energy dependence. These results are computed using a 33 groups energy mesh whose energy structure can be read from Table A.1.

Table A.1 – 33 groups energy mesh

Group number	Lower bound [eV]	Upper bound [eV]
1	10000000.0	19640300.0
2	6065307.0	10000000.0
3	3678794.0	6065307.0
4	2231302.0	3678794.0
5	1353353.0	2231302.0
6	820850.0	1353353.0
7	497870.7	820850.0
8	301973.8	497870.7
9	183156.4	301973.8
10	111090.0	183156.4
11	67379.47	111090.0
12	40867.71	67379.47
13	24787.52	40867.71
14	15034.39	24787.52
15	9118.82	15034.39
16	5530.844	9118.82
17	3354.626	5530.844
18	2034.684	3354.626
19	1234.098	2034.684
20	748.5183	1234.098
21	453.9993	748.5183
22	304.3248	453.9993
23	148.6254	304.3248
24	91.66088	148.6254
25	67.90405	91.66088
26	40.169	67.90405
27	22.60329	40.169
28	13.70959	22.60329
29	8.315287	13.70959
30	4.0	8.315287
31	0.54	4.0
32	0.1	0.54
33	1.00001e-05	0.1

Table A.2 – O 16

Groups	Capture	Fission	Elastic	Inelastic	NXN	ν	ν_D	χ	χ_d	TOTAL
1	1.26 e-04	-	3.27 e-05	6.29 e-05	-1.22 e-09	-	-	-	-	2.21 e-04
2	8.84 e-04	-	1.93 e-04	-1.01 e-04	0.00 e+00	-	-	-	-	9.75 e-04
3	1.14 e-03	-	1.96 e-04	0.00 e+00	0.00 e+00	-	-	-	-	1.34 e-03
4	1.30 e-05	-	-4.08 e-03	0.00 e+00	0.00 e+00	-	-	-	-	-4.07 e-03
5	1.92 e-09	-	-1.75 e-02	0.00 e+00	0.00 e+00	-	-	-	-	-1.75 e-02
6	2.84 e-09	-	-3.04 e-03	0.00 e+00	0.00 e+00	-	-	-	-	-3.04 e-03
7	3.94 e-09	-	2.09 e-03	0.00 e+00	0.00 e+00	-	-	-	-	2.09 e-03
8	1.80 e-09	-	1.28 e-03	0.00 e+00	0.00 e+00	-	-	-	-	1.28 e-03
9	7.28 e-10	-	6.41 e-04	0.00 e+00	0.00 e+00	-	-	-	-	6.41 e-04
10	-7.12 e-10	-	1.21 e-04	0.00 e+00	0.00 e+00	-	-	-	-	1.21 e-04
11	-2.08 e-09	-	-4.19 e-04	0.00 e+00	0.00 e+00	-	-	-	-	-4.19 e-04
12	-2.78 e-09	-	-5.17 e-04	0.00 e+00	0.00 e+00	-	-	-	-	-5.17 e-04
13	-3.37 e-09	-	-3.65 e-04	0.00 e+00	0.00 e+00	-	-	-	-	-3.65 e-04
14	-4.73 e-09	-	-7.14 e-05	0.00 e+00	0.00 e+00	-	-	-	-	-7.14 e-05
15	-4.52 e-09	-	8.04 e-05	0.00 e+00	0.00 e+00	-	-	-	-	8.04 e-05
16	-3.93 e-09	-	-9.99 e-06	0.00 e+00	0.00 e+00	-	-	-	-	-9.99 e-06
17	-3.37 e-09	-	-1.77 e-04	0.00 e+00	0.00 e+00	-	-	-	-	-1.77 e-04
18	-1.62 e-09	-	-7.45 e-06	0.00 e+00	0.00 e+00	-	-	-	-	-7.46 e-06
19	-4.69 e-09	-	-2.19 e-04	0.00 e+00	0.00 e+00	-	-	-	-	-2.19 e-04
20	-3.67 e-09	-	2.58 e-04	0.00 e+00	0.00 e+00	-	-	-	-	2.58 e-04
21	-2.69 e-09	-	-1.09 e-05	0.00 e+00	0.00 e+00	-	-	-	-	-1.09 e-05
22	-1.30 e-09	-	-4.35 e-05	0.00 e+00	0.00 e+00	-	-	-	-	-4.35 e-05
23	-1.25 e-09	-	-7.17 e-05	0.00 e+00	0.00 e+00	-	-	-	-	-7.17 e-05
24	-2.89 e-10	-	-7.53 e-06	0.00 e+00	0.00 e+00	-	-	-	-	-7.53 e-06
25	-8.27 e-11	-	-1.16 e-05	0.00 e+00	0.00 e+00	-	-	-	-	-1.16 e-05
26	-3.63 e-11	-	1.69 e-06	0.00 e+00	0.00 e+00	-	-	-	-	1.69 e-06
27	-3.74 e-11	-	-4.44 e-06	0.00 e+00	0.00 e+00	-	-	-	-	-4.44 e-06
28	2.67 e-12	-	8.75 e-07	0.00 e+00	0.00 e+00	-	-	-	-	8.75 e-07
29	-2.09 e-11	-	-7.50 e-07	0.00 e+00	0.00 e+00	-	-	-	-	-7.50 e-07
30	-9.83 e-12	-	-5.44 e-07	0.00 e+00	0.00 e+00	-	-	-	-	-5.44 e-07
31	-1.27 e-11	-	-1.46 e-07	0.00 e+00	0.00 e+00	-	-	-	-	-1.46 e-07
32	1.04 e-11	-	9.54 e-08	0.00 e+00	0.00 e+00	-	-	-	-	9.54 e-08
33	2.31 e-11	-	1.79 e-08	0.00 e+00	0.00 e+00	-	-	-	-	1.79 e-08
TOTAL	2.17 e-03	-	-2.16 e-02	-3.86 e-05	-1.22 e-09	-	-	-	-	-1.95 e-02

Table A.3 – Na 23

Groups	Capture	Fission	Elastic	Inelastic	NXN	ν	ν_d	χ	χ_d	TOTAL
1	3.99 e-05	-	3.54 e-06	2.21 e-05	-3.76 e-07	-	-	-	-	6.52 e-05
2	1.48 e-04	-	1.43 e-06	2.17 e-05	0.00 e+00	-	-	-	-	1.71 e-04
3	3.15 e-05	-	-2.41 e-04	-9.60 e-04	0.00 e+00	-	-	-	-	-1.17 e-03
4	3.47 e-06	-	-3.17 e-03	-2.87 e-03	0.00 e+00	-	-	-	-	-6.04 e-03
5	6.33 e-06	-	-5.91 e-03	-3.14 e-03	0.00 e+00	-	-	-	-	-9.04 e-03
6	7.11 e-06	-	-2.38 e-03	1.68 e-04	0.00 e+00	-	-	-	-	-2.21 e-03
7	1.26 e-05	-	-2.08 e-03	1.10 e-03	0.00 e+00	-	-	-	-	-9.68 e-04
8	7.88 e-06	-	-2.89 e-04	7.15 e-06	0.00 e+00	-	-	-	-	-2.74 e-04
9	8.56 e-06	-	-2.99 e-04	0.00 e+00	0.00 e+00	-	-	-	-	-2.90 e-04
10	2.22 e-06	-	-2.72 e-04	0.00 e+00	0.00 e+00	-	-	-	-	-2.69 e-04
11	-5.49 e-08	-	-2.29 e-04	0.00 e+00	0.00 e+00	-	-	-	-	-2.29 e-04
12	-7.33 e-06	-	-3.68 e-04	0.00 e+00	0.00 e+00	-	-	-	-	-3.75 e-04
13	-1.05 e-05	-	-2.32 e-04	0.00 e+00	0.00 e+00	-	-	-	-	-2.42 e-04
14	-1.90 e-07	-	-1.46 e-04	0.00 e+00	0.00 e+00	-	-	-	-	-1.46 e-04
15	-4.80 e-07	-	-9.53 e-05	0.00 e+00	0.00 e+00	-	-	-	-	-9.58 e-05
16	-8.06 e-06	-	-1.14 e-04	0.00 e+00	0.00 e+00	-	-	-	-	-1.22 e-04
17	-1.58 e-05	-	-4.05 e-04	0.00 e+00	0.00 e+00	-	-	-	-	-4.21 e-04
18	-6.27 e-05	-	-5.75 e-04	0.00 e+00	0.00 e+00	-	-	-	-	-6.37 e-04
19	-2.24 e-05	-	-2.46 e-04	0.00 e+00	0.00 e+00	-	-	-	-	-2.69 e-04
20	-6.52 e-06	-	-3.40 e-05	0.00 e+00	0.00 e+00	-	-	-	-	-4.05 e-05
21	-2.59 e-06	-	-5.85 e-05	0.00 e+00	0.00 e+00	-	-	-	-	-6.11 e-05
22	-7.27 e-07	-	-4.14 e-05	0.00 e+00	0.00 e+00	-	-	-	-	-4.22 e-05
23	6.84 e-07	-	-4.87 e-05	0.00 e+00	0.00 e+00	-	-	-	-	-4.80 e-05
24	7.92 e-07	-	-9.62 e-06	0.00 e+00	0.00 e+00	-	-	-	-	-8.83 e-06
25	3.67 e-07	-	1.08 e-06	0.00 e+00	0.00 e+00	-	-	-	-	1.44 e-06
26	6.20 e-07	-	5.98 e-06	0.00 e+00	0.00 e+00	-	-	-	-	6.60 e-06
27	1.30 e-07	-	-6.25 e-06	0.00 e+00	0.00 e+00	-	-	-	-	-6.12 e-06
28	4.09 e-07	-	1.14 e-06	0.00 e+00	0.00 e+00	-	-	-	-	1.55 e-06
29	5.64 e-08	-	7.63 e-08	0.00 e+00	0.00 e+00	-	-	-	-	1.33 e-07
30	9.18 e-09	-	-4.29 e-07	0.00 e+00	0.00 e+00	-	-	-	-	-4.20 e-07
31	6.24 e-08	-	-1.17 e-07	0.00 e+00	0.00 e+00	-	-	-	-	-5.47 e-08
32	1.27 e-08	-	2.83 e-08	0.00 e+00	0.00 e+00	-	-	-	-	4.10 e-08
33	2.22 e-08	-	3.09 e-09	0.00 e+00	0.00 e+00	-	-	-	-	2.52 e-08
TOTAL	1.33 e-04	-	-1.72 e-02	-5.65 e-03	-3.76 e-07	-	-	-	-	-2.28 e-02

Table A.4 – Fe 56

Groups	Capture	Fission	Elastic	Inelastic	NXN	ν	ν_d	χ	χ_d	TOTAL
1	4.47 e-05	-	9.43 e-07	9.62 e-05	-1.71 e-05	-	-	-	-	1.25 e-04
2	1.98 e-04	-	-5.13 e-05	-1.81 e-04	0.00 e+00	-	-	-	-	-3.47 e-05
3	5.77 e-05	-	-4.85 e-04	-5.80 e-03	0.00 e+00	-	-	-	-	-6.22 e-03
4	9.13 e-05	-	-2.95 e-03	-1.20 e-02	0.00 e+00	-	-	-	-	-1.48 e-02
5	1.47 e-04	-	-5.09 e-03	-1.44 e-02	0.00 e+00	-	-	-	-	-1.93 e-02
6	2.12 e-04	-	-2.34 e-03	2.47 e-03	0.00 e+00	-	-	-	-	3.36 e-04
7	2.89 e-04	-	-1.73 e-03	0.00 e+00	0.00 e+00	-	-	-	-	-1.44 e-03
8	1.95 e-04	-	-1.25 e-03	0.00 e+00	0.00 e+00	-	-	-	-	-1.06 e-03
9	9.68 e-05	-	-5.36 e-04	0.00 e+00	0.00 e+00	-	-	-	-	-4.39 e-04
10	1.85 e-05	-	-5.07 e-04	0.00 e+00	0.00 e+00	-	-	-	-	-4.88 e-04
11	-7.26 e-05	-	-6.42 e-04	0.00 e+00	0.00 e+00	-	-	-	-	-7.14 e-04
12	-7.38 e-05	-	-4.16 e-04	0.00 e+00	0.00 e+00	-	-	-	-	-4.89 e-04
13	-1.57 e-04	-	-1.51 e-03	0.00 e+00	0.00 e+00	-	-	-	-	-1.67 e-03
14	-5.55 e-05	-	-3.72 e-05	0.00 e+00	0.00 e+00	-	-	-	-	-9.27 e-05
15	-5.93 e-06	-	-1.49 e-04	0.00 e+00	0.00 e+00	-	-	-	-	-1.55 e-04
16	-4.52 e-06	-	-2.46 e-04	0.00 e+00	0.00 e+00	-	-	-	-	-2.51 e-04
17	-5.63 e-06	-	-2.71 e-04	0.00 e+00	0.00 e+00	-	-	-	-	-2.77 e-04
18	-5.40 e-06	-	-9.88 e-05	0.00 e+00	0.00 e+00	-	-	-	-	-1.04 e-04
19	-1.75 e-05	-	-3.99 e-04	0.00 e+00	0.00 e+00	-	-	-	-	-4.17 e-04
20	-6.52 e-04	-	-1.66 e-04	0.00 e+00	0.00 e+00	-	-	-	-	-8.18 e-04
21	-1.24 e-05	-	-2.51 e-04	0.00 e+00	0.00 e+00	-	-	-	-	-2.64 e-04
22	-5.70 e-06	-	-1.65 e-04	0.00 e+00	0.00 e+00	-	-	-	-	-1.71 e-04
23	2.54 e-06	-	-2.37 e-04	0.00 e+00	0.00 e+00	-	-	-	-	-2.34 e-04
24	5.93 e-06	-	-5.68 e-05	0.00 e+00	0.00 e+00	-	-	-	-	-5.09 e-05
25	3.13 e-06	-	1.68 e-06	0.00 e+00	0.00 e+00	-	-	-	-	4.81 e-06
26	6.34 e-06	-	2.62 e-05	0.00 e+00	0.00 e+00	-	-	-	-	3.25 e-05
27	1.24 e-07	-	-4.55 e-05	0.00 e+00	0.00 e+00	-	-	-	-	-4.53 e-05
28	4.74 e-06	-	4.27 e-06	0.00 e+00	0.00 e+00	-	-	-	-	9.01 e-06
29	-2.73 e-07	-	-5.56 e-06	0.00 e+00	0.00 e+00	-	-	-	-	-5.83 e-06
30	-5.00 e-07	-	-6.69 e-06	0.00 e+00	0.00 e+00	-	-	-	-	-7.19 e-06
31	6.67 e-07	-	-1.28 e-06	0.00 e+00	0.00 e+00	-	-	-	-	-6.12 e-07
32	1.37 e-07	-	2.36 e-07	0.00 e+00	0.00 e+00	-	-	-	-	3.73 e-07
33	2.14 e-07	-	1.33 e-08	0.00 e+00	0.00 e+00	-	-	-	-	2.27 e-07
TOTAL	3.05 e-04	-	-1.96 e-02	-2.97 e-02	-1.71 e-05	-	-	-	-	-4.91 e-02

Table A.5 – U 238

Groups	Capture	Fission	Elastic	Inelastic	NXN	ν	ν_d	χ	χ_d	TOTAL
1	5.28 e-07	2.16 e-05	-1.46 e-06	1.97 e-05	-2.02 e-04	-1.27 e-03	1.08 e-03	-3.96 e-04	-	-7.43 e-04
2	3.82 e-06	4.97 e-03	-3.93 e-05	-3.95 e-04	-1.69 e-03	-1.54 e-02	1.82 e-02	-5.79 e-03	1.29 e-06	-1.29 e-04
3	2.83 e-05	3.03 e-02	-2.06 e-04	-9.09 e-03	0.00 e+00	-3.77 e-02	6.29 e-02	-2.32 e-02	2.82 e-04	2.33 e-02
4	3.53 e-04	9.83 e-02	-7.01 e-04	-2.99 e-02	0.00 e+00	-8.79 e-02	1.74 e-01	-4.45 e-02	3.93 e-03	1.14 e-01
5	1.89 e-03	1.08 e-01	-1.24 e-03	-2.39 e-02	0.00 e+00	-7.87 e-02	1.74 e-01	-5.26 e-02	2.20 e-02	1.49 e-01
6	4.32 e-03	1.12 e-02	-1.12 e-03	3.83 e-03	0.00 e+00	-5.65 e-03	1.57 e-02	-4.41 e-02	6.44 e-02	4.86 e-02
7	5.30 e-03	1.42 e-03	-1.77 e-03	9.93 e-04	0.00 e+00	-4.75 e-04	1.82 e-03	-2.77 e-02	1.09 e-01	8.84 e-02
8	1.73 e-03	2.70 e-04	-9.15 e-04	3.15 e-04	0.00 e+00	-6.30 e-05	3.28 e-04	-1.49 e-02	9.97 e-02	8.65 e-02
9	5.88 e-04	1.52 e-04	-1.01 e-03	1.91 e-04	0.00 e+00	-2.82 e-05	1.79 e-04	-7.39 e-03	6.55 e-02	5.82 e-02
10	-5.19 e-04	1.17 e-04	-8.74 e-04	1.07 e-04	0.00 e+00	-1.84 e-05	1.35 e-04	-3.50 e-03	3.88 e-02	3.42 e-02
11	-1.66 e-03	3.59 e-05	-7.91 e-04	1.87 e-05	0.00 e+00	-4.95 e-06	4.12 e-05	-1.63 e-03	2.14 e-02	1.74 e-02
12	-2.60 e-03	5.17 e-05	-7.11 e-04	1.92 e-05	0.00 e+00	-6.54 e-06	5.88 e-05	-7.42 e-04	9.60 e-03	5.67 e-03
13	-3.37 e-03	2.47 e-05	-7.04 e-04	0.00 e+00	0.00 e+00	-2.95 e-06	2.80 e-05	-3.49 e-04	5.49 e-03	1.12 e-03
14	-4.51 e-03	5.13 e-05	-5.39 e-04	0.00 e+00	0.00 e+00	-5.69 e-06	5.77 e-05	-1.79 e-04	4.50 e-03	-6.32 e-04
15	-4.12 e-03	2.84 e-05	-4.16 e-04	0.00 e+00	0.00 e+00	-2.94 e-06	3.18 e-05	-9.11 e-05	2.87 e-03	-1.70 e-03
16	-3.29 e-03	2.93 e-05	-3.85 e-04	0.00 e+00	0.00 e+00	-3.01 e-06	3.29 e-05	-3.80 e-05	6.07 e-04	-3.04 e-03
17	-2.41 e-03	3.77 e-09	-2.93 e-04	0.00 e+00	0.00 e+00	-3.83 e-10	4.22 e-09	-1.91 e-05	3.78 e-04	-2.35 e-03
18	-1.29 e-03	2.68 e-10	-1.30 e-04	0.00 e+00	0.00 e+00	-2.69 e-11	3.00 e-10	-9.51 e-06	2.33 e-04	-1.19 e-03
19	-2.62 e-03	1.63 e-08	-2.72 e-04	0.00 e+00	0.00 e+00	-1.67 e-09	1.82 e-08	-4.82 e-06	1.43 e-04	-2.76 e-03
20	-2.39 e-03	5.73 e-05	-1.65 e-04	0.00 e+00	0.00 e+00	-5.97 e-06	6.43 e-05	-2.48 e-06	8.80 e-05	-2.36 e-03
21	-1.48 e-03	4.24 e-05	-1.12 e-04	0.00 e+00	0.00 e+00	-4.53 e-06	4.77 e-05	-1.41 e-06	5.93 e-05	-1.45 e-03
22	-5.04 e-04	7.28 e-08	-4.96 e-05	0.00 e+00	0.00 e+00	-7.93 e-09	8.21 e-08	-6.34 e-07	3.11 e-05	-5.23 e-04
23	-5.65 e-04	4.23 e-08	-6.76 e-05	0.00 e+00	0.00 e+00	-4.86 e-09	4.77 e-08	-6.27 e-07	3.54 e-05	-5.98 e-04
24	-1.07 e-04	1.32 e-09	-1.59 e-05	0.00 e+00	0.00 e+00	-1.56 e-10	1.49 e-09	-1.93 e-07	1.26 e-05	-1.10 e-04
25	-1.94 e-05	4.49 e-09	-5.52 e-06	0.00 e+00	0.00 e+00	-5.59 e-10	5.09 e-09	-9.31 e-08	6.59 e-06	-1.84 e-05
26	-1.60 e-05	1.00 e-08	-2.61 e-06	0.00 e+00	0.00 e+00	-1.35 e-09	1.14 e-08	-8.11 e-08	6.18 e-06	-1.25 e-05
27	-2.11 e-05	1.10 e-09	-1.77 e-06	0.00 e+00	0.00 e+00	-1.65 e-10	1.27 e-09	-1.89 e-08	1.79 e-06	-2.11 e-05
28	3.12 e-06	4.17 e-09	-2.17 e-07	0.00 e+00	0.00 e+00	-7.00 e-10	4.86 e-09	-1.66 e-08	1.51 e-06	4.41 e-06
29	-4.75 e-07	1.22 e-10	-6.92 e-07	0.00 e+00	0.00 e+00	-2.01 e-11	1.44 e-10	-1.84 e-08	1.86 e-06	6.72 e-07
30	-3.59 e-06	1.54 e-10	-1.59 e-07	0.00 e+00	0.00 e+00	-2.64 e-11	1.83 e-10	-8.74 e-09	9.64 e-07	-2.79 e-06
31	-1.57 e-07	2.31 e-10	-1.44 e-07	0.00 e+00	0.00 e+00	-3.89 e-11	2.71 e-10	-9.88 e-20	3.85 e-07	8.48 e-08
32	5.97 e-08	5.01 e-12	4.31 e-08	0.00 e+00	0.00 e+00	-1.80 e-12	6.24 e-12	-1.26 e-19	1.48 e-07	2.51 e-07
33	1.28 e-07	6.25 e-12	1.91 e-09	0.00 e+00	0.00 e+00	-2.93 e-12	7.92 e-12	-7.17 e-20	3.79 e-08	1.68 e-07
TOTAL	-1.73 e-02	2.55 e-01	-1.25 e-02	-5.78 e-02	-1.89 e-03	-2.27 e-01	4.49 e-01	-2.27 e-01	4.49 e-01	6.09 e-01

Table A.6 – Pu 239

Groups	Capture	Fission	Elastic	Inelastic	NXN	ν	ν_d	χ	χ_d	TOTAL
1	7.15 e-08	-3.59 e-04	-1.95 e-07	9.39 e-07	-6.32 e-06	-4.67 e-04	3.90 e-05	-1.30 e-03	-	-2.09 e-03
2	7.73 e-07	-4.62 e-03	-5.36 e-06	-2.41 e-05	-7.93 e-05	-6.07 e-03	6.83 e-04	-1.45 e-02	2.17 e-07	-2.46 e-02
3	5.14 e-06	-1.46 e-02	-2.86 e-05	-5.60 e-04	-1.54 e-06	-2.11 e-02	4.03 e-03	-5.01 e-02	7.11 e-05	-8.22 e-02
4	4.51 e-05	-3.33 e-02	-9.94 e-05	-1.60 e-03	0.00 e+00	-5.11 e-02	1.18 e-02	-8.29 e-02	1.60 e-03	-1.56 e-01
5	1.65 e-04	-3.83 e-02	-1.58 e-04	-1.15 e-03	0.00 e+00	-6.38 e-02	1.63 e-02	-1.17 e-01	1.21 e-02	-1.92 e-01
6	3.00 e-04	-2.91 e-02	-1.16 e-04	1.20 e-04	0.00 e+00	-5.72 e-02	1.83 e-02	-1.16 e-01	4.84 e-02	-1.36 e-01
7	4.92 e-04	-3.05 e-02	-1.75 e-04	1.95 e-04	0.00 e+00	-7.08 e-02	3.10 e-02	-7.11 e-02	7.97 e-02	-6.12 e-02
8	2.40 e-04	-1.44 e-02	-1.04 e-04	3.04 e-05	0.00 e+00	-4.36 e-02	2.62 e-02	-3.71 e-02	7.39 e-02	5.24 e-03
9	8.89 e-05	-1.00 e-02	-1.26 e-04	3.02 e-06	0.00 e+00	-4.08 e-02	3.00 e-02	-1.80 e-02	4.43 e-02	5.38 e-03
10	-1.22 e-04	-6.22 e-03	-1.12 e-04	3.08 e-07	0.00 e+00	-3.66 e-02	3.13 e-02	-8.46 e-03	2.60 e-02	5.73 e-03
11	-3.22 e-04	-2.63 e-03	-1.01 e-04	-2.30 e-06	0.00 e+00	-2.83 e-02	2.74 e-02	-3.92 e-03	1.47 e-02	6.81 e-03
12	-4.24 e-04	-8.71 e-04	-8.84 e-05	-2.11 e-06	0.00 e+00	-2.07 e-02	2.16 e-02	-1.80 e-03	6.76 e-03	4.45 e-03
13	-5.36 e-04	-3.88 e-05	-8.36 e-05	-9.10 e-07	0.00 e+00	-1.59 e-02	1.75 e-02	-8.34 e-04	3.93 e-03	4.02 e-03
14	-8.15 e-04	7.43 e-04	-6.23 e-05	8.99 e-06	0.00 e+00	-1.51 e-02	1.78 e-02	-3.97 e-04	3.12 e-03	5.25 e-03
15	-8.58 e-04	1.01 e-03	-4.90 e-05	1.38 e-05	0.00 e+00	-1.00 e-02	1.26 e-02	-1.92 e-04	1.98 e-03	4.48 e-03
16	-8.52 e-04	7.56 e-04	-4.49 e-05	2.01 e-06	0.00 e+00	-7.58 e-03	9.57 e-03	-9.28 e-05	5.38 e-04	2.30 e-03
17	-7.87 e-04	5.70 e-04	-3.38 e-05	0.00 e+00	0.00 e+00	-5.72 e-03	7.26 e-03	-4.54 e-05	3.36 e-04	1.58 e-03
18	-4.09 e-04	3.01 e-04	-1.30 e-05	0.00 e+00	0.00 e+00	-2.75 e-03	3.54 e-03	-2.19 e-05	2.07 e-04	8.50 e-04
19	-1.10 e-03	6.42 e-04	-2.86 e-05	0.00 e+00	0.00 e+00	-7.47 e-03	9.35 e-03	-1.06 e-05	1.27 e-04	1.51 e-03
20	-7.43 e-04	4.59 e-04	-1.50 e-05	0.00 e+00	0.00 e+00	-7.07 e-03	8.61 e-03	-5.24 e-06	7.86 e-05	1.31 e-03
21	-6.44 e-04	1.31 e-04	-1.29 e-05	0.00 e+00	0.00 e+00	-5.05 e-03	5.97 e-03	-2.80 e-06	5.30 e-05	4.44 e-04
22	-2.55 e-04	5.61 e-06	-5.12 e-06	0.00 e+00	0.00 e+00	-1.81 e-03	2.10 e-03	-1.18 e-06	2.78 e-05	5.95 e-05
23	-2.81 e-04	-1.57 e-04	-6.15 e-06	0.00 e+00	0.00 e+00	-3.11 e-03	3.30 e-03	-1.09 e-06	3.19 e-05	-2.24 e-04
24	-3.87 e-05	-7.11 e-05	-1.14 e-06	0.00 e+00	0.00 e+00	-8.74 e-04	8.52 e-04	-3.05 e-07	1.14 e-05	-1.22 e-04
25	-7.88 e-06	-5.10 e-05	-2.98 e-07	0.00 e+00	0.00 e+00	-4.53 e-04	4.17 e-04	-1.39 e-07	6.03 e-06	-8.91 e-05
26	2.62 e-06	-7.10 e-05	-6.68 e-08	0.00 e+00	0.00 e+00	-4.63 e-04	3.88 e-04	-1.13 e-07	5.72 e-06	-1.38 e-04
27	-1.55 e-06	-6.90 e-06	-1.77 e-07	0.00 e+00	0.00 e+00	-2.75 e-05	2.23 e-05	-2.06 e-08	1.66 e-06	-1.23 e-05
28	1.90 e-06	-2.81 e-05	7.32 e-08	0.00 e+00	0.00 e+00	-1.28 e-04	9.67 e-05	-1.85 e-08	1.41 e-06	-5.56 e-05
29	-2.08 e-06	-1.72 e-05	9.40 e-08	0.00 e+00	0.00 e+00	-6.19 e-05	4.79 e-05	-1.71 e-08	1.67 e-06	-3.14 e-05
30	-1.36 e-06	-7.20 e-06	4.91 e-08	0.00 e+00	0.00 e+00	-2.30 e-05	1.76 e-05	-7.17 e-09	9.03 e-07	-1.30 e-05
31	5.15 e-09	-4.16 e-06	-1.16 e-08	0.00 e+00	0.00 e+00	-1.55 e-05	1.14 e-05	-2.81 e-19	3.39 e-07	-8.01 e-06
32	3.48 e-06	-6.19 e-06	1.16 e-08	0.00 e+00	0.00 e+00	-1.78 e-05	5.69 e-06	-3.87 e-19	1.35 e-07	-1.47 e-05
33	2.74 e-06	-5.48 e-06	4.77 e-10	0.00 e+00	0.00 e+00	-1.69 e-05	5.10 e-06	-2.19 e-19	3.49 e-08	-1.45 e-05
TOTAL	-6.85 e-03	-1.81 e-01	-1.47 e-03	-2.96 e-03	-8.71 e-05	-5.24 e-01	3.18 e-01	-5.24 e-01	3.18 e-01	-6.04 e-01

Appendix B

EPICURE sensitivity tables

This appendix contains the tables with the sensitivities of the β-effective for the EPICURE case, presented in section 4.2, to the five main isotopes. The main addition to those presented in section 4.2 is in the energy dependence. These results are computed using a 26 groups energy mesh whose energy structure can be read from Table B.1.

Table B.2 – H1_H2O

Groups	Capture	Fission	Elastic	Inelastic	NXN	ν	ν_d	χ	χ_d	TOTAL
1	4.90 e-07	-	-3.03 e-03	-	-	-	-	-	-	-3.03 e-03
2	2.66 e-06	-	-3.74 e-02	-	-	-	-	-	-	-3.74 e-02
3	2.29 e-06	-	-3.33 e-02	-	-	-	-	-	-	-3.33 e-02
4	2.60 e-06	-	-1.61 e-02	-	-	-	-	-	-	-1.61 e-02
5	4.52 e-07	-	2.06 e-03	-	-	-	-	-	-	2.06 e-03
6	1.68 e-07	-	3.36 e-03	-	-	-	-	-	-	3.36 e-03
7	3.05 e-07	-	2.12 e-03	-	-	-	-	-	-	2.12 e-03
8	3.10 e-07	-	1.75 e-03	-	-	-	-	-	-	1.75 e-03
9	1.28 e-06	-	1.97 e-03	-	-	-	-	-	-	1.97 e-03
10	2.43 e-06	-	1.81 e-03	-	-	-	-	-	-	1.81 e-03
11	4.89 e-06	-	5.35 e-03	-	-	-	-	-	-	5.35 e-03
12	-9.46 e-06	-	7.17 e-03	-	-	-	-	-	-	7.16 e-03
13	-5.48 e-05	-	-6.75 e-03	-	-	-	-	-	-	-6.81 e-03
14	-1.98 e-05	-	-3.25 e-03	-	-	-	-	-	-	-3.27 e-03
15	-1.26 e-05	-	-1.94 e-03	-	-	-	-	-	-	-1.96 e-03
16	-3.21 e-05	-	-4.56 e-03	-	-	-	-	-	-	-4.59 e-03
17	-1.59 e-05	-	-2.07 e-03	-	-	-	-	-	-	-2.08 e-03
18	-2.54 e-05	-	-3.06 e-03	-	-	-	-	-	-	-3.08 e-03
19	-5.70 e-05	-	-4.50 e-03	-	-	-	-	-	-	-4.56 e-03
20	-1.34 e-04	-	1.45 e-04	-	-	-	-	-	-	1.05 e-05
21	-2.34 e-04	-	3.18 e-03	-	-	-	-	-	-	2.94 e-03
22	-5.93 e-04	-	2.78 e-03	-	-	-	-	-	-	2.18 e-03
23	-1.92 e-03	-	7.56 e-04	-	-	-	-	-	-	-1.17 e-03
24	-4.80 e-03	-	-1.83 e-03	-	-	-	-	-	-	-6.63 e-03
25	-4.99 e-03	-	-5.19 e-04	-	-	-	-	-	-	-5.51 e-03
26	-1.73 e-03	-	7.28 e-04	-	-	-	-	-	-	-1.01 e-03
TOTAL	-1.46 e-02	-	-8.52 e-02	-	-	-	-	-	-	-9.98 e-02

Table B.1 – 26 groups energy mesh

Group number	Lower bound [eV]	Upper bound [eV]
1	4965850.0	19640300.0
2	2231300.0	4965850.0
3	1336940.0	2231300.0
4	494002.0	1336940.0
5	195008.0	494002.0
6	67379.5	195008.0
7	24999.099	67379.5
8	9118.821	24999.099
9	1910.4499	9118.821
10	410.796	1910.4499
11	52.6726	410.796
12	4.0	52.6726
13	1.2509399	4.0
14	1.148	1.2509399
15	1.104	1.148
16	1.009	1.104
17	0.96396	1.009
18	0.88003	0.96396
19	0.625	0.88003
20	0.35299	0.625
21	0.231193	0.35299
22	0.13799999	0.231193
23	0.076497	0.13799999
24	0.0343998	0.076497
25	0.0104505	0.0343998
26	0.00011	0.0104505

Table B.3 – O 16

Groups	Capture	Fission	Elastic	Inelastic	NXN	ν	ν_d	χ	χ_d	TOTAL
1	1.35 e-03	-	-1.28 e-03	-3.39 e-04	-2.35 e-06	-	-	-	-	-2.67 e-04
2	9.54 e-04	-	-7.98 e-03	0.00 e+00	0.00 e+00	-	-	-	-	-7.02 e-03
3	1.63 e-09	-	-1.08 e-02	0.00 e+00	0.00 e+00	-	-	-	-	-1.08 e-02
4	2.66 e-09	-	-7.32 e-03	0.00 e+00	0.00 e+00	-	-	-	-	-7.32 e-03
5	5.88 e-10	-	-5.42 e-04	0.00 e+00	0.00 e+00	-	-	-	-	-5.42 e-04
6	2.46 e-10	-	3.15 e-04	0.00 e+00	0.00 e+00	-	-	-	-	3.15 e-04
7	3.49 e-10	-	2.59 e-04	0.00 e+00	0.00 e+00	-	-	-	-	2.59 e-04
8	3.92 e-10	-	2.34 e-04	0.00 e+00	0.00 e+00	-	-	-	-	2.34 e-04
9	1.33 e-09	-	3.17 e-04	0.00 e+00	0.00 e+00	-	-	-	-	3.17 e-04
10	2.69 e-09	-	2.82 e-04	0.00 e+00	0.00 e+00	-	-	-	-	2.82 e-04
11	6.68 e-09	-	4.95 e-04	0.00 e+00	0.00 e+00	-	-	-	-	4.95 e-04
12	8.74 e-09	-	7.61 e-04	0.00 e+00	0.00 e+00	-	-	-	-	7.61 e-04
13	-1.75 e-08	-	1.33 e-03	0.00 e+00	0.00 e+00	-	-	-	-	1.33 e-03
14	-1.17 e-08	-	1.12 e-04	0.00 e+00	0.00 e+00	-	-	-	-	1.12 e-04
15	-7.90 e-09	-	-5.81 e-05	0.00 e+00	0.00 e+00	-	-	-	-	-5.81 e-05
16	-2.10 e-08	-	-1.89 e-04	0.00 e+00	0.00 e+00	-	-	-	-	-1.89 e-04
17	-1.02 e-08	-	-1.32 e-04	0.00 e+00	0.00 e+00	-	-	-	-	-1.32 e-04
18	-1.55 e-08	-	-2.43 e-04	0.00 e+00	0.00 e+00	-	-	-	-	-2.43 e-04
19	-2.92 e-08	-	-2.24 e-04	0.00 e+00	0.00 e+00	-	-	-	-	-2.24 e-04
20	-7.66 e-08	-	1.39 e-04	0.00 e+00	0.00 e+00	-	-	-	-	1.39 e-04
21	-1.57 e-07	-	2.66 e-04	0.00 e+00	0.00 e+00	-	-	-	-	2.65 e-04
22	-3.12 e-07	-	2.59 e-04	0.00 e+00	0.00 e+00	-	-	-	-	2.59 e-04
23	-8.67 e-07	-	1.18 e-04	0.00 e+00	0.00 e+00	-	-	-	-	1.17 e-04
24	-2.01 e-06	-	-8.84 e-05	0.00 e+00	0.00 e+00	-	-	-	-	-9.04 e-05
25	-1.96 e-06	-	-6.48 e-05	0.00 e+00	0.00 e+00	-	-	-	-	-6.68 e-05
26	-6.32 e-07	-	1.89 e-05	0.00 e+00	0.00 e+00	-	-	-	-	1.83 e-05
TOTAL	2.30 e-03	-	-2.40 e-02	-3.39 e-04	-2.35 e-06	-	-	-	-	-2.21 e-02

Table B.4 – U 235

Groups	Capture	Fission	Elastic	Inelastic	NXN	ν	ν_d	χ	χ_d	TOTAL
1	2.64 e-07	-4.83 e-04	-5.89 e-06	-4.44 e-05	-3.07 e-05	-8.75 e-04	3.00 e-04	-2.05 e-02	1.07 e-05	-2.16 e-02
2	1.10 e-05	-1.27 e-03	-3.94 e-05	-3.32 e-04	0.00 e+00	-3.72 e-03	1.96 e-03	-1.08 e-01	2.72 e-03	-1.09 e-01
3	2.62 e-05	-7.48 e-04	-3.54 e-05	-1.65 e-04	0.00 e+00	-2.98 e-03	1.78 e-03	-1.03 e-01	2.19 e-02	-8.34 e-02
4	2.99 e-05	2.02 e-06	-4.20 e-05	-2.20 e-05	0.00 e+00	-3.40 e-03	3.12 e-03	-1.44 e-01	2.46 e-01	1.01 e-01
5	-3.73 e-05	5.30 e-04	-1.37 e-05	4.55 e-06	0.00 e+00	-1.35 e-03	2.08 e-03	-4.68 e-02	2.61 e-01	2.15 e-01
6	-6.56 e-05	5.23 e-04	-7.01 e-06	1.49 e-06	0.00 e+00	-1.06 e-03	1.84 e-03	-1.38 e-02	1.23 e-01	1.11 e-01
7	-6.61 e-05	4.16 e-04	-3.27 e-06	1.64 e-07	0.00 e+00	-9.25 e-04	1.55 e-03	-2.83 e-03	3.25 e-02	3.07 e-02
8	-8.65 e-05	4.70 e-04	-2.07 e-06	8.19 e-09	0.00 e+00	-1.07 e-03	1.79 e-03	-6.88 e-04	1.54 e-02	1.58 e-02
9	-2.28 e-04	1.04 e-03	-2.21 e-06	-2.89 e-13	0.00 e+00	-2.61 e-03	4.23 e-03	-1.74 e-04	3.20 e-03	5.46 e-03
10	-5.41 e-04	2.00 e-03	-2.03 e-06	0.00 e+00	0.00 e+00	-5.37 e-03	8.56 e-03	-1.84 e-05	6.81 e-04	5.32 e-03
11	-1.63 e-03	5.07 e-03	-1.59 e-06	0.00 e+00	0.00 e+00	-1.46 e-02	2.29 e-02	-2.39 e-06	1.68 e-04	1.19 e-02
12	-4.47 e-03	8.59 e-03	1.22 e-07	0.00 e+00	0.00 e+00	-2.75 e-02	4.25 e-02	-1.78 e-07	2.40 e-05	1.91 e-02
13	-7.78 e-04	1.56 e-03	1.57 e-06	0.00 e+00	0.00 e+00	-6.00 e-03	9.27 e-03	-6.68 e-09	1.58 e-06	4.06 e-03
14	-1.68 e-04	3.66 e-04	3.80 e-07	0.00 e+00	0.00 e+00	-1.45 e-03	2.28 e-03	-2.49 e-10	6.01 e-08	1.03 e-03
15	-9.26 e-05	2.57 e-04	1.31 e-07	0.00 e+00	0.00 e+00	-1.01 e-03	1.61 e-03	-1.06 e-10	2.58 e-08	7.68 e-04
16	-1.26 e-04	4.82 e-04	4.64 e-07	0.00 e+00	0.00 e+00	-1.85 e-03	2.98 e-03	-2.29 e-10	5.57 e-08	1.49 e-03
17	-3.78 e-05	1.92 e-04	2.07 e-07	0.00 e+00	0.00 e+00	-7.41 e-04	1.19 e-03	-1.10 e-10	2.65 e-08	6.03 e-04
18	-5.78 e-05	3.46 e-04	4.24 e-07	0.00 e+00	0.00 e+00	-1.35 e-03	2.14 e-03	-2.06 e-10	4.96 e-08	1.08 e-03
19	-1.93 e-04	1.33 e-03	1.62 e-06	0.00 e+00	0.00 e+00	-5.26 e-03	8.25 e-03	-6.37 e-10	1.52 e-07	4.13 e-03
20	-6.89 e-04	3.62 e-03	3.51 e-06	0.00 e+00	0.00 e+00	-1.43 e-02	2.26 e-02	-6.85 e-10	1.63 e-07	1.12 e-02
21	-1.54 e-03	4.71 e-03	3.37 e-06	0.00 e+00	0.00 e+00	-1.87 e-02	3.02 e-02	-3.07 e-10	7.38 e-08	1.47 e-02
22	-2.05 e-03	6.88 e-03	3.72 e-06	0.00 e+00	0.00 e+00	-2.78 e-02	4.49 e-02	-2.34 e-10	5.66 e-08	2.20 e-02
23	-3.85 e-03	1.44 e-02	1.54 e-06	0.00 e+00	0.00 e+00	-5.88 e-02	9.63 e-02	-1.54 e-10	3.76 e-08	4.80 e-02
24	-7.62 e-03	2.78 e-02	-1.64 e-06	0.00 e+00	0.00 e+00	-1.15 e-01	1.90 e-01	-1.05 e-10	2.59 e-08	9.51 e-02
25	-6.97 e-03	2.30 e-02	-1.73 e-06	0.00 e+00	0.00 e+00	-9.70 e-02	1.61 e-01	-5.95 e-11	1.48 e-08	7.97 e-02
26	-1.95 e-03	5.88 e-03	-1.23 e-07	0.00 e+00	0.00 e+00	-2.49 e-02	4.12 e-02	-2.56 e-11	6.33 e-09	2.02 e-02
TOTAL	-3.32 e-02	1.07 e-01	-1.41 e-04	-5.57 e-04	-3.07 e-05	-4.40 e-01	7.06 e-01	-4.40 e-01	7.06 e-01	6.06 e-01

Table B.5 – U 238

Groups	Capture	Fission	Elastic	Inelastic	NXN	ν	ν_d	χ	χ_d	TOTAL
1	5.19 e-06	8.94 e-04	-1.32 e-04	-2.77 e-03	-1.73 e-03	-1.96 e-02	1.80 e-02	-6.27 e-03	5.80 e-06	-1.15 e-02
2	2.56 e-04	3.38 e-02	-9.18 e-04	-1.87 e-02	0.00 e+00	-6.96 e-02	9.28 e-02	-3.40 e-02	1.14 e-03	4.73 e-03
3	9.75 e-04	2.74 e-02	-9.95 e-04	-9.61 e-03	0.00 e+00	-3.93 e-02	5.96 e-02	-3.05 e-02	6.89 e-03	1.45 e-02
4	2.33 e-03	2.59 e-03	-1.77 e-03	-1.80 e-03	0.00 e+00	-1.98 e-03	4.29 e-03	-4.04 e-02	6.14 e-02	2.46 e-02
5	3.03 e-04	3.23 e-05	-6.34 e-04	-9.76 e-05	0.00 e+00	-1.50 e-05	4.66 e-05	-1.40 e-02	6.34 e-02	4.91 e-02
6	1.14 e-04	7.11 e-06	-3.57 e-04	-1.10 e-05	0.00 e+00	-2.99 e-06	1.00 e-05	-4.23 e-03	3.00 e-02	2.55 e-02
7	2.07 e-04	3.30 e-06	-1.90 e-04	3.15 e-07	0.00 e+00	-1.40 e-06	4.67 e-06	-8.81 e-04	7.46 e-03	6.60 e-03
8	2.37 e-04	3.97 e-06	-1.45 e-04	0.00 e+00	0.00 e+00	-1.67 e-06	5.61 e-06	-2.30 e-04	3.82 e-03	3.69 e-03
9	6.26 e-04	2.39 e-06	-2.17 e-04	0.00 e+00	0.00 e+00	-1.02 e-06	3.38 e-06	-5.47 e-05	6.14 e-04	9.72 e-04
10	9.48 e-04	2.21 e-05	-2.19 e-04	0.00 e+00	0.00 e+00	-9.47 e-06	3.13 e-05	-6.25 e-06	1.30 e-04	8.96 e-04
11	1.63 e-03	2.40 e-07	-4.18 e-04	0.00 e+00	0.00 e+00	-1.02 e-07	3.40 e-07	-9.12 e-07	3.20 e-05	1.24 e-03
12	3.00 e-03	4.53 e-07	-1.85 e-04	0.00 e+00	0.00 e+00	-1.92 e-07	6.41 e-07	-8.41 e-08	4.55 e-06	2.82 e-03
13	-5.62 e-05	1.20 e-07	6.91 e-05	0.00 e+00	0.00 e+00	-4.98 e-08	1.70 e-07	-4.34 e-09	2.94 e-07	1.34 e-05
14	-5.14 e-05	9.28 e-09	1.33 e-05	0.00 e+00	0.00 e+00	-3.48 e-09	1.32 e-08	-1.46 e-10	1.06 e-08	-3.81 e-05
15	-3.52 e-05	3.75 e-09	8.62 e-07	0.00 e+00	0.00 e+00	-1.23 e-09	5.29 e-09	-5.92 e-11	4.37 e-09	-3.43 e-05
16	-9.53 e-05	8.46 e-09	7.55 e-06	0.00 e+00	0.00 e+00	-2.52 e-09	1.18 e-08	-1.26 e-10	9.38 e-09	-8.78 e-05
17	-4.50 e-05	4.74 e-09	-2.66 e-06	0.00 e+00	0.00 e+00	-1.52 e-09	6.66 e-09	-6.21 e-11	4.56 e-09	-4.76 e-05
18	-6.59 e-05	1.08 e-08	-1.18 e-05	0.00 e+00	0.00 e+00	-3.83 e-09	1.52 e-08	-1.24 e-10	8.92 e-09	-7.77 e-05
19	-1.12 e-04	4.98 e-08	2.75 e-05	0.00 e+00	0.00 e+00	-1.90 e-08	6.98 e-08	-4.08 e-10	2.88 e-08	-8.49 e-05
20	-3.01 e-04	9.93 e-08	8.83 e-05	0.00 e+00	0.00 e+00	-3.63 e-08	1.38 e-07	-4.49 e-10	3.18 e-08	-2.12 e-04
21	-6.41 e-04	7.67 e-08	7.20 e-05	0.00 e+00	0.00 e+00	-2.42 e-08	1.07 e-07	-2.04 e-10	1.45 e-08	-5.69 e-04
22	-1.01 e-03	1.50 e-07	8.47 e-05	0.00 e+00	0.00 e+00	-4.95 e-08	2.09 e-07	-1.55 e-10	1.12 e-08	-9.26 e-04
23	-2.21 e-03	3.08 e-07	5.65 e-05	0.00 e+00	0.00 e+00	-1.01 e-07	4.31 e-07	-1.02 e-10	7.41 e-09	-2.16 e-03
24	-4.37 e-03	5.43 e-07	4.73 e-06	0.00 e+00	0.00 e+00	-1.74 e-07	7.61 e-07	-6.95 e-11	5.10 e-09	-4.37 e-03
25	-3.66 e-03	4.25 e-07	-1.85 e-05	0.00 e+00	0.00 e+00	-1.35 e-07	5.96 e-07	-3.90 e-11	2.90 e-09	-3.67 e-03
26	-9.26 e-04	1.04 e-07	-2.13 e-06	0.00 e+00	0.00 e+00	-3.30 e-08	1.47 e-07	-1.68 e-11	1.24 e-09	-9.28 e-04
TOTAL	-2.95 e-03	6.47 e-02	-5.79 e-03	-3.30 e-02	-1.73 e-03	-1.31 e-01	1.75 e-01	-1.31 e-01	1.75 e-01	1.10 e-01

Table B.6 – Pu 239

Groups	Capture	Fission	Elastic	Inelastic	NXN	ν	ν_d	χ	χ_d	TOTAL
1	1.58 e-07	-8.13 e-04	-2.39 e-07	-1.79 e-05	-1.09 e-05	-1.03 e-03	7.79 e-05	-2.01 e-02	1.06 e-06	-2.19 e-02
2	4.73 e-06	-3.25 e-03	-3.69 e-06	-1.21 e-04	0.00 e+00	-4.57 e-03	5.62 e-04	-9.70 e-02	2.99 e-04	-1.04 e-01
3	1.24 e-05	-2.42 e-03	-4.36 e-06	-5.28 e-05	0.00 e+00	-3.62 e-03	4.94 e-04	-8.37 e-02	2.58 e-03	-8.67 e-02
4	4.28 e-05	-3.22 e-03	-8.35 e-06	-2.50 e-05	0.00 e+00	-5.12 e-03	8.59 e-04	-1.08 e-01	3.08 e-02	-8.50 e-02
5	4.59 e-05	-1.42 e-03	-5.99 e-06	-2.69 e-06	0.00 e+00	-2.38 e-03	4.72 e-04	-3.57 e-02	3.03 e-02	-8.70 e-03
6	5.64 e-05	-9.67 e-04	-5.35 e-06	-7.68 e-07	0.00 e+00	-1.66 e-03	3.45 e-04	-1.06 e-02	1.31 e-02	2.57 e-04
7	6.81 e-05	-6.40 e-04	-3.54 e-06	-4.50 e-07	0.00 e+00	-1.11 e-03	2.34 e-04	-2.22 e-03	3.37 e-03	-3.03 e-04
8	1.16 e-04	-6.06 e-04	-3.16 e-06	-8.79 e-07	0.00 e+00	-1.07 e-03	2.28 e-04	-5.24 e-04	1.59 e-03	-2.73 e-04
9	4.22 e-04	-1.24 e-03	-4.39 e-06	-1.30 e-07	0.00 e+00	-2.22 e-03	4.78 e-04	-1.36 e-04	3.26 e-04	-2.38 e-03
10	8.79 e-04	-2.79 e-03	-4.35 e-06	0.00 e+00	0.00 e+00	-5.09 e-03	1.11 e-03	-1.38 e-05	6.88 e-05	-5.84 e-03
11	3.27 e-03	-1.22 e-02	-8.64 e-06	0.00 e+00	0.00 e+00	-2.27 e-02	5.05 e-03	-1.62 e-06	1.67 e-05	-2.66 e-02
12	6.55 e-03	-1.72 e-02	-2.23 e-06	0.00 e+00	0.00 e+00	-3.33 e-02	7.52 e-03	-9.89 e-08	2.34 e-06	-3.65 e-02
13	2.94 e-04	-2.51 e-03	2.02 e-06	0.00 e+00	0.00 e+00	-5.11 e-03	1.16 e-03	-3.16 e-09	1.42 e-07	-6.16 e-03
14	2.26 e-05	-2.23 e-04	3.36 e-07	0.00 e+00	0.00 e+00	-4.14 e-04	9.45 e-05	-8.31 e-11	4.28 e-09	-5.19 e-04
15	3.78 e-06	-4.58 e-05	-7.39 e-08	0.00 e+00	0.00 e+00	-7.95 e-05	1.82 e-05	-2.96 e-11	1.54 e-09	-1.03 e-04
16	1.76 e-06	-2.13 e-05	-4.46 e-08	0.00 e+00	0.00 e+00	-3.66 e-05	8.41 e-06	-6.14 e-11	3.21 e-09	-4.77 e-05
17	5.47 e-06	-5.37 e-05	-3.25 e-07	0.00 e+00	0.00 e+00	-9.65 e-05	2.22 e-05	-3.24 e-11	1.71 e-09	-1.23 e-04
18	3.84 e-05	-2.65 e-04	-9.97 e-07	0.00 e+00	0.00 e+00	-5.23 e-04	1.20 e-04	-7.31 e-11	3.91 e-09	-6.31 e-04
19	5.69 e-04	-2.20 e-03	-1.24 e-07	0.00 e+00	0.00 e+00	-5.00 e-03	1.15 e-03	-2.65 e-10	1.48 e-08	-5.48 e-03
20	6.93 e-03	-1.34 e-02	1.54 e-06	0.00 e+00	0.00 e+00	-3.38 e-02	7.88 e-03	-2.93 e-10	1.72 e-08	-3.24 e-02
21	1.28 e-02	-1.77 e-02	9.18 e-07	0.00 e+00	0.00 e+00	-4.83 e-02	1.14 e-02	-1.32 e-10	8.10 e-09	-4.19 e-02
22	9.64 e-03	-1.49 e-02	7.41 e-07	0.00 e+00	0.00 e+00	-3.96 e-02	9.39 e-03	-9.68 e-11	6.24 e-09	-3.55 e-02
23	8.16 e-03	-1.61 e-02	1.14 e-06	0.00 e+00	0.00 e+00	-4.25 e-02	1.01 e-02	-6.23 e-11	4.14 e-09	-4.03 e-02
24	8.57 e-03	-2.07 e-02	1.19 e-06	0.00 e+00	0.00 e+00	-5.48 e-02	1.32 e-02	-4.11 e-11	2.85 e-09	-5.39 e-02
25	5.03 e-03	-1.37 e-02	3.56 e-07	0.00 e+00	0.00 e+00	-3.62 e-02	8.66 e-03	-2.26 e-11	1.62 e-09	-3.61 e-02
26	1.06 e-03	-2.99 e-03	-6.74 e-09	0.00 e+00	0.00 e+00	-7.83 e-03	1.87 e-03	-9.49 e-12	6.92 e-10	-7.90 e-03
TOTAL	6.46 e-02	-1.52 e-01	-4.76 e-05	-2.22 e-04	-1.09 e-05	-3.58 e-01	8.25 e-02	-3.58 e-01	8.25 e-02	-6.39 e-01

Appendix C

ASTRID: PK and MPK Coefficient tables

This appendix is a collection of all the parameters computed for the ASTRID case discussed in section 5.1. This case has nominal and perturbed configurations and they are described in section 5.1. The parameters related to the Kobayashi's MPK are named as in Table 3.3 while the parameters related to Avery's MPK are named as in Table 3.2.

C.1 ASTRID core coefficients

β-effective = 3.689553 e-03

Mean neutron generation time (Λ) = 3.845961 e-07

k-effective = 1.014748 e+00

Table C.1 – β effective by family

Family 1 - 4	5.895871 e-05	6.036456 e-04	2.227123 e-04	5.311924 e-04
Family 5 - 8	1.163077 e-03	4.812419 e-04	4.261865 e-04	2.025387 e-04

Table C.2 – l_j (Kobayashi nominal)

4.401790 e-07	4.401743 e-07	4.401743 e-07

Table C.3 – S_j (Kobayashi nominal)

3.333333 e-01	3.333333 e-01	3.333333 e-01

Table C.4 – k_{jk} (Kobayashi nominal)

9.406318 e-01	3.722610 e-02	3.714574 e-02
3.714572 e-02	9.406311 e-01	3.722614 e-02
3.722614 e-02	3.714572 e-02	9.406311 e-01

Table C.5 – β_{jk} (Kobayashi nominal)

3.677049 e-03	3.642572 e-03	3.628413 e-03
3.628410 e-03	3.677049 e-03	3.642571 e-03
3.642571 e-03	3.628410 e-03	3.677049 e-03

Table C.6 – β_{ij} (Kobayashi nominal)

Family 1 - 4	7.729443 e-05	7.092247 e-04	2.848756 e-04	6.549710 e-04
	7.729443 e-05	7.092247 e-04	2.848756 e-04	6.549710 e-04
	7.729443 e-05	7.092247 e-04	2.848756 e-04	6.549710 e-04
Family 5 - 8	1.412396 e-03	5.955051 e-04	5.201692 e-04	2.455544 e-04
	1.412396 e-03	5.955051 e-04	5.201692 e-04	2.455544 e-04
	1.412396 e-03	5.955051 e-04	5.201692 e-04	2.455544 e-04

Table C.7 – k_{ij}^d (Kobayashi nominal)

Family 1	7.202077 e-01	2.552535 e-02	2.540697 e-02
	2.540691 e-02	7.202072 e-01	2.552536 e-02
	2.552536 e-02	2.540691 e-02	7.202072 e-01
Family 2	7.954133 e-01	3.252842 e-02	3.238699 e-02
	3.238695 e-02	7.954127 e-01	3.252845 e-02
	3.252845 e-02	3.238695 e-02	7.954127 e-01
Family 3	7.362856 e-01	2.695461 e-02	2.682047 e-02
	2.682042 e-02	7.362851 e-01	2.695462 e-02
	2.695462 e-02	2.682042 e-02	7.362851 e-01
Family 4	7.604321 e-01	2.973346 e-02	2.956052 e-02
	2.956047 e-02	7.604316 e-01	2.973348 e-02
	2.973348 e-02	2.956047 e-02	7.604316 e-01
Family 5	7.717819 e-01	3.035469 e-02	3.017864 e-02
	3.017859 e-02	7.717814 e-01	3.035470 e-02
	3.035470 e-02	3.017859 e-02	7.717814 e-01
Family 6	7.579498 e-01	2.949906 e-02	2.926277 e-02
	2.926273 e-02	7.579493 e-01	2.949907 e-02
	2.949907 e-02	2.926273 e-02	7.579493 e-01
Family 7	7.690404 e-01	2.968736 e-02	2.949264 e-02
	2.949259 e-02	7.690399 e-01	2.968738 e-02
	2.968738 e-02	2.949259 e-02	7.690399 e-01
Family 8	7.724888 e-01	3.062635 e-02	3.035328 e-02
	3.035323 e-02	7.724883 e-01	3.062637 e-02
	3.062637 e-02	3.035323 e-02	7.724883 e-01

Table C.8 – k_{ij} (Avery nominal)

9.273158 e-01	3.559637 e-02	3.557232 e-02
3.557232 e-02	9.273155 e-01	3.559637 e-02
3.559637 e-02	3.557232 e-02	9.273155 e-01

Table C.9 – β_{jk} (Avery nominal)

3.689396 e-03	3.644194 e-03	3.629282 e-03
3.629266 e-03	3.689396 e-03	3.644192 e-03
3.644192 e-03	3.629266 e-03	3.689396 e-03

Table C.10 – l_{jk} (Avery nominal)

3.685684 e-07	7.085108 e-07	7.048390 e-07
7.048835 e-07	3.685699 e-07	7.085212 e-07
7.085212 e-07	7.048836 e-07	3.685699 e-07

Table C.11 – β_{ki} (Avery nominal)

Family 1 - 4	7.729443 e-05	7.092247 e-04	2.848756 e-04	6.549710 e-04
	7.729443 e-05	7.092247 e-04	2.848756 e-04	6.549710 e-04
	7.729443 e-05	7.092247 e-04	2.848756 e-04	6.549710 e-04
Family 5 - 8	1.412396 e-03	5.955051 e-04	5.201692 e-04	2.455544 e-04
	1.412396 e-03	5.955051 e-04	5.201692 e-04	2.455544 e-04
	1.412396 e-03	5.955051 e-04	5.201692 e-04	2.455544 e-04

Table C.12 – S_{jk} (Avery nominal)

3.095745 e-01	1.188347 e-02	1.187544 e-02
1.187544 e-02	3.095744 e-01	1.188347 e-02
1.188347 e-02	1.187544 e-02	3.095744 e-01

Table C.13 – $k^d_{jk,i}$ (Avery nominal)

Family 1	7.129002 e-01	2.442677 e-02	2.435240 e-02
	2.435283 e-02	7.129005 e-01	2.442683 e-02
	2.442683 e-02	2.435283 e-02	7.129005 e-01
Family 2	7.873124 e-01	3.115665 e-02	3.106498 e-02
	3.106536 e-02	7.873128 e-01	3.115671 e-02
	3.115671 e-02	3.106537 e-02	7.873128 e-01
Family 3	7.290124 e-01	2.580520 e-02	2.571568 e-02
	2.571609 e-02	7.290127 e-01	2.580526 e-02
	2.580526 e-02	2.571609 e-02	7.290127 e-01
Family 4	7.525335 e-01	2.845765 e-02	2.832996 e-02
	2.833036 e-02	7.525338 e-01	2.845771 e-02
	2.845772 e-02	2.833036 e-02	7.525338 e-01
Family 5	7.638062 e-01	2.905841 e-02	2.892831 e-02
	2.892871 e-02	7.638065 e-01	2.905847 e-02
	2.905848 e-02	2.892871 e-02	7.638065 e-01
Family 6	7.498021 e-01	2.821578 e-02	2.802117 e-02
	2.802157 e-02	7.498024 e-01	2.821584 e-02
	2.821584 e-02	2.802157 e-02	7.498024 e-01
Family 7	7.609005 e-01	2.841395 e-02	2.826302 e-02
	2.826342 e-02	7.609008 e-01	2.841401 e-02
	2.841401 e-02	2.826342 e-02	7.609008 e-01
Family 8	7.641773 e-01	2.929607 e-02	2.906443 e-02
	2.906482 e-02	7.641776 e-01	2.929613 e-02
	2.929613 e-02	2.906482 e-02	7.641776 e-01

C.2 ASTRID core coefficient without rod

β-effective = 3.689982 e-03

Mean neutron generation time (Λ) = 3.893813 e-07

k-effective = 1.018296 e+00

Table C.14 – β effective by family (perturbed)

Family 1 - 4	5.907414 e-05	6.040008 e-04	2.230306 e-04	5.313872 e-04
Family 5 - 8	1.163327 e-03	4.808380 e-04	4.261119 e-04	2.022119 e-04

Table C.15 – l_j (Kobayashi perturbed)

4.526114 e-07	4.426223 e-07	4.428333 e-07

Table C.16 – S_j (Kobayashi perturbed)

4.134671 e-01	2.959042 e-01	2.906288 e-01

Table C.17 – k_{jk} (Kobayashi perturbed)

9.591129 e-01	4.268151 e-02	4.173273 e-02
3.320646 e-02	9.369456 e-01	3.598427 e-02
3.191957 e-02	3.540174 e-02	9.372325 e-01

Table C.18 – β_{jk} (Kobayashi perturbed)

3.681641 e-03	3.646116 e-03	3.631242 e-03
3.613543 e-03	3.672789 e-03	3.636731 e-03
3.627929 e-03	3.623078 e-03	3.672736 e-03

Table C.19 – β_{ij} (Kobayashi perturbed)

Family 1 - 4	7.723222 e-05	7.084555 e-04	2.845613 e-04	6.536983 e-04
	7.728309 e-05	7.089406 e-04	2.847691 e-04	6.545012 e-04
	7.728112 e-05	7.089108 e-04	2.847567 e-04	6.544512 e-04
Family 5 - 8	1.409670 e-03	5.934844 e-04	5.189225 e-04	2.445552 e-04
	1.411268 e-03	5.946400 e-04	5.196222 e-04	2.450976 e-04
	1.411155 e-03	5.945553 e-04	5.195689 e-04	2.450541 e-04

Table C.20 – $k_i^d jk$ (Kobayashi perturbed)

Family 1	7.367716 e-01	2.940426 e-02	2.866784 e-02
	2.255616 e-02	7.173191 e-01	2.466014 e-02
	2.173639 e-02	2.419581 e-02	7.175672 e-01
Family 2	8.136701 e-01	3.731673 e-02	3.640563 e-02
	2.892909 e-02	7.920436 e-01	3.143747 e-02
	2.787144 e-02	3.086581 e-02	7.923369 e-01
Family 3	7.531829 e-01	3.101853 e-02	3.023425 e-02
	2.385118 e-02	7.332972 e-01	2.604107 e-02
	2.299248 e-02	2.554445 e-02	7.335565 e-01
Family 4	7.780954 e-01	3.415743 e-02	3.327164 e-02
	2.636449 e-02	7.572204 e-01	2.872440 e-02
	2.543814 e-02	2.815715 e-02	7.575073 e-01
Family 5	7.895597 e-01	3.486339 e-02	3.396044 e-02
	2.692527 e-02	7.685312 e-01	2.932450 e-02
	2.597854 e-02	2.874611 e-02	7.688204 e-01
Family 6	7.755970 e-01	3.389786 e-02	3.294719 e-02
	2.611067 e-02	7.547000 e-01	2.848258 e-02
	2.524949 e-02	2.785732 e-02	7.550003 e-01
Family 7	7.865708 e-01	3.411081 e-02	3.320148 e-02
	2.630716 e-02	7.658267 e-01	2.867335 e-02
	2.540138 e-02	2.808475 e-02	7.661149 e-01
Family 8	7.904075 e-01	3.517539 e-02	3.415961 e-02
	2.711444 e-02	7.691384 e-01	2.956584 e-02
	2.624426 e-02	2.889117 e-02	7.694504 e-01

Table C.21 – k_{ij} (Avery perturbed)

9.494318 e-01	3.564171 e-02	3.346459 e-02
3.611281 e-02	9.159824 e-01	3.272460 e-02
3.398219 e-02	3.272747 e-02	9.169218 e-01

Table C.22 – β_{jk} (Avery perturbed)

3.696195 e-03	3.636529 e-03	3.621204 e-03
3.621316 e-03	3.684097 e-03	3.635856 e-03
3.636102 e-03	3.622468 e-03	3.684078 e-03

Table C.23 – l_{jk} (Avery perturbed)

3.869252 e-07	7.171242 e-07	7.136829 e-07
7.066575 e-07	3.653489 e-07	7.193046 e-07
7.126060 e-07	7.146183 e-07	3.662211 e-07

Table C.24 – β_{ki} (Avery perturbed)

Family 1 - 4	7.723222 e-05	7.084555 e-04	2.845613 e-04	6.536983 e-04
	7.728309 e-05	7.089406 e-04	2.847691 e-04	6.545012 e-04
	7.728112 e-05	7.089108 e-04	2.847567 e-04	6.544512 e-04
Family 5 - 8	1.409670 e-03	5.934844 e-04	5.189225 e-04	2.445552 e-04
	1.411268 e-03	5.946400 e-04	5.196222 e-04	2.450976 e-04
	1.411155 e-03	5.945553 e-04	5.195689 e-04	2.450541 e-04

Table C.25 – S_{jk} (Avery perturbed)

3.931348 e-01	1.056200 e-02	9.740042 e-03
1.495337 e-02	2.714407 e-01	9.524665 e-03
1.407113 e-02	9.698403 e-03	2.668749 e-01

Table C.26 – $k^d_{jk,i}$ (Avery perturbed)

Family 1	7.332279 e-01	2.439413 e-02	2.283957 e-02
	2.468388 e-02	7.041917 e-01	2.243028 e-02
	2.326996 e-02	2.238631 e-02	7.049484 e-01
Family 2	8.094673 e-01	3.116746 e-02	2.919988 e-02
	3.153626 e-02	7.772048 e-01	2.864145 e-02
	2.974394 e-02	2.858700 e-02	7.780977 e-01
Family 3	7.496977 e-01	2.578377 e-02	2.413367 e-02
	2.607904 e-02	7.200049 e-01	2.369788 e-02
	2.459937 e-02	2.364154 e-02	7.207834 e-01
Family 4	7.739213 e-01	2.845191 e-02	2.661135 e-02
	2.875960 e-02	7.429204 e-01	2.613326 e-02
	2.716363 e-02	2.604540 e-02	7.437541 e-01
Family 5	7.853568 e-01	2.905834 e-02	2.717909 e-02
	2.936958 e-02	7.540531 e-01	2.668518 e-02
	2.773990 e-02	2.659525 e-02	7.548938 e-01
Family 6	7.710222 e-01	2.821231 e-02	2.632455 e-02
	2.846615 e-02	7.400930 e-01	2.587803 e-02
	2.695308 e-02	2.573078 e-02	7.409072 e-01
Family 7	7.821183 e-01	2.841367 e-02	2.655284 e-02
	2.869945 e-02	7.512337 e-01	2.607832 e-02
	2.712863 e-02	2.596925 e-02	7.520505 e-01
Family 8	7.856557 e-01	2.930302 e-02	2.731622 e-02
	2.954208 e-02	7.541830 e-01	2.685900 e-02
	2.800261 e-02	2.667944 e-02	7.550043 e-01

Appendix D

Coupled Fast-Thermal reactor: PK and MPK Coefficient tables

This appendix is a collection of all the parameters computed for the coupled fast-thermal reactor case discussed in section 5.2. This case has nominal and perturbed configurations using 4 of 6 regions as described in section 5.2. The parameters related to the Kobayashi's MPK are named as in Table 3.3 while the parameters related to Avery's MPK are named as in Table 3.2.

D.1 4 Regions - Nominal

β-effective = 5.869554 e-03

Mean neutron generation time (Λ) = 9.991501 e-06

k-effective = 1.117068 e+00

Table D.1 – Decay constant by family

Family 1 - 4	0.0124667	0.0282917	0.0425244	0.133042
Family 5 - 8	0.292467	0.666488	1.63478	3.55460

Table D.2 – β effective by family

Family 1 - 4	1.546197 e-04	8.633193 e-04	4.667864 e-04	1.039692 e-03
Family 5 - 8	1.866730 e-03	6.693078 e-04	5.669312 e-04	2.421670 e-04

Table D.3 – l_j (Kobayashi nominal)

3.125243 e-07	4.241243 e-07	3.722716 e-06	2.823202 e-05

Table D.4 – S_j (Kobayashi nominal)

2.837599 e-01	3.458717 e-02	1.928776 e-01	4.887753 e-01

Table D.5 – k_{jk} (Kobayashi nominal)

8.892396 e-01	2.933488 e-01	1.529153 e-01	5.134308 e-02
3.203326 e-02	1.212539 e-01	7.372552 e-02	2.288876 e-02
1.213460 e-01	2.868032 e-01	3.848769 e-01	1.983441 e-01
1.604824 e-01	4.163781 e-01	5.668357 e-01	7.704573 e-01

Table D.6 – β_{jk} (Kobayashi nominal)

3.324368 e-03	1.097126 e-02	4.973596 e-03	2.992518 e-03
1.193957 e-03	2.899534 e-03	1.700528 e-03	1.944113 e-03
3.398791 e-03	1.486325 e-02	7.763905 e-03	7.150381 e-03
3.042483 e-03	1.371868 e-02	7.276371 e-03	8.073548 e-03

Table D.7 – β_{ij} (Kobayashi nominal)

Family 1 - 4	7.509912 e-05	6.496067 e-04	2.662088 e-04	5.788504 e-04
	1.577333 e-04	1.544016 e-03	6.246718 e-04	2.042958 e-03
	2.169260 e-04	1.038917 e-03	6.414830 e-04	1.374969 e-03
	2.154923 e-04	1.051669 e-03	6.183833 e-04	1.360550 e-03
Family 5 - 8	1.278033 e-03	4.757664 e-04	4.449008 e-04	2.174297 e-04
	4.225047 e-03	2.663192 e-03	1.765291 e-03	1.232738 e-03
	2.259826 e-03	7.844469 e-04	6.684247 e-04	2.484974 e-04
	2.306283 e-03	7.389272 e-04	6.276080 e-04	2.245502 e-04

Table D.8 – k^d_{ijk} (Kobayashi nominal)

Family 1	6.938350 e-01	1.859416 e-01	7.845122 e-02	1.114325 e-02
	7.641340 e-03	1.885453 e-02	1.476405 e-02	5.165832 e-03
	8.479262 e-02	3.071822 e-01	4.486988 e-01	1.956143 e-01
	8.997018 e-02	3.671487 e-01	5.562497 e-01	9.232677 e-01
Family 2	7.616274 e-01	2.462257 e-01	1.195024 e-01	2.625151 e-02
	9.686500 e-03	2.148068 e-02	1.617478 e-02	6.116048 e-03
	1.131562 e-01	2.943361 e-01	3.917658 e-01	1.969489 e-01
	1.390188 e-01	4.193110 e-01	5.797193 e-01	8.437187 e-01
Family 3	7.095683 e-01	1.977334 e-01	8.701310 e-02	1.426419 e-02
	8.010851 e-03	1.936752 e-02	1.498744 e-02	5.358564 e-03
	9.051115 e-02	3.052171 e-01	4.385109 e-01	1.965050 e-01
	1.001526 e-01	3.775389 e-01	5.599905 e-01	9.071494 e-01
Family 4	7.343520 e-01	2.221413 e-01	1.034890 e-01	2.016308 e-02
	8.966520 e-03	2.081020 e-02	1.581581 e-02	5.823007 e-03
	1.021989 e-01	2.997190 e-01	4.139853 e-01	1.974086 e-01
	1.198322 e-01	3.994389 e-01	5.708837 e-01	8.756508 e-01
Family 5	7.436696 e-01	2.278273 e-01	1.072908 e-01	2.223040 e-02
	9.709618 e-03	2.453100 e-02	1.787207 e-02	6.343475 e-03
	1.042892 e-01	2.985996 e-01	4.100915 e-01	1.978949 e-01
	1.238279 e-01	4.027077 e-01	5.717794 e-01	8.669313 e-01
Family 6	7.374707 e-01	2.214766 e-01	1.033567 e-01	2.165289 e-02
	9.817359 e-03	2.576114 e-02	1.864870 e-02	6.679098 e-03
	1.013071 e-01	3.003233 e-01	4.163150 e-01	2.028837 e-01
	1.184926 e-01	3.973322 e-01	5.683188 e-01	8.722222 e-01
Family 7	7.429218 e-01	2.227599 e-01	1.049490 e-01	2.275762 e-02
	1.042271 e-02	2.933029 e-02	2.060632 e-02	7.114463 e-03
	1.008605 e-01	2.992602 e-01	4.168633 e-01	2.007959 e-01
	1.192773 e-01	3.948210 e-01	5.652702 e-01	8.696785 e-01
Family 8	7.519537 e-01	2.319270 e-01	1.109436 e-01	2.596278 e-02
	1.076289 e-02	2.985117 e-02	2.098397 e-02	7.511148 e-03
	1.055325 e-01	2.979092 e-01	4.077820 e-01	2.071637 e-01
	1.263711 e-01	4.042573 e-01	5.698722 e-01	8.550742 e-01

Table D.9 – k_{jk} (Avery nominal)

7.999294 e-01	2.576321 e-01	1.343349 e-01	4.504825 e-02
2.874681 e-02	1.085613 e-01	6.592927 e-02	2.046984 e-02
1.086718 e-01	2.568826 e-01	3.446775 e-01	1.774675 e-01
1.509754 e-01	3.868276 e-01	5.244137 e-01	6.777642 e-01

Table D.10 – β_{jk} (Avery nominal)

3.327851 e-03	1.097153 e-02	4.967651 e-03	2.984334 e-03
1.192906 e-03	2.899227 e-03	1.700732 e-03	1.943267 e-03
3.398853 e-03	1.486114 e-02	7.762142 e-03	7.147207 e-03
3.077907 e-03	1.390732 e-02	7.387935 e-03	8.094742 e-03

Table D.11 – l_{jk} (Avery nominal)

2.465552 e-07	3.491411 e-07	3.935861 e-07	4.495084 e-07
2.938236 e-07	1.370451 e-07	2.646137 e-07	6.829774 e-07
2.812069 e-06	2.577694 e-06	2.400735 e-06	4.275512 e-06
1.788613 e-05	1.888784 e-05	1.917967 e-05	2.546375 e-05

Table D.12 – β_{ki} (Avery nominal)

Family 1 - 4	7.509912 e-05	6.496067 e-04	2.662088 e-04	5.788504 e-04
	1.577333 e-04	1.544016 e-03	6.246718 e-04	2.042958 e-03
	2.169260 e-04	1.038917 e-03	6.414830 e-04	1.374969 e-03
	2.154923 e-04	1.051669 e-03	6.183833 e-04	1.360550 e-03
Family 5 - 8	1.278033 e-03	4.757664 e-04	4.449008 e-04	2.174297 e-04
	4.225047 e-03	2.663192 e-03	1.765291 e-03	1.232738 e-03
	2.259826 e-03	7.844469 e-04	6.684247 e-04	2.484974 e-04
	2.306283 e-03	7.389272 e-04	6.276080 e-04	2.245502 e-04

Table D.13 – S_{jk} (Avery nominal)

2.269773 e-01	8.910346 e-03	2.590899 e-02	2.201744 e-02
8.156810 e-03	3.754652 e-03	1.271569 e-02	1.000469 e-02
3.083525 e-02	8.884426 e-03	6.647748 e-02	8.673766 e-02
4.283877 e-02	1.337865 e-02	1.011430 e-01	3.312589 e-01

Table D.14 – $k^d_{jk,i}$ (Avery nominal)

Family 1	6.254200 e-01	1.629402 e-01	6.865399 e-02	9.706959 e-03
	6.851720 e-03	1.687837 e-02	1.320426 e-02	4.617686 e-03
	7.594669 e-02	2.751087 e-01	4.017343 e-01	1.749154 e-01
	8.637883 e-02	3.495982 e-01	5.286960 e-01	8.154678 e-01
Family 2	6.855506 e-01	2.164729 e-01	1.049814 e-01	2.300655 e-02
	8.684891 e-03	1.923054 e-02	1.446738 e-02	5.468299 e-03
	1.013391 e-01	2.635783 e-01	3.507660 e-01	1.761575 e-01
	1.319692 e-01	3.929420 e-01	5.410195 e-01	7.426238 e-01
Family 3	6.394060 e-01	1.734161 e-01	7.623324 e-02	1.245426 e-02
	7.182846 e-03	1.733777 e-02	1.340437 e-02	4.790227 e-03
	8.106598 e-02	2.733463 e-01	3.926174 e-01	1.757219 e-01
	9.583475 e-02	3.581724 e-01	5.301986 e-01	8.009097 e-01
Family 4	6.613355 e-01	1.951005 e-01	9.081346 e-02	1.764614 e-02
	8.039653 e-03	1.862990 e-02	1.414579 e-02	5.205917 e-03
	9.152965 e-02	2.684091 e-01	3.706576 e-01	1.765496 e-01
	1.141595 e-01	3.765407 e-01	5.365920 e-01	7.721284 e-01
Family 5	6.696490 e-01	2.001195 e-01	9.416982 e-02	1.946539 e-02
	8.706818 e-03	2.196108 e-02	1.598429 e-02	5.671493 e-03
	9.340105 e-02	2.674069 e-01	3.671749 e-01	1.769906 e-01
	1.178286 e-01	3.790858 e-01	5.365906 e-01	7.643095 e-01
Family 6	6.641405 e-01	1.944714 e-01	9.068148 e-02	1.895275 e-02
	8.803917 e-03	2.306238 e-02	1.667860 e-02	5.971612 e-03
	9.073149 e-02	2.689534 e-01	3.727509 e-01	1.814516 e-01
	1.128752 e-01	3.746788 e-01	5.344231 e-01	7.706109 e-01
Family 7	6.690819 e-01	1.955731 e-01	9.208532 e-02	1.992808 e-02
	9.347597 e-03	2.625790 e-02	1.842900 e-02	6.361121 e-03
	9.033140 e-02	2.680070 e-01	3.732468 e-01	1.795853 e-01
	1.134820 e-01	3.720145 e-01	5.312567 e-01	7.678576 e-01
Family 8	6.770363 e-01	2.037203 e-01	9.738568 e-02	2.274423 e-02
	9.652592 e-03	2.672425 e-02	1.876677 e-02	6.715952 e-03
	9.451432 e-02	2.667900 e-01	3.651178 e-01	1.852926 e-01
	1.201387 e-01	3.801851 e-01	5.342650 e-01	7.561031 e-01

D.2 4 Regions - Perturbed

β-effective = 5.093797 e-03

Mean neutron generation time (Λ) = 6.479059 e-06

k-effective = 1.120244 e+00

Table D.15 – β effective by family (perturbed)

Family 1 - 4	1.249487 e-04	7.743577 e-04	3.863769 e-04	8.670063 e-04
Family 5 - 8	1.633062 e-03	5.812800 e-04	5.041977 e-04	2.225677 e-04

Table D.16 – l_j (Kobayashi perturbed)

4.478120 e-07	1.013323 e-05	1.181440 e-05	1.755106 e-05

Table D.17 – S_j (Kobayashi perturbed)

3.783075 e-01	4.777713 e-02	1.494485 e-02	5.589705 e-01

Table D.18 – k_{jk} (Kobayashi perturbed)

9.514795 e-01	3.650743 e-01	2.139427 e-01	7.730377 e-02
5.071692 e-02	1.482248 e-01	1.101859 e-01	4.582911 e-02
1.009092 e-02	2.843498 e-02	4.569019 e-02	1.947574 e-02
2.579153 e-01	5.655059 e-01	7.236982 e-01	8.780217 e-01

Table D.19 – β_{jk} (Kobayashi perturbed)

3.349978 e-03	9.963719 e-03	7.839042 e-03	3.665953 e-03
2.051857 e-03	4.280099 e-03	4.963883 e-03	4.518932 e-03
3.004593 e-03	7.367873 e-03	5.290648 e-03	5.206116 e-03
3.286156 e-03	1.142255 e-02	1.041454 e-02	7.948542 e-03

Table D.20 – β_{ij} (Kobayashi perturbed)

Family 1 - 4	7.487500 e-05	6.433136 e-04	2.643394 e-04	5.681552 e-04
	1.810508 e-04	1.353089 e-03	6.280878 e-04	1.783720 e-03
	1.922862 e-04	1.248409 e-03	6.238115 e-04	1.637709 e-03
	2.161209 e-04	1.046447 e-03	6.179697 e-04	1.352786 e-03
Family 5 - 8	1.255013 e-03	4.563876 e-04	4.338196 e-04	2.081418 e-04
	3.476057 e-03	1.924415 e-03	1.331491 e-03	8.451138 e-04
	3.074855 e-03	1.521999 e-03	1.092517 e-03	6.352113 e-04
	2.285763 e-03	7.168069 e-04	6.143121 e-04	2.129400 e-04

Table D.21 – k^d_{ijk} (Kobayashi perturbed)

Family 1	7.695735 e-01	2.734577 e-01	1.396195 e-01	2.689538 e-02
	2.386761 e-02	5.180257 e-02	5.514341 e-02	2.910438 e-02
	6.798688 e-03	1.855452 e-02	2.471248 e-02	1.458665 e-02
	1.770075 e-01	5.455024 e-01	7.490318 e-01	1.038455 e+00
Family 2	8.342350 e-01	3.310251 e-01	1.813986 e-01	4.652131 e-02
	2.727304 e-02	5.119544 e-02	5.082313 e-02	2.858822 e-02
	8.247388 e-03	1.758273 e-02	2.236066 e-02	1.388949 e-02
	2.388912 e-01	5.781517 e-01	7.550084 e-01	9.606783 e-01
Family 3	7.847301 e-01	2.868757 e-01	1.483065 e-01	3.096294 e-02
	2.448333 e-02	5.165859 e-02	5.430864 e-02	2.905292 e-02
	7.077327 e-03	1.828667 e-02	2.424706 e-02	1.447331 e-02
	1.894804 e-01	5.495928 e-01	7.499657 e-01	1.022983 e+00
Family 4	8.095293 e-01	3.107205 e-01	1.650487 e-01	3.862692 e-02
	2.599190 e-02	5.174436 e-02	5.280661 e-02	2.894618 e-02
	7.681131 e-03	1.793677 e-02	2.339553 e-02	1.423462 e-02
	2.142951 e-01	5.628231 e-01	7.530691 e-01	9.924546 e-01
Family 5	8.181513 e-01	3.170289 e-01	1.689460 e-01	4.110319 e-02
	2.683961 e-02	5.510325 e-02	5.450298 e-02	2.932956 e-02
	7.817619 e-03	1.818616 e-02	2.408594 e-02	1.432805 e-02
	2.189753 e-01	5.630155 e-01	7.521236 e-01	9.839117 e-01
Family 6	8.148185 e-01	3.158059 e-01	1.646483 e-01	3.989274 e-02
	2.667761 e-02	5.654016 e-02	5.592658 e-02	3.003093 e-02
	7.647571 e-03	1.830014 e-02	2.471440 e-02	1.467373 e-02
	2.109803 e-01	5.539522 e-01	7.511251 e-01	9.917176 e-01
Family 7	8.175252 e-01	3.154887 e-01	1.662690 e-01	4.137997 e-02
	2.730661 e-02	6.002950 e-02	5.799975 e-02	3.038684 e-02
	7.666126 e-03	1.864275 e-02	2.554285 e-02	1.476324 e-02
	2.116446 e-01	5.524848 e-01	7.476677 e-01	9.875315 e-01
Family 8	8.284913 e-01	3.263906 e-01	1.719920 e-01	4.480768 e-02
	2.780212 e-02	6.004494 e-02	5.740356 e-02	3.074509 e-02
	7.890440 e-03	1.848192 e-02	2.525278 e-02	1.487468 e-02
	2.202989 e-01	5.568704 e-01	7.501823 e-01	9.767958 e-01

Table D.22 – k_{jk} (Avery perturbed)

8.535217 e-01	3.181417 e-01	1.861089 e-01	6.700577 e-02
4.620883 e-02	1.330276 e-01	9.670046 e-02	4.025645 e-02
9.008863 e-03	2.540699 e-02	4.080667 e-02	1.738107 e-02
2.437470 e-01	5.263459 e-01	6.698148 e-01	7.721802 e-01

Table D.23 – β_{jk} (Avery perturbed)

3.349970 e-03	9.939597 e-03	7.797221 e-03	3.626415 e-03
2.021464 e-03	4.233959 e-03	4.959272 e-03	4.488570 e-03
3.003619 e-03	7.360540 e-03	5.287172 e-03	5.205200 e-03
3.323732 e-03	1.158827 e-02	1.058041 e-02	7.957564 e-03

Table D.24 – l_{jk} (Avery perturbed)

3.321384 e-07	5.472347 e-07	6.792203 e-07	8.429560 e-07
6.460955 e-06	4.103354 e-06	6.620207 e-06	1.222259 e-05
1.209166 e-05	7.939842 e-06	5.819977 e-06	1.063388 e-05
1.385390 e-05	1.385728 e-05	1.377444 e-05	1.547767 e-05

Table D.25 – β_{ki} (Avery perturbed)

Family 1 - 4	7.487500 e-05	6.433136 e-04	2.643394 e-04	5.681552 e-04
	1.810508 e-04	1.353089 e-03	6.280878 e-04	1.783720 e-03
	1.922862 e-04	1.248409 e-03	6.238115 e-04	1.637709 e-03
	2.161209 e-04	1.046447 e-03	6.179697 e-04	1.352786 e-03
Family 5 - 8	1.255013 e-03	4.563876 e-04	4.338196 e-04	2.081418 e-04
	3.476057 e-03	1.924415 e-03	1.331491 e-03	8.451138 e-04
	3.074855 e-03	1.521999 e-03	1.092517 e-03	6.352113 e-04
	2.285763 e-03	7.168069 e-04	6.143121 e-04	2.129400 e-04

Table D.26 – S_{jk} (Avery perturbed)

3.228757 e-01	1.519905 e-02	2.781216 e-03	3.745217 e-02
1.748018 e-02	6.355325 e-03	1.445094 e-03	2.250092 e-02
3.407931 e-03	1.213805 e-03	6.098157 e-04	9.714967 e-03
9.220619 e-02	2.514590 e-02	1.000973 e-02	4.316020 e-01

Table D.27 – $k^d_{jk,i}$ (Avery perturbed)

Family 1	6.903092 e-01	2.366330 e-01	1.200565 e-01	2.282420 e-02
	2.144619 e-02	4.586891 e-02	4.832556 e-02	2.536116 e-02
	6.068422 e-03	1.656051 e-02	2.205438 e-02	1.301540 e-02
	1.705105 e-01	5.202190 e-01	7.123699 e-01	9.153026 e-01
Family 2	7.481065 e-01	2.883369 e-01	1.573477 e-01	4.002324 e-02
	2.444386 e-02	4.539277 e-02	4.458027 e-02	2.495502 e-02
	7.361247 e-03	1.569396 e-02	1.995696 e-02	1.239367 e-02
	2.276446 e-01	5.431121 e-01	7.054990 e-01	8.446173 e-01
Family 3	7.039031 e-01	2.485973 e-01	1.278026 e-01	2.638798 e-02
	2.198589 e-02	4.576248 e-02	4.760269 e-02	2.532506 e-02
	6.317075 e-03	1.632163 e-02	2.163932 e-02	1.291434 e-02
	1.819954 e-01	5.224486 e-01	7.107486 e-01	9.014267 e-01
Family 4	7.261179 e-01	2.700493 e-01	1.427559 e-01	3.310226 e-02
	2.331903 e-02	4.587086 e-02	4.630303 e-02	2.525034 e-02
	6.855927 e-03	1.600972 e-02	2.088006 e-02	1.270151 e-02
	2.049570 e-01	5.318080 e-01	7.086770 e-01	8.736728 e-01
Family 5	7.338464 e-01	2.756512 e-01	1.462237 e-01	3.527361 e-02
	2.409749 e-02	4.891779 e-02	4.778850 e-02	2.559370 e-02
	6.977817 e-03	1.623332 e-02	2.149741 e-02	1.278496 e-02
	2.092098 e-01	5.312811 e-01	7.066647 e-01	8.659975 e-01
Family 6	7.310969 e-01	2.744302 e-01	1.423825 e-01	3.419956 e-02
	2.396907 e-02	5.023525 e-02	4.903293 e-02	2.620504 e-02
	6.826109 e-03	1.633529 e-02	2.205862 e-02	1.309343 e-02
	2.018083 e-01	5.236617 e-01	7.070909 e-01	8.741488 e-01
Family 7	7.334399 e-01	2.740750 e-01	1.438015 e-01	3.551284 e-02
	2.455822 e-02	5.339219 e-02	5.085153 e-02	2.652341 e-02
	6.842770 e-03	1.664206 e-02	2.279903 e-02	1.317338 e-02
	2.022367 e-01	5.219287 e-01	7.035212 e-01	8.701321 e-01
Family 8	7.433644 e-01	2.838765 e-01	1.489244 e-01	3.849900 e-02
	2.499266 e-02	5.342735 e-02	5.033055 e-02	2.684240 e-02
	7.042939 e-03	1.649858 e-02	2.254048 e-02	1.327287 e-02
	2.103220 e-01	5.250857 e-01	7.040924 e-01	8.614766 e-01

D.3 6 Regions - Nominal

β-effective = 5.869550 e-03

Mean neutron generation time (Λ) = 9.991443 e-06

k-effective = 1.117067 e+00

Table D.28 – β effective by family

Family 1 - 4	1.546193 e-04	8.633183 e-04	4.667854 e-04	1.039691 e-03
Family 5 - 8	1.866729 e-03	6.693083 e-04	5.669314 e-04	2.421676 e-04

Table D.29 – l_j (Kobayashi nominal)

3.638865 e-07	2.866609 e-07	4.238131 e-07	3.718982 e-06	1.547261 e-05	3.728018 e-05

Table D.30 – S_j (Kobayashi nominal) 6

1.534923 e-01	1.302698 e-01	3.458730 e-02	1.928769 e-01	2.028717 e-01	2.859020 e-01

Table D.31 – k_{jk} (Kobayashi nominal)

6.327164 e-01	3.605657 e-01	1.242074 e-01	6.495573 e-02	3.416779 e-02	1.284805 e-02
3.423109 e-01	4.276155 e-01	1.691558 e-01	8.798182 e-02	4.680699 e-02	1.758582 e-02
2.182383 e-02	4.411222 e-02	1.212615 e-01	7.372988 e-02	3.563675 e-02	1.384502 e-02
1.029658 e-01	1.428713 e-01	2.867800 e-01	3.848604 e-01	2.835329 e-01	1.378638 e-01
7.556089 e-02	1.079871 e-01	2.181371 e-01	2.896969 e-01	3.394702 e-01	2.399383 e-01
5.610669 e-02	8.652877 e-02	1.982451 e-01	2.771318 e-01	4.005380 e-01	5.520529 e-01

Table D.32 – β_{jk} (Kobayashi nominal)

3.350527 e-03	3.391955 e-03	1.093370 e-02	4.879850 e-03	3.456529 e-03	1.829169 e-03
3.378963 e-03	3.170142 e-03	1.099849 e-02	5.042588 e-03	3.674942 e-03	1.938571 e-03
1.417299 e-03	1.063155 e-03	2.899464 e-03	1.700470 e-03	2.096646 e-03	1.665011 e-03
3.262563 e-03	3.514037 e-03	1.486362 e-02	7.764016 e-03	7.933647 e-03	6.007645 e-03
3.094956 e-03	3.361753 e-03	1.481399 e-02	7.933671 e-03	8.504931 e-03	7.836094 e-03
2.675441 e-03	2.870828 e-03	1.251351 e-02	6.589420 e-03	7.503237 e-03	8.282464 e-03

Table D.33 – β_{ij} (Kobayashi nominal)

Family 1 - 4	7.508247 e-05	6.491414 e-04	2.660704 e-04	5.780541 e-04
	7.511873 e-05	6.501551 e-04	2.663719 e-04	5.797889 e-04
	1.577334 e-04	1.544016 e-03	6.246718 e-04	2.042958 e-03
	2.169259 e-04	1.038917 e-03	6.414830 e-04	1.374969 e-03
	2.146237 e-04	1.060329 e-03	6.205048 e-04	1.374896 e-03
	2.161086 e-04	1.045524 e-03	6.168781 e-04	1.350370 e-03
Family 5 - 8	1.276324 e-03	4.743223 e-04	4.440766 e-04	2.167381 e-04
	1.280047 e-03	4.774682 e-04	4.458722 e-04	2.182448 e-04
	4.225046 e-03	2.663192 e-03	1.765291 e-03	1.232738 e-03
	2.259827 e-03	7.844480 e-04	6.684254 e-04	2.484980 e-04
	2.339434 e-03	7.783509 e-04	6.520381 e-04	2.451391 e-04
	2.282760 e-03	7.109532 e-04	6.102731 e-04	2.099409 e-04

Table D.34 – k^d_{ijk} (Kobayashi nominal)

Family 1	5.102707 e-01	2.816855 e-01	7.579863 e-02	3.134770 e-02	8.689310 e-03	1.165957 e-03
	2.666865 e-01	3.142767 e-01	1.101488 e-01	4.711217 e-02	1.411446 e-02	1.858687 e-03
	6.165623 e-03	9.381296 e-03	1.885467 e-02	1.476412 e-02	9.047346 e-03	2.430026 e-03
	6.614422 e-02	1.066726 e-01	3.071718 e-01	4.486903 e-01	3.241585 e-01	1.050058 e-01
	4.322858 e-02	7.239532 e-02	2.207092 e-01	3.309627 e-01	4.358322 e-01	2.771984 e-01
	2.475323 e-02	4.351539 e-02	1.464426 e-01	2.252872 e-01	4.112411 e-01	6.997140 e-01
Family 2	5.402480 e-01	3.177847 e-01	1.054470 e-01	5.057659 e-02	1.995123 e-02	4.334482 e-03
	3.017513 e-01	3.492877 e-01	1.407860 e-01	6.894052 e-02	2.828238 e-02	6.216250 e-03
	8.078327 e-03	1.158621 e-02	2.148146 e-02	1.617515 e-02	9.864555 e-03	3.417870 e-03
	9.382391 e-02	1.357474 e-01	2.943159 e-01	3.917519 e-01	2.985306 e-01	1.238192 e-01
	6.670218 e-02	1.005803 e-01	2.304744 e-01	3.109776 e-01	3.743067 e-01	2.602756 e-01
	4.415764 e-02	7.164918 e-02	1.888424 e-01	2.687393 e-01	4.160353 e-01	6.217927 e-01
Family 3	5.185133 e-01	2.889988 e-01	8.164231 e-02	3.537869 e-02	1.103243 e-02	1.786574 e-03
	2.739064 e-01	3.230722 e-01	1.160970 e-01	5.164423 e-02	1.705036 e-02	2.717207 e-03
	6.526201 e-03	9.761498 e-03	1.936780 e-02	1.498757 e-02	9.186971 e-03	2.625513 e-03
	7.180204 e-02	1.124310 e-01	3.052045 e-01	4.385011 e-01	3.192065 e-01	1.089024 e-01
	4.812279 e-02	7.814253 e-02	2.224501 e-01	3.262160 e-01	4.236910 e-01	2.740108 e-01
	2.883523 e-02	4.936244 e-02	1.550926 e-01	2.337742 e-01	4.117805 e-01	6.842465 e-01
Family 4	5.278979 e-01	3.034634 e-01	9.370075 e-02	4.309374 e-02	1.540775 e-02	3.002806 e-03
	2.879748 e-01	3.351250 e-01	1.284469 e-01	6.040741 e-02	2.257857 e-02	4.394050 e-03
	7.387815 e-03	1.082718 e-02	2.081080 e-02	1.581611 e-02	9.646898 e-03	3.059827 e-03
	8.313722 e-02	1.244642 e-01	2.997025 e-01	4.139735 e-01	3.092723 e-01	1.165644 e-01
	5.759190 e-02	8.961339 e-02	2.271107 e-01	3.191838 e-01	3.990501 e-01	2.676967 e-01
	3.651456 e-02	6.050882 e-02	1.723330 e-01	2.516986 e-01	4.137865 e-01	6.532783 e-01
Family 5	5.334990 e-01	3.073895 e-01	9.630319 e-02	4.482309 e-02	1.676480 e-02	3.533467 e-03
	2.916814 e-01	3.405214 e-01	1.315310 e-01	6.248068 e-02	2.430782 e-02	5.107186 e-03
	7.855224 e-03	1.189703 e-02	2.453199 e-02	1.787257 e-02	1.044046 e-02	3.363732 e-03
	8.520989 e-02	1.265752 e-01	2.985825 e-01	4.100792 e-01	3.071520 e-01	1.184167 e-01
	5.941310 e-02	9.170011 e-02	2.271794 e-01	3.168801 e-01	3.932518 e-01	2.657398 e-01
	3.823593 e-02	6.295494 e-02	1.755331 e-01	2.548977 e-01	4.131270 e-01	6.451669 e-01
Family 6	5.311127 e-01	3.039500 e-01	9.312466 e-02	4.293279 e-02	1.592839 e-02	3.296013 e-03
	2.883770 e-01	3.375258 e-01	1.283589 e-01	6.043626 e-02	2.333558 e-02	4.786056 e-03
	7.846476 e-03	1.213293 e-02	2.576214 e-02	1.864923 e-02	1.085450 e-02	3.435120 e-03
	8.224536 e-02	1.234990 e-01	3.003074 e-01	4.163034 e-01	3.123933 e-01	1.177857 e-01
	5.684598 e-02	8.863361 e-02	2.263758 e-01	3.186281 e-01	3.990647 e-01	2.695505 e-01
	3.609214 e-02	5.983675 e-02	1.709609 e-01	2.496893 e-01	4.091839 e-01	6.523135 e-01
Family 7	5.362467 e-01	3.048998 e-01	9.351084 e-02	4.364721 e-02	1.669961 e-02	3.730858 e-03
	2.892865 e-01	3.410792 e-01	1.292559 e-01	6.131457 e-02	2.423939 e-02	5.353593 e-03
	8.173857 e-03	1.307220 e-02	2.933156 e-02	2.060699 e-02	1.160152 e-02	3.712394 e-03
	8.197708 e-02	1.228991 e-01	2.992437 e-01	4.168512 e-01	3.104501 e-01	1.176363 e-01
	5.700259 e-02	8.848426 e-02	2.240256 e-01	3.160672 e-01	3.979385 e-01	2.673608 e-01
	3.681562 e-02	6.073699 e-02	1.708000 e-01	2.492015 e-01	4.092420 e-01	6.496432 e-01
Family 8	5.390748 e-01	3.105780 e-01	9.806214 e-02	4.642270 e-02	1.854298 e-02	4.164401 e-03
	2.947368 e-01	3.455973 e-01	1.338725 e-01	6.453450 e-02	2.666724 e-02	5.965363 e-03
	8.487669 e-03	1.343694 e-02	2.985261 e-02	2.098473 e-02	1.188761 e-02	3.884905 e-03
	8.641032 e-02	1.277801 e-01	2.978917 e-01	4.077695 e-01	3.096670 e-01	1.222085 e-01
	6.048878 e-02	9.287949 e-02	2.268774 e-01	3.140766 e-01	3.880129 e-01	2.677321 e-01
	3.939194 e-02	6.456017 e-02	1.773847 e-01	2.557938 e-01	4.066928 e-01	6.373027 e-01

Table D.35 – k_{jk} (Avery nominal)

5.671133 e-01	3.223961 e-01	1.110823 e-01	5.805897 e-02	3.051602 e-02	1.139364 e-02
3.087929 e-01	3.825649 e-01	1.498194 e-01	7.795392 e-02	4.146689 e-02	1.556607 e-02
1.955529 e-02	3.957798 e-02	1.085621 e-01	6.592899 e-02	3.187076 e-02	1.237987 e-02
9.226993 e-02	1.280097 e-01	2.568845 e-01	3.446735 e-01	2.537565 e-01	1.233343 e-01
6.791708 e-02	9.704855 e-02	1.959361 e-01	2.603266 e-01	3.039884 e-01	2.136764 e-01
5.170782 e-02	7.946208 e-02	1.809346 e-01	2.520657 e-01	3.617271 e-01	4.871658 e-01

Table D.36 – β_{jk} (Avery nominal)

3.350425 e-03	3.392685 e-03	1.093215 e-02	4.878613 e-03	3.453289 e-03	1.803963 e-03
3.380819 e-03	3.172583 e-03	1.100344 e-02	5.040854 e-03	3.671250 e-03	1.933891 e-03
1.416355 e-03	1.062078 e-03	2.899138 e-03	1.700666 e-03	2.096031 e-03	1.663782 e-03
3.262698 e-03	3.514043 e-03	1.486149 e-02	7.762256 e-03	7.930609 e-03	6.003698 e-03
3.097721 e-03	3.364397 e-03	1.481911 e-02	7.931168 e-03	8.503731 e-03	7.822294 e-03
2.697026 e-03	2.896641 e-03	1.264190 e-02	6.669085 e-03	7.577345 e-03	8.288919 e-03

Table D.37 – l_{jk} (Avery nominal)

2.270960 e-07	3.170967 e-07	4.625038 e-07	5.279461 e-07	6.264822 e-07	1.217649 e-06
2.781133 e-07	1.899617 e-07	2.634898 e-07	3.068007 e-07	3.396388 e-07	4.341082 e-07
3.884437 e-07	2.386710 e-07	1.369773 e-07	2.644146 e-07	5.597242 e-07	9.023576 e-07
2.838312 e-06	2.787708 e-06	2.576258 e-06	2.399145 e-06	3.596083 e-06	5.249359 e-06
1.326571 e-05	1.321921 e-05	1.305442 e-05	1.269530 e-05	1.290280 e-05	1.579062 e-05
2.501048 e-05	2.570185 e-05	2.697905 e-05	2.775579 e-05	2.927837 e-05	3.599815 e-05

Table D.38 – β_{ki} (Avery nominal)

Family 1 - 4	7.508247 e-05	6.491414 e-04	2.660704 e-04	5.780541 e-04
	7.511873 e-05	6.501551 e-04	2.663719 e-04	5.797889 e-04
	1.577334 e-04	1.544016 e-03	6.246718 e-04	2.042958 e-03
	2.169259 e-04	1.038917 e-03	6.414830 e-04	1.374969 e-03
	2.146237 e-04	1.060329 e-03	6.205048 e-04	1.374896 e-03
	2.161086 e-04	1.045524 e-03	6.168781 e-04	1.350370 e-03
Family 5 - 8	1.276324 e-03	4.743223 e-04	4.440766 e-04	2.167381 e-04
	1.280047 e-03	4.774682 e-04	4.458722 e-04	2.182448 e-04
	4.225046 e-03	2.663192 e-03	1.765291 e-03	1.232738 e-03
	2.259827 e-03	7.844480 e-04	6.684254 e-04	2.484980 e-04
	2.339434 e-03	7.783509 e-04	6.520381 e-04	2.451391 e-04
	2.282760 e-03	7.109532 e-04	6.102731 e-04	2.099409 e-04

Table D.39 – S_{jk} (Avery nominal)

8.704118 e-02	4.199541 e-02	3.841757 e-03	1.119742 e-02	6.190384 e-03	3.257226 e-03
4.739389 e-02	4.983301 e-02	5.181471 e-03	1.503442 e-02	8.411844 e-03	4.450045 e-03
3.001368 e-03	5.155439 e-03	3.754596 e-03	1.271525 e-02	6.465203 e-03	3.539170 e-03
1.416169 e-02	1.667458 e-02	8.884292 e-03	6.647471 e-02	5.147625 e-02	3.525896 e-02
1.042399 e-02	1.264157 e-02	6.776405 e-03	5.020733 e-02	6.166614 e-02	6.108606 e-02
7.936175 e-03	1.035075 e-02	6.257582 e-03	4.861410 e-02	7.337883 e-02	1.392715 e-01

Table D.40 – $k^d_{jk,i}$ (Avery nominal)

Family 1	4.573263 e-01	2.518365 e-01	6.775922 e-02	2.801689 e-02	7.753828 e-03	9.955609 e-04
	2.410550 e-01	2.815152 e-01	9.752742 e-02	4.169027 e-02	1.246948 e-02	1.634721 e-03
	5.529136 e-03	8.412111 e-03	1.687863 e-02	1.320438 e-02	8.088628 e-03	2.171417 e-03
	5.924612 e-02	9.554150 e-02	2.750989 e-01	4.017265 e-01	2.899421 e-01	9.383231 e-02
	3.894392 e-02	6.518249 e-02	1.985151 e-01	2.976265 e-01	3.903113 e-01	2.460938 e-01
	2.313505 e-02	4.058694 e-02	1.360354 e-01	2.090350 e-01	3.774552 e-01	6.186425 e-01
Family 2	4.841726 e-01	2.841857 e-01	9.429827 e-02	4.522039 e-02	1.782280 e-02	3.827668 e-03
	2.722452 e-01	3.126799 e-01	1.248044 e-01	6.110123 e-02	2.504516 e-02	5.495284 e-03
	7.243153 e-03	1.038869 e-02	1.923134 e-02	1.446778 e-02	8.821228 e-03	3.055089 e-03
	8.403143 e-02	1.215697 e-01	2.635601 e-01	3.507533 e-01	2.670839 e-01	1.106959 e-01
	6.001536 e-02	9.043345 e-02	2.069617 e-01	2.791468 e-01	3.350161 e-01	2.314708 e-01
	4.098670 e-02	6.628295 e-02	1.736245 e-01	2.464838 e-01	3.780316 e-01	5.485370 e-01
Family 3	4.647142 e-01	2.583842 e-01	7.299073 e-02	3.162351 e-02	9.848782 e-03	1.550239 e-03
	2.474897 e-01	2.893579 e-01	1.028230 e-01	4.572078 e-02	1.507566 e-02	2.395244 e-03
	5.852209 e-03	8.752825 e-03	1.733814 e-02	1.340455 e-02	8.213876 e-03	2.346296 e-03
	6.431231 e-02	1.006964 e-01	2.733346 e-01	3.926085 e-01	2.855255 e-01	9.732493 e-02
	4.333657 e-02	7.032970 e-02	2.000128 e-01	2.932602 e-01	3.794042 e-01	2.433433 e-01
	2.689024 e-02	4.592622 e-02	1.436932 e-01	2.163094 e-01	3.771912 e-01	6.047643 e-01
Family 4	4.731129 e-01	2.713546 e-01	8.378450 e-02	3.852594 e-02	1.376068 e-02	2.637505 e-03
	2.599852 e-01	3.000711 e-01	1.138232 e-01	5.351407 e-02	1.998226 e-02	3.880744 e-03
	6.624215 e-03	9.708218 e-03	1.863048 e-02	1.414609 e-02	8.625867 e-03	2.734781 e-03
	7.446238 e-02	1.114689 e-01	2.683941 e-01	3.706468 e-01	2.766664 e-01	1.041921 e-01
	5.183851 e-02	8.060962 e-02	2.040675 e-01	2.867241 e-01	3.572592 e-01	2.379033 e-01
	3.395980 e-02	5.611621 e-02	1.590137 e-01	2.318273 e-01	3.775183 e-01	5.768993 e-01
Family 5	4.781316 e-01	2.748646 e-01	8.611343 e-02	4.007320 e-02	1.497470 e-02	3.113514 e-03
	2.633044 e-01	3.048815 e-01	1.165585 e-01	5.535507 e-02	2.151655 e-02	4.512871 e-03
	7.042716 e-03	1.066820 e-02	2.196174 e-02	1.598463 e-02	9.335627 e-03	3.006607 e-03
	7.631819 e-02	1.133588 e-01	2.673913 e-01	3.671638 e-01	2.747776 e-01	1.058534 e-01
	5.347185 e-02	8.247759 e-02	2.041096 e-01	2.846316 e-01	3.520608 e-01	2.362008 e-01
	3.553265 e-02	5.833221 e-02	1.618024 e-01	2.345074 e-01	3.765681 e-01	5.696594 e-01
Family 6	4.759930 e-01	2.717801 e-01	8.326783 e-02	3.838182 e-02	1.422724 e-02	2.902176 e-03
	2.603705 e-01	3.022125 e-01	1.137314 e-01	5.353512 e-02	2.065218 e-02	4.228362 e-03
	7.035215 e-03	1.088045 e-02	2.306307 e-02	1.667896 e-02	9.705797 e-03	3.070470 e-03
	7.366374 e-02	1.106051 e-01	2.689389 e-01	3.727403 e-01	2.794637 e-01	1.052852 e-01
	5.116813 e-02	7.973158 e-02	2.034257 e-01	2.862631 e-01	3.573211 e-01	2.395580 e-01
	3.356022 e-02	5.548438 e-02	1.577563 e-01	2.299956 e-01	3.734470 e-01	5.763364 e-01
Family 7	4.806041 e-01	2.726210 e-01	8.361381 e-02	3.902144 e-02	1.491740 e-02	3.291875 e-03
	2.612181 e-01	3.053974 e-01	1.145164 e-01	5.431388 e-02	2.145516 e-02	4.731709 e-03
	7.329014 e-03	1.172399 e-02	2.625880 e-02	1.842948 e-02	1.037401 e-02	3.318571 e-03
	7.342312 e-02	1.100680 e-01	2.679920 e-01	3.732358 e-01	2.777256 e-01	1.051547 e-01
	5.130294 e-02	7.958991 e-02	2.013187 e-01	2.839902 e-01	3.563113 e-01	2.376062 e-01
	3.420100 e-02	5.626473 e-02	1.574809 e-01	2.293718 e-01	3.733656 e-01	5.739256 e-01
Family 8	4.831274 e-01	2.777120 e-01	8.768708 e-02	4.150423 e-02	1.656581 e-02	3.680320 e-03
	2.660506 e-01	3.094047 e-01	1.186294 e-01	5.717640 e-02	2.360845 e-02	5.273533 e-03
	7.609640 e-03	1.205055 e-02	2.672511 e-02	1.876722 e-02	1.062999 e-02	3.472801 e-03
	7.739303 e-02	1.144377 e-01	2.667742 e-01	3.651064 e-01	2.770405 e-01	1.092488 e-01
	5.443594 e-02	8.353299 e-02	2.038316 e-01	2.821124 e-01	3.474224 e-01	2.380216 e-01
	3.658212 e-02	5.977551 e-02	1.633866 e-01	2.351385 e-01	3.705813 e-01	5.630734 e-01

D.4 6 Regions - Perturbed

β-effective = 5.093746 e-03

Mean neutron generation time (Λ) = 6.478777 e-06

k-effective = 1.120243 e+00

Table D.41 – β effective by family (perturbed)

Family 1 - 4	1.249463 e-04	7.743509 e-04	3.863709 e-04	8.669939 e-04
Family 5 - 8	1.633045 e-03	5.812762 e-04	5.041946 e-04	2.225678 e-04

Table D.42 – l_j (Kobayashi perturbed)

3.903454 e-07	5.110203 e-07	1.013258 e-05	1.181318 e-05	1.360145 e-05	2.052059 e-05

Table D.43 – S_j (Kobayashi perturbed)

1.980757 e-01	1.802376 e-01	4.777728 e-02	1.494467 e-02	2.399209 e-01	3.190438 e-01

Table D.44 – k_{jk} (Kobayashi perturbed)

6.509644 e-01	3.790449 e-01	1.465317 e-01	8.403558 e-02	4.627592 e-02	1.643749 e-02
3.874216 e-01	4.769136 e-01	2.185411 e-01	1.299057 e-01	7.521585 e-02	2.763422 e-02
3.751032 e-02	6.527986 e-02	1.482334 e-01	1.101912 e-01	6.759939 e-02	2.946086 e-02
8.315539 e-03	1.205787 e-02	2.843754 e-02	4.569165 e-02	2.875654 e-02	1.249713 e-02
1.350343 e-01	1.829816 e-01	3.170213 e-01	3.921188 e-01	4.196555 e-01	2.738057 e-01
8.117725 e-02	1.208872 e-01	2.485087 e-01	3.315937 e-01	4.462764 e-01	6.132979 e-01

Table D.45 – β_{jk} (Kobayashi perturbed)

3.354447 e-03	3.352974 e-03	9.655979 e-03	7.340943 e-03	3.764434 e-03	2.000158 e-03
3.474190 e-03	3.229925 e-03	1.017008 e-02	8.161325 e-03	4.582136 e-03	2.657275 e-03
2.359408 e-03	1.856717 e-03	4.279945 e-03	4.963694 e-03	4.669150 e-03	4.259046 e-03
3.069032 e-03	2.953931 e-03	7.367509 e-03	5.290529 e-03	5.260301 e-03	5.111935 e-03
3.395993 e-03	3.575353 e-03	1.239691 e-02	1.141520 e-02	8.351410 e-03	7.540010 e-03
2.902245 e-03	2.996865 e-03	1.017939 e-02	9.231226 e-03	7.249949 e-03	8.305847 e-03

Table D.46 – β_{ij} (Kobayashi perturbed)

Family 1 - 4	7.503825 e-05	6.474435 e-04	2.655970 e-04	5.751416 e-04
	7.469560 e-05	6.387750 e-04	2.629574 e-04	5.604776 e-04
	1.810507 e-04	1.353091 e-03	6.280879 e-04	1.783722 e-03
	1.922857 e-04	1.248413 e-03	6.238117 e-04	1.637715 e-03
	2.159442 e-04	1.049752 e-03	6.201976 e-04	1.359765 e-03
	2.162538 e-04	1.043962 e-03	6.162944 e-04	1.347538 e-03
Family 5 - 8	1.270000 e-03	4.688936 e-04	4.410033 e-04	2.141230 e-04
	1.238543 e-03	4.426442 e-04	4.259251 e-04	2.015688 e-04
	3.476063 e-03	1.924421 e-03	1.331495 e-03	8.451169 e-04
	3.074871 e-03	1.522015 e-03	1.092527 e-03	6.352196 e-04
	2.297667 e-03	7.348658 e-04	6.261816 e-04	2.222960 e-04
	2.276812 e-03	7.032278 e-04	6.053869 e-04	2.059049 e-04

Table D.47 – k^d_{ijk} (Kobayashi perturbed)

Family 1	5.279140 e-01	3.057894 e-01	1.003391 e-01	4.734141 e-02	1.532704 e-02	1.848347 e-03
	3.161819 e-01	3.815080 e-01	1.731192 e-01	9.227836 e-02	3.731232 e-02	5.713836 e-03
	1.939860 e-02	2.880762 e-02	5.180288 e-02	5.514310 e-02	4.624886 e-02	1.622889 e-02
	5.377789 e-03	8.372412 e-03	1.855476 e-02	2.471223 e-02	2.267571 e-02	8.511873 e-03
	9.361754 e-02	1.496192 e-01	3.506468 e-01	4.741499 e-01	5.359549 e-01	2.991783 e-01
	4.271615 e-02	7.238717 e-02	1.948712 e-01	2.748911 e-01	4.444768 e-01	7.828287 e-01
Family 2	5.601569 e-01	3.408673 e-01	1.320479 e-01	6.886898 e-02	2.919440 e-02	5.998796 e-03
	3.515465 e-01	4.070433 e-01	1.989742 e-01	1.125274 e-01	5.408973 e-02	1.272042 e-02
	2.339604 e-02	3.160304 e-02	5.119668 e-02	5.082352 e-02	4.207403 e-02	1.838976 e-02
	6.973256 e-03	9.673171 e-03	1.758350 e-02	2.236083 e-02	1.997115 e-02	9.290382 e-03
	1.275244 e-01	1.816606 e-01	3.416399 e-01	4.324180 e-01	4.669213 e-01	2.902174 e-01
	6.799880 e-02	1.056423 e-01	2.365319 e-01	3.226018 e-01	4.604437 e-01	6.956356 e-01
Family 3	5.365625 e-01	3.129640 e-01	1.072741 e-01	5.178607 e-02	1.819500 e-02	2.669530 e-03
	3.232000 e-01	3.884703 e-01	1.796015 e-01	9.652017 e-02	4.074761 e-02	7.117652 e-03
	2.014392 e-02	2.930760 e-02	5.165912 e-02	5.430848 e-02	4.540565 e-02	1.667658 e-02
	5.694029 e-03	8.618064 e-03	1.828702 e-02	2.424690 e-02	2.213408 e-02	8.675458 e-03
	1.004935 e-01	1.558946 e-01	3.472000 e-01	4.656536 e-01	5.224301 e-01	2.976747 e-01
	4.797892 e-02	7.920053 e-02	2.024095 e-01	2.843218 e-01	4.475133 e-01	7.654285 e-01
Family 4	5.470501 e-01	3.277880 e-01	1.205758 e-01	6.045534 e-02	2.360073 e-02	4.269651 e-03
	3.377169 e-01	3.968726 e-01	1.901433 e-01	1.045922 e-01	4.733307 e-02	9.839594 e-03
	2.191592 e-02	3.059813 e-02	5.174526 e-02	5.280674 e-02	4.388234 e-02	1.761123 e-02
	6.366090 e-03	9.170363 e-03	1.793737 e-02	2.339556 e-02	2.110816 e-02	9.018427 e-03
	1.144777 e-01	1.690592 e-01	3.438237 e-01	4.493551 e-01	4.948289 e-01	2.945695 e-01
	5.810139 e-02	9.238262 e-02	2.190181 e-01	3.037246 e-01	4.542162 e-01	7.308084 e-01
Family 5	5.527087 e-01	3.314129 e-01	1.237005 e-01	6.240464 e-02	2.518029 e-02	4.938394 e-03
	3.412473 e-01	4.012934 e-01	1.933267 e-01	1.065400 e-01	4.924993 e-02	1.087082 e-02
	2.251764 e-02	3.172037 e-02	5.510431 e-02	5.450321 e-02	4.424363 e-02	1.801049 e-02
	6.498904 e-03	9.310537 e-03	1.818690 e-02	2.408605 e-02	2.115780 e-02	9.144702 e-03
	1.168748 e-01	1.711175 e-01	3.414062 e-01	4.447817 e-01	4.881355 e-01	2.933642 e-01
	6.022914 e-02	9.514624 e-02	2.216284 e-01	3.073528 e-01	4.548613 e-01	7.215811 e-01
Family 6	5.502282 e-01	3.297524 e-01	1.223321 e-01	6.015896 e-02	2.384287 e-02	4.635530 e-03
	3.379203 e-01	3.996818 e-01	1.934726 e-01	1.044884 e-01	4.771299 e-02	1.037317 e-02
	2.229788 e-02	3.178695 e-02	5.654127 e-02	5.592683 e-02	4.515864 e-02	1.814225 e-02
	6.344087 e-03	9.172019 e-03	1.830086 e-02	2.471449 e-02	2.162115 e-02	9.213937 e-03
	1.132062 e-01	1.669851 e-01	3.393075 e-01	4.491262 e-01	4.953880 e-01	2.970212 e-01
	5.744438 e-02	9.105048 e-02	2.146638 e-01	3.020096 e-01	4.523533 e-01	7.292397 e-01
Family 7	5.548694 e-01	3.290642 e-01	1.217956 e-01	6.085389 e-02	2.484592 e-02	5.165088 e-03
	3.380235 e-01	4.026831 e-01	1.936918 e-01	1.054139 e-01	4.882716 e-02	1.109407 e-02
	2.249306 e-02	3.279606 e-02	6.003092 e-02	5.800019 e-02	4.588751 e-02	1.832925 e-02
	6.321626 e-03	9.203061 e-03	1.864352 e-02	2.554298 e-02	2.187233 e-02	9.233303 e-03
	1.125743 e-01	1.663859 e-01	3.372507 e-01	4.460882 e-01	4.933759 e-01	2.947205 e-01
	5.803236 e-02	9.205711 e-02	2.152531 e-01	3.015904 e-01	4.513113 e-01	7.261218 e-01
Family 8	5.583850 e-01	3.360963 e-01	1.278366 e-01	6.387324 e-02	2.669742 e-02	5.760495 e-03
	3.440342 e-01	4.060690 e-01	1.985523 e-01	1.081174 e-01	5.119481 e-02	1.218487 e-02
	2.321896 e-02	3.316481 e-02	6.004634 e-02	5.740400 e-02	4.530223 e-02	1.892611 e-02
	6.596388 e-03	9.408883 e-03	1.848282 e-02	2.525299 e-02	2.149695 e-02	9.498150 e-03
	1.181369 e-01	1.713598 e-01	3.362914 e-01	4.409901 e-01	4.831710 e-01	2.972060 e-01
	6.158673 e-02	9.641537 e-02	2.205989 e-01	3.092033 e-01	4.535938 e-01	7.120773 e-01

Table D.48 – k_{jk} (Avery perturbed)

5.819106 e-01	3.378930 e-01	1.306735 e-01	7.494576 e-02	4.122487 e-02	1.466610 e-02
3.486210 e-01	4.253714 e-01	1.926154 e-01	1.144088 e-01	6.611910 e-02	2.427896 e-02
3.399744 e-02	5.962970 e-02	1.330320 e-01	9.670304 e-02	5.939114 e-02	2.586824 e-02
7.414885 e-03	1.076166 e-02	2.540790 e-02	4.080704 e-02	2.566211 e-02	1.115356 e-02
1.212798 e-01	1.642457 e-01	2.841932 e-01	3.514850 e-01	3.748454 e-01	2.430950 e-01
7.478374 e-02	1.109682 e-01	2.265033 e-01	3.011373 e-01	4.023290 e-01	5.403139 e-01

Table D.49 – β_{jk} (Avery perturbed)

3.354104 e-03	3.353339 e-03	9.652312 e-03	7.337226 e-03	3.761736 e-03	1.999330 e-03
3.472134 e-03	3.229140 e-03	1.016096 e-02	8.140387 e-03	4.559528 e-03	2.637987 e-03
2.335843 e-03	1.823770 e-03	4.233849 e-03	4.959156 e-03	4.641859 e-03	4.223491 e-03
3.068131 e-03	2.952664 e-03	7.360133 e-03	5.287043 e-03	5.259515 e-03	5.110760 e-03
3.399472 e-03	3.579023 e-03	1.240562 e-02	1.141804 e-02	8.352908 e-03	7.522906 e-03
2.925534 e-03	3.024046 e-03	1.028639 e-02	9.339542 e-03	7.316925 e-03	8.302597 e-03

Table D.50 – l_{jk} (Avery perturbed)

2.658746 e-07	3.832037 e-07	5.767838 e-07	6.594630 e-07	7.205497 e-07	7.623539 e-07
4.202024 e-07	3.202960 e-07	5.244253 e-07	6.941455 e-07	8.649901 e-07	1.034389 e-06
7.661747 e-06	5.708253 e-06	4.103360 e-06	6.619993 e-06	1.071235 e-05	1.482935 e-05
1.277621 e-05	1.157207 e-05	7.939367 e-06	5.819478 e-06	9.252456 e-06	1.302193 e-05
1.245256 e-05	1.230534 e-05	1.195749 e-05	1.161943 e-05	1.150471 e-05	1.278044 e-05
1.673573 e-05	1.676528 e-05	1.688270 e-05	1.696678 e-05	1.712916 e-05	1.872312 e-05

Table D.51 – β_{ki} (Avery perturbed)

Family 1 - 4	7.503825 e-05	6.474435 e-04	2.655970 e-04	5.751416 e-04
	7.469560 e-05	6.387750 e-04	2.629574 e-04	5.604776 e-04
	1.810507 e-04	1.353091 e-03	6.280879 e-04	1.783722 e-03
	1.922857 e-04	1.248413 e-03	6.238117 e-04	1.637715 e-03
	2.159442 e-04	1.049752 e-03	6.201976 e-04	1.359765 e-03
	2.162538 e-04	1.043962 e-03	6.162944 e-04	1.347538 e-03
Family 5 - 8	1.270000 e-03	4.688936 e-04	4.410033 e-04	2.141230 e-04
	1.238543 e-03	4.426442 e-04	4.259251 e-04	2.015688 e-04
	3.476063 e-03	1.924421 e-03	1.331495 e-03	8.451169 e-04
	3.074871 e-03	1.522015 e-03	1.092527 e-03	6.352196 e-04
	2.297667 e-03	7.348658 e-04	6.261816 e-04	2.222960 e-04
	2.276812 e-03	7.032278 e-04	6.053869 e-04	2.059049 e-04

Table D.52 – S_{jk} (Avery perturbed)

1.152547 e-01	6.089699 e-02	6.242810 e-03	1.119965 e-03	9.890051 e-03	4.678817 e-03
6.904875 e-02	7.666284 e-02	9.202027 e-03	1.709689 e-03	1.586230 e-02	7.745536 e-03
6.733618 e-03	1.074680 e-02	6.355483 e-03	1.445099 e-03	1.424823 e-02	8.252553 e-03
1.468611 e-03	1.939527 e-03	1.213840 e-03	6.098073 e-04	6.156467 e-03	3.558238 e-03
2.402099 e-02	2.960130 e-02	1.357708 e-02	5.252478 e-03	8.992727 e-02	7.755281 e-02
1.481186 e-02	1.999932 e-02	1.082099 e-02	4.500099 e-03	9.652071 e-02	1.723724 e-01

Table D.53 – $k^d_{jk,i}$ (Avery perturbed)

Family 1	4.718862 e-01	2.725489 e-01	8.939525 e-02	4.216454 e-02	1.364377 e-02	1.647078 e-03
	2.846383 e-01	3.400343 e-01	1.521494 e-01	8.083823 e-02	3.250639 e-02	4.949599 e-03
	1.744987 e-02	2.586076 e-02	4.586897 e-02	4.832529 e-02	4.034710 e-02	1.410747 e-02
	4.800199 e-03	7.472986 e-03	1.656073 e-02	2.205417 e-02	2.023355 e-02	7.594704 e-03
	8.422775 e-02	1.345317 e-01	3.148403 e-01	4.255649 e-01	4.789847 e-01	2.646021 e-01
	3.992093 e-02	6.749196 e-02	1.807556 e-01	2.545715 e-01	4.069569 e-01	6.898496 e-01
Family 2	5.007381 e-01	3.039562 e-01	1.177276 e-01	6.138861 e-02	2.601768 e-02	5.347379 e-03
	3.161303 e-01	3.630000 e-01	1.753641 e-01	9.896120 e-02	4.740454 e-02	1.110711 e-02
	2.097696 e-02	2.830585 e-02	4.539270 e-02	4.458005 e-02	3.677255 e-02	1.601853 e-02
	6.224112 e-03	8.633793 e-03	1.569466 e-02	1.995714 e-02	1.782077 e-02	8.289611 e-03
	1.145805 e-01	1.630953 e-01	3.062453 e-01	3.873785 e-01	4.170298 e-01	2.572882 e-01
	6.313311 e-02	9.770773 e-02	2.172145 e-01	2.953788 e-01	4.175222 e-01	6.121627 e-01
Family 3	4.796311 e-01	2.789668 e-01	9.559073 e-02	4.613401 e-02	1.620305 e-02	2.379200 e-03
	2.909086 e-01	3.462912 e-01	1.579329 e-01	8.463009 e-02	3.555766 e-02	6.182946 e-03
	1.810479 e-02	2.629610 e-02	4.576252 e-02	4.760243 e-02	3.962473 e-02	1.450321 e-02
	5.082427 e-03	7.692205 e-03	1.632195 e-02	2.163919 e-02	1.975035 e-02	7.740719 e-03
	9.038032 e-02	1.401218 e-01	3.116499 e-01	4.178068 e-01	4.668489 e-01	2.633947 e-01
	4.475113 e-02	7.367809 e-02	1.872945 e-01	2.626108 e-01	4.089268 e-01	6.743919 e-01
Family 4	4.890118 e-01	2.922453 e-01	1.074751 e-01	5.387533 e-02	2.102653 e-02	3.805786 e-03
	3.038075 e-01	3.538850 e-01	1.674164 e-01	9.185963 e-02	4.140458 e-02	8.574511 e-03
	1.967325 e-02	2.743176 e-02	4.587086 e-02	4.630279 e-02	3.832430 e-02	1.532911 e-02
	5.682245 e-03	8.185102 e-03	1.601026 e-02	2.088010 e-02	1.883514 e-02	8.046853 e-03
	1.029031 e-01	1.518626 e-01	3.084076 e-01	4.028670 e-01	4.420748 e-01	2.608982 e-01
	5.405264 e-02	8.566786 e-02	2.018552 e-01	2.792637 e-01	4.134543 e-01	6.435412 e-01
Family 5	4.940735 e-01	2.954810 e-01	1.102660 e-01	5.561593 e-02	2.243596 e-02	4.402119 e-03
	3.069786 e-01	3.578421 e-01	1.702501 e-01	9.359894 e-02	4.310616 e-02	9.482928 e-03
	2.021937 e-02	2.846872 e-02	4.891777 e-02	4.778826 e-02	3.865214 e-02	1.568340 e-02
	5.800854 e-03	8.310347 e-03	1.623399 e-02	2.149754 e-02	1.887955 e-02	8.159602 e-03
	1.050460 e-01	1.536931 e-01	3.062065 e-01	3.987234 e-01	4.360759 e-01	2.598862 e-01
	5.599046 e-02	8.815472 e-02	2.040622 e-01	2.822785 e-01	4.136645 e-01	6.353851 e-01
Family 6	4.918526 e-01	2.939844 e-01	1.090388 e-01	5.361014 e-02	2.124227 e-02	4.132036 e-03
	3.040199 e-01	3.564537 e-01	1.703374 e-01	9.176119 e-02	4.173901 e-02	9.045089 e-03
	2.003467 e-02	2.855089 e-02	5.023531 e-02	4.903272 e-02	3.944845 e-02	1.579765 e-02
	5.662720 e-03	8.186800 e-03	1.633595 e-02	2.205872 e-02	1.929300 e-02	8.221384 e-03
	1.017632 e-01	1.500070 e-01	3.043864 e-01	4.027039 e-01	4.425947 e-01	2.630784 e-01
	5.343354 e-02	8.442789 e-02	1.978717 e-01	2.777012 e-01	4.118244 e-01	6.424899 e-01
Family 7	4.960145 e-01	2.933620 e-01	1.085614 e-01	5.423147 e-02	2.213797 e-02	4.604513 e-03
	3.041686 e-01	3.590854 e-01	1.705032 e-01	9.257755 e-02	4.272984 e-02	9.682683 e-03
	2.022019 e-02	2.949551 e-02	5.339217 e-02	5.085128 e-02	4.009451 e-02	1.596704 e-02
	5.642744 e-03	8.214678 e-03	1.664278 e-02	2.279918 e-02	1.951724 e-02	8.238741 e-03
	1.011854 e-01	1.494594 e-01	3.025512 e-01	4.000199 e-01	4.408026 e-01	2.610373 e-01
	5.393652 e-02	8.528919 e-02	1.982681 e-01	2.771261 e-01	4.107542 e-01	6.397034 e-01
Family 8	4.991516 e-01	2.996546 e-01	1.139567 e-01	5.692700 e-02	2.378943 e-02	5.135128 e-03
	3.094938 e-01	3.621863 e-01	1.748744 e-01	9.500425 e-02	4.482932 e-02	1.063905 e-02
	2.086349 e-02	2.981421 e-02	5.342736 e-02	5.033033 e-02	3.959322 e-02	1.649025 e-02
	5.887970 e-03	8.398343 e-03	1.649941 e-02	2.254071 e-02	1.918235 e-02	8.475090 e-03
	1.061728 e-01	1.539007 e-01	3.016102 e-01	3.953103 e-01	4.316462 e-01	2.633616 e-01
	5.721671 e-02	8.927227 e-02	2.029860 e-01	2.837413 e-01	4.122760 e-01	6.274772 e-01

Appendix E

MUSE: PK and MPK Coefficient tables

This appendix is a collection of all the parameters computed for the MUSE case discussed in section 5.3. This case has only the nominal configuration and the parameters related to PK and to Kobayashi's MPK. The parameters related to the Kobayashi's MPK are named as in Table 3.3.

E.1 MUSE - Nominal case

β-effective = 3.328177 e-03

Mean neutron generation time (Λ) = 4.653594 e-07

k-effective = 9.709812 e-01

Table E.1 – Decay constant by family

Family 1 - 4	0.0124667	0.0282917	0.0425244	0.133042
Family 5 - 8	0.292467	0.666488	1.63478	3.55460

Table E.2 – β effective by family

Family 1 - 4	6.265543 e-05	5.662745 e-04	2.237621 e-04	4.814289 e-04
Family 5 - 8	1.072509 e-03	3.806861 e-04	3.697593 e-04	1.712787 e-04

Table E.3 – l_j (Kobayashi nominal)

2.871538 e-07	2.768729 e-07	4.033583 e-07	9.694875 e-07	7.287803 e-06

Table E.4 – S_j (Kobayashi nominal)

6.851666 e-02	2.957154 e-01	3.249993 e-01	3.098917 e-01	8.769487 e-04

Table E.5 – k_{jk} (Kobayashi nominal)

2.441617 e-01	9.390358 e-02	4.153881 e-02	2.785265 e-02	2.237968 e-03
4.399657 e-01	4.595483 e-01	2.357504 e-01	1.451588 e-01	1.716348 e-02
2.693566 e-01	3.198707 e-01	3.842187 e-01	2.531898 e-01	4.205024 e-02
2.271085 e-01	2.499891 e-01	3.085480 e-01	3.616621 e-01	8.078420 e-02
4.236750 e-04	5.946081 e-04	8.423972 e-04	1.004688 e-03	5.777652 e-02

Table E.6 – β_{jk} (Kobayashi nominal)

3.255307 e-03	3.492318 e-03	3.389938 e-03	3.099735 e-03	2.047714 e-03
3.439994 e-03	3.354126 e-03	3.369433 e-03	3.119304 e-03	2.164866 e-03
3.413587 e-03	3.451682 e-03	3.263229 e-03	3.135361 e-03	2.329223 e-03
3.443458 e-03	3.532698 e-03	3.456114 e-03	3.132899 e-03	2.539884 e-03
2.990841 e-03	3.343687 e-03	3.612893 e-03	3.579579 e-03	1.963242 e-03

Table E.7 – β_{ij} (Kobayashi nominal)

Family 1 - 4	7.242759 e-05	6.327325 e-04	2.566205 e-04	5.467130 e-04
	7.266330 e-05	6.375863 e-04	2.581801 e-04	5.551779 e-04
	7.248038 e-05	6.334031 e-04	2.568316 e-04	5.479979 e-04
	7.173948 e-05	6.168814 e-04	2.514675 e-04	5.194960 e-04
	9.009638 e-04	1.796223 e-04	2.698242 e-04	6.777048 e-05
Family 5 - 8	1.209441 e-03	4.322041 e-04	4.160737 e-04	1.928089 e-04
	1.227244 e-03	4.470292 e-04	4.246034 e-04	1.998316 e-04
	1.211853 e-03	4.342648 e-04	4.172890 e-04	1.936592 e-04
	1.150792 e-03	3.837255 e-04	3.882478 e-04	1.692407 e-04
	6.907394 e-05	5.520494 e-04	2.297208 e-04	4.063740 e-04

Table E.8 – k^d_{ijk} (Kobayashi nominal)

	2.125241 e-01	8.457027 e-02	3.502904 e-02	2.194660 e-02	1.110847 e-03
	3.955171 e-01	3.956591 e-01	2.020891 e-01	1.178903 e-01	9.921699 e-03
Family 1	2.293289 e-01	2.779618 e-01	3.250595 e-01	2.167048 e-01	2.951853 e-02
	1.941710 e-01	2.215462 e-01	2.824025 e-01	3.230563 e-01	7.052887 e-02
	2.449366 e-04	4.205002 e-04	7.238509 e-04	9.770499 e-04	4.497646 e-02
	2.091787 e-01	8.620300 e-02	3.846293 e-02	2.519482 e-02	2.014107 e-03
	4.048213 e-01	4.044271 e-01	2.140504 e-01	1.308762 e-01	1.588209 e-02
Family 2	2.521582 e-01	2.935552 e-01	3.340165 e-01	2.244327 e-01	4.021238 e-02
	2.150903 e-01	2.357483 e-01	2.824571 e-01	3.140304 e-01	7.994539 e-02
	3.839859 e-04	5.717231 e-04	8.537199 e-04	1.041115 e-03	3.980864 e-02
	2.138963 e-01	8.499572 e-02	3.562801 e-02	2.256269 e-02	1.314666 e-03
	3.978268 e-01	3.993874 e-01	2.046400 e-01	1.203717 e-01	1.123625 e-02
Family 3	2.331830 e-01	2.809876 e-01	3.284994 e-01	2.187598 e-01	3.175992 e-02
	1.974493 e-01	2.234107 e-01	2.821820 e-01	3.229371 e-01	7.214998 e-02
	2.744552 e-04	4.511272 e-04	7.466090 e-04	9.817338 e-04	4.562969 e-02
	2.098747 e-01	8.540464 e-02	3.714931 e-02	2.408885 e-02	1.670455 e-03
	4.007454 e-01	4.004700 e-01	2.095030 e-01	1.264481 e-01	1.362739 e-02
Family 4	2.432969 e-01	2.872983 e-01	3.302240 e-01	2.219321 e-01	3.618549 e-02
	2.070853 e-01	2.301769 e-01	2.819533 e-01	3.171323 e-01	7.638619 e-02
	3.310473 e-04	5.149403 e-04	8.053694 e-04	1.014028 e-03	4.177763 e-02
	2.112751 e-01	8.585145 e-02	3.748320 e-02	2.438484 e-02	1.730383 e-03
	4.028782 e-01	4.034344 e-01	2.111351 e-01	1.277810 e-01	1.401585 e-02
Family 5	2.453910 e-01	2.893626 e-01	3.329527 e-01	2.235835 e-01	3.687598 e-02
	2.088332 e-01	2.316326 e-01	2.831073 e-01	3.186642 e-01	7.701352 e-02
	3.408595 e-04	5.247711 e-04	8.128050 e-04	1.017282 e-03	4.219438 e-02
	2.115715 e-01	8.567265 e-02	3.723224 e-02	2.440700 e-02	1.628294 e-03
	4.024878 e-01	4.032322 e-01	2.107295 e-01	1.279981 e-01	1.335906 e-02
Family 6	2.434284 e-01	2.881791 e-01	3.328821 e-01	2.246829 e-01	3.574947 e-02
	2.070713 e-01	2.305243 e-01	2.832177 e-01	3.202612 e-01	7.613379 e-02
	3.260646 e-04	5.097055 e-04	8.006639 e-04	1.005096 e-03	4.273952 e-02
	2.150096 e-01	8.616516 e-02	3.711153 e-02	2.413573 e-02	1.640374 e-03
	4.041339 e-01	4.066213 e-01	2.110246 e-01	1.271706 e-01	1.332456 e-02
Family 7	2.423063 e-01	2.885386 e-01	3.358235 e-01	2.254939 e-01	3.535292 e-02
	2.052355 e-01	2.293691 e-01	2.848343 e-01	3.249669 e-01	7.507478 e-02
	3.246437 e-04	5.015076 e-04	7.824649 e-04	9.869989 e-04	4.550263 e-02
	2.127309 e-01	8.622426 e-02	3.782630 e-02	2.501324 e-02	1.758335 e-03
	4.052855 e-01	4.068837 e-01	2.133475 e-01	1.306072 e-01	1.419416 e-02
Family 8	2.471198 e-01	2.913616 e-01	3.364196 e-01	2.273735 e-01	3.720007 e-02
	2.102257 e-01	2.329303 e-01	2.844272 e-01	3.215659 e-01	7.735724 e-02
	3.463214 e-04	5.301112 e-04	8.157094 e-04	1.009237 e-03	4.303544 e-02